

University of Windsor

Scholarship at UWindor

Electronic Theses and Dissertations

Theses, Dissertations, and Major Papers

2010

Measuring the Sensitivity of Interfacial Gaps in Laser Transmission Welding Using Manufactured Voids

Stephanie Masse
University of Windsor

Follow this and additional works at: <https://scholar.uwindsor.ca/etd>

Recommended Citation

Masse, Stephanie, "Measuring the Sensitivity of Interfacial Gaps in Laser Transmission Welding Using Manufactured Voids" (2010). *Electronic Theses and Dissertations*. 199.
<https://scholar.uwindsor.ca/etd/199>

This online database contains the full-text of PhD dissertations and Masters' theses of University of Windsor students from 1954 forward. These documents are made available for personal study and research purposes only, in accordance with the Canadian Copyright Act and the Creative Commons license—CC BY-NC-ND (Attribution, Non-Commercial, No Derivative Works). Under this license, works must always be attributed to the copyright holder (original author), cannot be used for any commercial purposes, and may not be altered. Any other use would require the permission of the copyright holder. Students may inquire about withdrawing their dissertation and/or thesis from this database. For additional inquiries, please contact the repository administrator via email (scholarship@uwindsor.ca) or by telephone at 519-253-3000ext. 3208.

Measuring the Sensitivity of Interfacial Gaps in Laser Transmission Welding Using Manufactured Voids

By:
Stephanie Lynn Masse

A Thesis

Submitted to the Faculty of Graduate Studies
through Engineering Materials
in Partial Fulfillment of the Requirements for
the Degree of Master of Applied Science at the
University of Windsor

Windsor, Ontario, Canada

January 2010

© Stephanie Lynn Masse

Measuring the Sensitivity of Interfacial Gaps in Laser Transmission Welding Using Manufactured Voids

By:
Stephanie Lynn Masse

APPROVED BY:

Dr. S. H. Eichhorn
Department of Chemistry and Biochemistry

Dr. A. Edrisky
Department of Mechanical, Automotive, & Materials Engineering

Dr. B. Baylis
Formally of Mahle Air Filter Systems Canada

Dr. D. F. Watt, Advisor
Department of Mechanical, Automotive, & Materials Engineering

Dr. H. Hu, Chair of Defence
Department of Mechanical, Automotive, and Materials Engineering

21 January 2010

Measuring the Sensitivity of Interfacial Gaps in Laser Transmission Welding
Using Manufactured Voids

By:
Stephanie Lynn Masse

APPROVED BY:



Dr. S. H. Eichhorn
Department of Chemistry and Biochemistry



Dr. A. Edrissy
Department of Mechanical, Automotive, & Materials Engineering



Dr. B. Baylis
Formerly of Mahle Air Filter Systems Canada



Dr. D. F. Watt, Advisor
Department of Mechanical, Automotive, & Materials Engineering



Dr. H. Hu, Chair of Defense
Department of Mechanical, Automotive, and Materials Engineering

21 January 2010

Declaration of Co-Authorship / Previous Publication

I. Co-Authorship Declaration

I hereby declare that this thesis incorporates material that is result of joint research, as follows: The concept of manufactured voids, and the injection mould that was used to produce the parts with these voids was done by Dr. Watt, and he and Dr. Baylis had the parts injection moulded with the differing levels of carbon black. All of this occurred before I joined this research. Therefore Dr. Watt was the primary author of sections 3.1 and 3.2. The micrographs shown in Sections 3.3 and Appendix I were obtained from the Optical Profilometer, which is owned by Dr. Ahmet Alpas, were made by Dr. Alpas's Graduate Student, Ming Chen, who is one of only a few persons qualified to use it. The laser welding fixture was designed by Dr. Watt, and built by Andy Jenner. The welding schedule was directed by Dr. Baylis and Dr. Watt and carried out by Hans Hurfurth of the Fraunhofer Laser Laboratory in Plymouth Michigan. All of these mentioned collaborations are described in Chapter 3.

I am aware of the University of Windsor Senate Policy on Authorship and I certify that I have properly acknowledged the contribution of other researchers to my thesis, and have obtained written permission from each of the co-author(s) to include the above material(s) in my thesis.

I certify that, with the above qualification, this thesis, and the major body of this thesis, and the research to which it refers, is the product of my own work, carried out with guidance from Dr. Watt.

II. Declaration of Previous Publication

This thesis includes one original paper that has been previously published/submitted for publication in peer reviewed journals, as follows:

Thesis Chapter	Publication title/full citation	Publication status*
<i>Mainly Chapter 3</i>	Watt, D. F., Masse, S., & Baylis, B., An Experimental Method to Study the Sensitivity of Transmission Laser Welding of Plastic Parts to Interfacial Gaps, in SAE World Congress 2009, SAE International: Technical Paper 2009-01-1298.	<i>published</i>

I certify that I have obtained a written permission from the copyright owner(s) to include the above published material(s) in my thesis. I certify that the above material describes work completed during my registration as graduate student at the University of Windsor.

I declare that, to the best of my knowledge, my thesis does not infringe upon anyone's copyright nor violate any proprietary rights and that any ideas, techniques, quotations, or any other material from the work of other people included in my thesis, published or otherwise, are fully acknowledged in accordance with the standard referencing practices. Furthermore, to the extent that I have included copyrighted material that surpasses the bounds of fair dealing within the meaning of the Canada

Copyright Act, I certify that I have obtained a written permission from the copyright owner(s) to include such material(s) in my thesis.

I declare that this is a true copy of my thesis, including any final revisions, as approved by my thesis committee and the Graduate Studies office, and that this thesis has not been submitted for a higher degree to any other University or Institution.

Abstract

The efforts of this research were to determine the sensitivity to interfacial gaps in laser transmission welding using various laser welding parameters. Note that the melting of the transparent side of the interface relies mainly on heat conduction from the absorbing side since the laser beam energy is mainly absorbed in the non-transparent material. If a gap exists between the parts at the faying surface, the weld may not form at that location.

For this study, interfacial gaps created via manufactured voids were moulded into the components to be welded. After welding, the samples were then assessed using microstructural analysis, fracture surface analysis and hydraulic burst testing.

The research has shown laser transmission welding has the potential of obtaining strong welds, exceeding those of linear vibration welds of similar geometry

Surprisingly, very strong bonds were observed even with a large degree of porosity/voids in the weld.

*To Addie,
for her constant and unassuming love*

Acknowledgements

I would like to thank my advisor Dr. Watt, for his guidance and continuous encouragement throughout this research. His enthusiasm for research, support and valuable suggestions are very much appreciated. I would also like to thank Dr. Bobbye Baylis, formally of Mahle Air Filter Systems Canada, for her contributions to my research through her vast knowledge and experience.

I would like to express my gratitude to the committee members, Dr. A. Edrisy and Dr. S. H. Eichhorn for their beneficial comments to improve this thesis.

Many thanks to the technical staff, especially Andy Jenner, Matthew St. Louis and Steven Budinsky from the University of Windsor, Hans Herfurth from Fraunhofer Center for Laser Technology, and Gary St. Amor, Rick Krzemien and John Mamarella from Mahle Air Filter Systems Canada.

Funding from Auto21 Network Centers for Excellence and Mahle Air Filters Systems Canada for partial support is also greatly acknowledged. I owe many thanks to family, Stacey, Sean, Lisa, Layla and my father Michael for their continual support. Special thanks to my mother Denise for her guidance, love, support and making me who I am. Finally, I would like to thank my friends, especially Christopher Kelly and Melissa Power for their companionship and for always being there.

Table of Contents

Declaration of Co-Authorship / Previous Publication.....	iii
Abstract.....	vi
Acknowledgements	viii
List of Figures	xi
List of Tables.....	xiii
List of Equations	xiii
Nomenclature	xiv
Chapter 1 : Introduction.....	1
1.1 Objectives of the Research.....	2
1.2 Thesis Map	4
Chapter 2 : Plastic Joining and Laser Transmission Welding	5
2.1 Various Welding Techniques (Thermal, Friction, Electromagnetic)	6
2.2 Lasers - An Overview	7
2.3 Process Review- Plastics Welding with Lasers.....	10
2.3.1 Surface Heating.....	10
2.3.2 Infrared/Laser Transmission Welding.....	11
2.3.3 Infrared/Laser Staking	12
2.3.4 Heating Using Transmitted Radiation.....	12
2.4 Porosity/Voids in Polymers.....	17
2.5 Laser Transmission Welding – Literature Review	19
2.5.1 Previous Measurements of Gap Bridging and Factors Affecting Transmission Laser Welding Tensile Strengths.....	23
2.6 Material Background- Nylons (Polyamides).....	25
Chapter 3 : The Creation, Characterization and Welding of Manufactured Voids.....	28
3.1 The Concept of Manufactured Voids.....	28
3.2 Moulding the Parts, and Characterization of the Voids	32
3.2.1 Characterization of the Voids	32
3.3 Laser Welding of the Parts	33
Chapter 4 : Welding - Quality Assessment Methods	36
4.1 Microstructural Analysis (Sectioning)	36
4.2 Fractured Surface Analysis	39
4.3 Burst Test	40
Chapter 5 : Laser Transmission Welding Results – Burst Test	42
5.1 Influence of Variations in Welding Parameters on Burst Strengths.....	43
5.1.1 Power - A (P180, S1500, CB S/2, LE7.2), vs. B (P270, S1500, CB S/2, LE10.8).....	44
5.1.2 Carbon Black Level - A (P180, S1500, CB S/2, LE7.2), vs. C (P180, S1500, CB S, LE7.2)	44
5.1.3 Beam Traverse Speed - B (P270, S1500, CB S/2, LE10.8), vs. D (P270, S1800, CB S/2, LE9)	45
5.1.4 Line Speed Effect at Constant Line Energy - C (P180, S1500, CB S, LE7.2) vs. E(P240, S2000, CB S, LE7.2).....	45
Chapter 6 : Laser Transmission Welding Results - Fractured Surface Analysis	47
6.1 Power A (P180, S1500, CB S/2, LE7.2), vs. B (P270, S1500, CB S/2, LE10.8)....	56

6.2 Carbon Black Level - A (P180, S1500, CB S/2, LE7.2), vs. C (P180, S1500, CB S, LE7.2)	57
6.3 Beam Traverse Speed - B (P270, S1500, CB S/2, LE10.8), vs. D (P270, S1800, CB S/2, LE9)	57
6.4 Line Speed Effect at Constant Line Energy - C (P180, S1500, CB S, LE7.2) vs. E(P240, S2000, CB S, LE7.2)	58
Chapter 7 : Laser Transmission Welding Results - Microstructural Analysis.....	59
7.1 Cross-sections Perpendicular to the Direction of the Laser Beam	63
7.2 Mechanisms for Porosity Formation.....	65
7.2.1 Air Encapsulation During Welding.....	65
7.2.2 Water Vapour Evolved from Moist Resin During Processing	66
7.2.3 Excessive Volume Contraction of the Polymer During Cooling (Shrinkage)..	66
7.3 Graphical Data and Results	68
7.3.1 Comparison of Welding Conditions.....	72
7.3.1.1 Power - A (P180, S1500, CB S/2, LE7.2), vs. B (P270, S1500, CB S/2, LE10.8).....	72
7.3.1.2 Carbon Black Level - A (P180, S1500, CB S/2, LE7.2), vs. C (P180, S1500, CB S, LE7.2).....	74
7.3.1.3 Beam Traverse Speed - B (P270, S1500, CB S/2, LE10.8), vs. D (P270, S1800, CB S/2, LE9).....	76
7.3.1.4 Line Speed Effect at Constant Line Energy - C (P180, S1500, CB S, LE7.2) vs. E(P240, S2000, CB S, LE7.2)	78
Chapter 8 : Discussion and Interpretation of Results	80
8.1 Overall Assessment of Each Welding Parameter	80
8.1.1 Power (Conditions A-B).....	81
8.1.2 Carbon Black Level (Conditions A-C).....	81
8.1.3 Laser Beam Traverse Speed (Conditions B-D)	82
8.1.4 Line Speed Effect at Constant Line Energy (Conditions C-E).....	83
Chapter 9 : Conclusions and Future Work.....	84
9.1 Conclusions	84
9.2 Recommendations for Future Work.....	86
References.....	88
Appendix I : Optical Profilometer Data and Micrographs	91
Appendix II : Microstructural Section Data and Micrographs	140
Conference Publication and Presentation	227
Vita Auctoris	228

List of Figures

Figure 1: The electromagnetic spectrum (UV-ultraviolet, IR- infrared) [9].....	7
Figure 2: Laser types used in material process categorized by the type of active medium [9]	8
Figure 3: Average power vs. wavelength for commercial lasers [9].....	8
Figure 4: Radiation processes associated with the interaction of light with matter spontaneous emission, stimulated emission and absorption [10].....	9
Figure 5: Amplification of light by stimulated emission of radiation [9].....	10
Figure 6: Surface heating using IR/laser welding [2].....	11
Figure 7: Infrared/laser transmission welding (LTW).....	11
Figure 8: Methods of delivery of the laser beam to the joint interface: a) contour welding, b) mask welding, c) simultaneous welding (form of continuous illumination), d) quasi-simultaneous welding (form of continuous illumination) [11]	12
Figure 9: Interaction of radiation from laser beam with plastic, reflection, transmission and absorption	13
Figure 10: Refraction of light through two materials with differing index of refraction [2]	14
Figure 11: Moving heat source (Scan welding) [2].....	16
Figure 12: Voids present in PVC that has been hot-gas welded. The ellipsoidal shape of the voids is due to the deformation of the material by the pressure applied during welding [12].....	18
Figure 13: Tree diagram illustrating the characterization of voids based on their appearance [12]	19
Figure 14: Transmission spectra for 30% GF PA6 [22]	22
Figure 15: Amide group [33]	25
Figure 16: Ring-opening polymerization of nylon 6 [33].....	26
Figure 17: Left: Removable ring for Mahle injection mould for hemispherical parts. Right: Sub insert from removable ring insert for injection mould.....	30
Figure 18: Left - Flange where reproducible voids are present on hemispherical component. Right - Each sub insert is labelled 1 though 10.....	30
Figure 19: Topographical image of manufactured void showing profile and depth.....	33
Figure 20: Equipment setup for the Nd:YAG laser at Fraunhofer Center for Laser Technology.....	34
Figure 21: Steps for assembly of stacked specimen. A- Welded sample. B- Two flanges cut from an un-welded hemisphere (preassembly). C- Un-welded flanges glued to welded hemisphere. D- Stacked specimen for each insert is cut out. E- Stacked specimen for one insert. F- Stacked specimen is mounted in a PVC pipe using epoxy.	37
Figure 22: Line of sight for the microscope. (Perpendicular to the center axis, z, of the assembly)	37
Figure 23: The location of laser beam with respect to the flange is obtained by images taken parallel to the direction of travel. Circled is the surface that is polished and microphotographed.....	38
Figure 24: Welded sample being separated for fracture surface analysis. Wedges are inserted between the welded inserts to “pry” apart the components. The clamps’ shadow	

prevented the laser beam from reaching the part between the inserts, thus these areas are not welded.	39
Figure 25: Shields used for burst tested samples	41
Figure 26: Axis system for burst tested samples.....	41
Figure 27: Image analysis using computer software techniques. Top- Before (left) and after (right) images of the transfer area defined by threshold technique. Bottom- Before (left) and after (right) images of the adhesion area defined by threshold technique.....	48
Figure 28: Fracture surface - Percent of transfer (top) and adhesion (bottom).....	55
Figure 29: Micrographs of the healed voids and un-welded cross-sections from a stacked specimen. N- Un-welded natural/transparent material. W-weld line, upper section is transparent material and lower section is absorbent material. B- Un-welded black/absorbent material. (Micrographs of welding condition B)	59
Figure 30: Montage of weld with voids that have not healed from welding (Micrographs of welding condition A).....	60
Figure 31: Porosity and unhealed voids is quantified as the average area (mm ²) of the pores on the cross section per unit length (mm).....	61
Figure 32: Area/length Porosity through Depth of B- HG 29.....	62
Figure 33: No Insert.....	62
Figure 34: Insert 3N8B	63
Figure 35: Insert 4N7B	63
Figure 36: A- HG 26 (Right is outer side of part, top is natural material)	64
Figure 37: B- HG 29 (Right is outer side of part, top is natural material).....	64
Figure 38: C- HG9 (Right is outer side of part, top is natural material)	64
Figure 39: D- HG 35 (Right is outer side of part, top is natural material)	64
Figure 40: E- HG 3 (Right is outer side of part, top is natural material).....	64
Figure 41: Manufactured voids and air encapsulation.....	65
Figure 42: Porosity/void formation by shrinkage	67
Figure 43: Area/length porosity through depth of A- HG 26	68
Figure 44: Area/length porosity through depth of B- HG 29.....	69
Figure 45: Area/length porosity through depth of C- HG 9.....	69
Figure 46: Area/length porosity through depth of D- HG 35	70
Figure 47: Area/length porosity through depth of E- HG 3.....	70
Figure 48: Insert 3N-8B, power level comparison, condition A and B.....	72
Figure 49: Insert 4N-7B, power level comparison, condition A and B.....	72
Figure 50: No insert, power level comparison, condition A and B.....	72
Figure 51: Insert 3N-8B, carbon black level comparison, condition A and C.....	74
Figure 52: Insert 4N-7B, carbon black level comparison, condition A and C.....	74
Figure 53: No insert, carbon black level comparison, condition A and C.....	74
Figure 54: Insert 3N-8B, beam traverse speed comparison, condition B and D.....	76
Figure 55: Insert 4N-7B, beam traverse speed comparison, condition B and D.....	76
Figure 56: No insert, beam traverse speed comparison, condition B and D.....	76
Figure 57: Insert 3N-8B, line speed effect, condition C and E.....	78
Figure 58: Insert 4N-7B, line speed effect, condition C and E.....	78
Figure 59: No insert, line speed effect, condition C and E.....	78

List of Tables

Table 1: Advantages and disadvantages of laser transmission welding [2-4]	2
Table 2: Vibration modes for chemical bonds during infrared radiation exposure [2].....	14
Table 3: Properties of Nylon 6 (30% GF) [34]	26
Table 4: Insert geometry on the moulded parts (Stereographic microscope with oblique lighting).....	31
Table 5: Welding parameters (S denotes commercial grade, S/2 denotes 50-50 mixture of natural and commercial grade).....	35
Table 6: Burst test results.....	43
Table 7: Fracture surfaces A- HG 25.....	49
Table 8: Fracture surfaces B- HG 28.....	50
Table 9: Fracture surfaces C- HG 8 (Welded backwards, L and R - flat area left and right of gate respectively).....	51
Table 10: Fracture samples D- HG34.....	52
Table 11: Fracture surfaces E- HG 2.....	53
Table 12: Fracture surfaces- All.....	54
Table 13: Depth of Penetration of Laser Beam.....	64

List of Equations

Equation 1: Snell's law [2]	14
Equation 2: Lambert Bouger's Law [2].....	15
Equation 3: Temperature distribution for moving heat source [2].....	16

Nomenclature

Abbreviations

ABS	Acrylonitrile butadiene styrene
CAD	Computer aided design
CNC	Computer numerical controlled
DAM	Dry as moulded
GF	Glass fibre filled
HAZ	Heat affected zone
HDPE	High density polyethylene
IR	Infrared radiation
LASER	Light amplification by stimulated emission of radiation
LET	Laser energy transmission
LTW	Laser transmission welding
Nd: YAG	Neodymium: Yttrium-Aluminum-Garnet
PA	Polyamide
PA6, PA46, PA mXD6	Variations of polyamide
PBT	Polybutyleneterephthalate
PC	Polycarbonate
PE	Polyethylene
PMMA	Polymethylmethacrylate
POM	Polyoxymethylene
PP	Polypropylene
PS	Polystyrene
PVC	Polyvinylchloride
UV	Ultraviolet

Symbols

A	Fraction of radiation absorbed
B	Black/absorbing material
CB	Carbon black addition level

I_A	Intensity of light absorbed
I_O	Intensity of radiation
I_R	Intensity of light reflected
I_T	Intensity of light transmitted
LE	Line energy
N	Natural/transparent material
n_a	Refraction index of material a
n_b	Refraction index of material b
P	Power
R	Fraction of radiation reflected
S	Standard commercial addition of carbon black
S	Speed
S/2	50-50 blend of natural and natural & standard commercial addition of carbon black materials
T	Fraction of radiation transmitted
W	Weld line
α	Absorption coefficient
θ_a	Angle of incidence
θ_b	Angle of refraction
θ_i	Initial temperature of the solid
κ	Thermal diffusivity
λ	Thermal conductivity

Chapter 1: Introduction

It is difficult to imagine a world without plastics. Plastics are utilized in automotive components, electronics, consumer goods and medical devices. The use of plastics is continually growing since plastics offer good strength-to-weight ratio, complex part geometries, low cost and an ease of recycling. As the need for plastic components grows, more complex components arise which cannot be manufactured as one piece, instead they need to be joined from two or more components. Joining methods for plastics is an evolving art that continually demands cost effective, environmentally friendly, and efficient processes with a high degree of quality. Joining techniques for plastics are categorized into the following: adhesive joining, mechanical joining/fastening and fusion bonding/welding (only for thermoplastics) [1]. With each method there are advantages and disadvantages. The current study utilizes a fusion bonding/welding technique known as laser transmission welding (LTW).

Laser transmission welding employs one material that is transparent to the laser beam and one that is absorbent. The laser goes through the transparent material and the energy is absorbed and converted to heat, mainly in the absorbent plastic near the interface of the two materials. The absorbent material being heated expands and transfers heat to the transparent material by conduction. The result is a melt pool bridging the interface, producing a weld after freezing. LTW has many advantages as summarized in Table 1 [2-4]. Laser welding of plastics is already utilized in industry for some applications [5, 6], for example electro-pneumatic pumps [7], with many more potential applications such as air intake manifolds, fluid reservoirs and medical devices. Medical devices may

especially benefit from laser welding since micro-welds with no particulates are obtainable.

Table 1: Advantages and disadvantages of laser transmission welding [2-4]

Advantages	Disadvantages
<ul style="list-style-type: none"> - no meltdown distance required - welds are stronger than vibration welds - greater flexibility in design geometry - reduced flash, small heat affected zone (HAZ) - reduction in material usage given proper joint design - aesthetically pleasing (no flash, markings) - possibility of re-welding - one laser welding machine can be reprogrammed to weld parts of differing geometry - no harmful fumes such are present when using adhesives - shock sensitive electric components can be welded - no mechanical stress on the joint components 	<ul style="list-style-type: none"> - no meltdown - continuous contact across faying surface requires tight dimensional control - limited welding thickness - somewhat higher capital cost initially

1.1 Objectives of the Research

The motivation of the present research is to demonstrate the ability of laser welding to overcome the shortfalls associated with other thermal welding techniques. Vibration welding for instance dominates the automotive field, being used for air induction modules, fluid reservoirs, and electrical modules. Linear vibration welding is limited to geometries that can tolerate relative movement in only one direction. Vibrations caused by ultrasonic or vibration welding may affect sensitive electrical components resulting in

the part being discarded. Hot plate welding, utilized for lighting assemblies, can encounter a poor fit when joining and as a result can have high residual stresses. As stated in Table 1 joint design flexibility is an advantage of laser welding. Since there is no relative movement of the components during laser welding, shock sensitive electrical components will not be damaged. These advantages have inspired research towards the further understanding and development of laser welding.

The purpose of the present study is to determine the sensitivity of interfacial gaps in laser transmission welding using various laser welding parameters. It is important to note that the melting of the transparent side of the interface relies mainly on heat conduction from the hotter absorbing side of the joint, since the laser beam energy is mainly absorbed in the non-transparent material. Gaps may be present between adjoining surfaces due to forming defects or warping of the components. If a gap exists between the parts at the faying surface, the weld may not form at that location.

For this study, interfacial gaps created via manufactured voids were moulded into the components to be welded. After welding, the samples were then assessed using microstructural analysis, fracture surface analysis and hydraulic burst testing. The main objective was to experimentally investigate the sensitivity to interfacial gaps in laser transmission welding.

1.2 Thesis Map

Chapter 2 gives an overview of the joining of plastics, including information about lasers, review on the different processes of laser welding, and a brief literature review on experimental and modeling work relating to laser transmission welding as well as optical properties, and process parameters. Included in Chapter 3 is an introduction of manufactured voids, an explanation of the design of the injection moulded specimen, and the type of laser welder used. The experimental approach is detailed in Chapter 4 along with an explanation of each assessment method. The experimental results for each assessment method: burst test analysis, fracture surface analysis and microstructural analysis are presented, analyzed and discussed in Chapters 5, 6 and 7, respectively. Chapter 8 includes discussion and interpretation of the results. Chapter 9 provides conclusions and recommendations for future work. Finally Appendix I and II includes the images and data generated for this research.

Chapter 2: Plastic Joining and Laser Transmission Welding

The intention of this chapter is to review scientific and technical documentation and interpretation in previous research on plastic joining, mainly centered on thermal plastic welding processes.

Thermoplastics have an advantage over other materials in that they may be formed to near net shape through fewer operations. Provided with the proper design of the mould, close tolerances can be held on plastics eliminating the need for post mould machining (excluding the specialized machining required for some joining purposes). Given that plastics have low cycle times enables high production. Colorants added to the plastic resin before moulding eliminate the need for painting and drying required by most other materials. Common operations used for producing thermoplastics include injection moulding, extrusion, blow moulding, compression moulding, thermoforming and variations of each [8].

Thermoplastic components often need to be assembled from two or more components for example due to the complexity of the part. For closed-hollow components made by injection moulding this is always true. Welding processes may also be necessary when aesthetics require varying colors and textures, or because of the size of part. Originally categorized by Stokes [1], joining of plastics may be completed using chemical techniques such as adhesives (mainly used for thermosets), mechanical technologies such as snap fits and fasteners, or thermal techniques such as welding (only for

thermoplastics). The current research uses hollow thermoplastic components joined by laser transmission welding.

2.1 Various Welding Techniques (Thermal, Friction, Electromagnetic)

The welding of the thermoplastic materials involves heating the interfaces to be welded until they have been melted or softened, followed by, or combined with pressing them together which induces intermolecular diffusion of the adjoining surfaces to create the weld. Therefore, the fundamental steps for welding thermoplastics include surface preparation, heating, pressing, intermolecular diffusion and cooling. Welding of thermoplastics is categorized by the heating method used; thermal, frictional/mechanical, or electromagnetic [2].

During thermal welding, heating relies on convection, conduction and/or radiation to heat the weld surface. Examples of thermal welding techniques for thermoplastics that use external heating are hot tool welding, hot gas welding, extrusion welding, implant induction welding, and resistive implant welding.

Frictional/mechanical welding relies on the conversion of mechanical energy into heat via surface friction or intermolecular friction. Examples of frictional/mechanical welding are ultrasonic welding and friction/vibration welding.

Electromagnetic welding relies on the absorption and conversion of electromagnetic radiation into heat. Examples of electromagnetic welding are radio frequency welding, infrared/laser welding and microwave welding.

2.2 Lasers - An Overview

The word laser is an acronym meaning **L**ight **A**mplification by **S**timulated **E**mission of **R**adiation. The basis of the LASER was originally concluded by Einstein; excited species (atoms, ions and molecules) could be stimulated to emit a photon by the arrival of another photon [9]. The generation of the laser light is due to the near-simultaneous transitions between the high and low energy states in species in various mediums. The electromagnetic spectrum shown in Figure 1 is the continuous range over which radiation can be produced with wavelength ranging from 10^{-7} nm to 10^{14} nm. The light produced by lasers has unique properties in that it is monochromatic, coherent, has low divergence and high brightness [9].

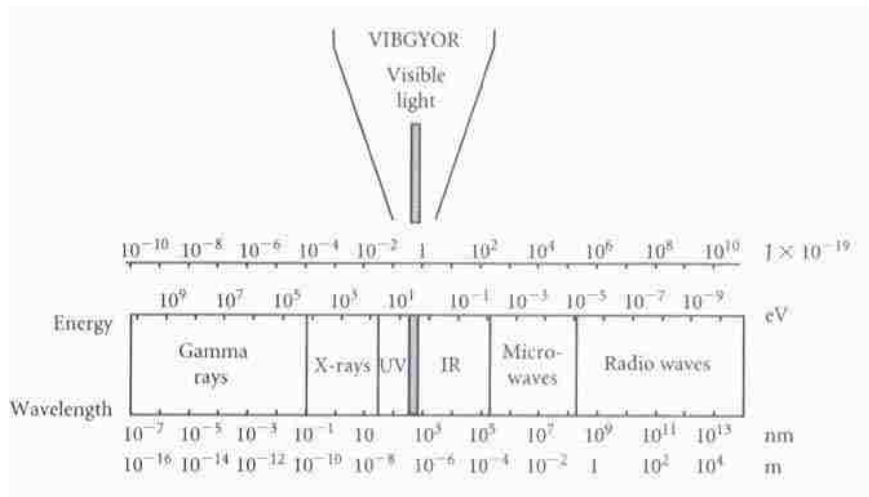


Figure 1: The electromagnetic spectrum (UV-ultraviolet, IR- infrared) [9]

Lasers have proven to be a flexible tool in industrial applications producing a beam of light with unique properties, high accuracy control, a small spot size, and being an intense source of energy. Lasers in manufacturing can be used for welding, cutting, drilling, surface hardening, and marking of various materials including plastics [9]. The

type of laser, active medium and parameters vary depending on the material and application. Examples of laser parameters include wavelength, power, energy and mode (pulse or continuous). The active medium can be gas, liquid or solid; Figure 2 gives a summary of the types of lasers for each category and Figure 3 shows various commercial lasers used in material processing, measurement and/or communication. Also shown is the average power versus the wavelength for each laser.

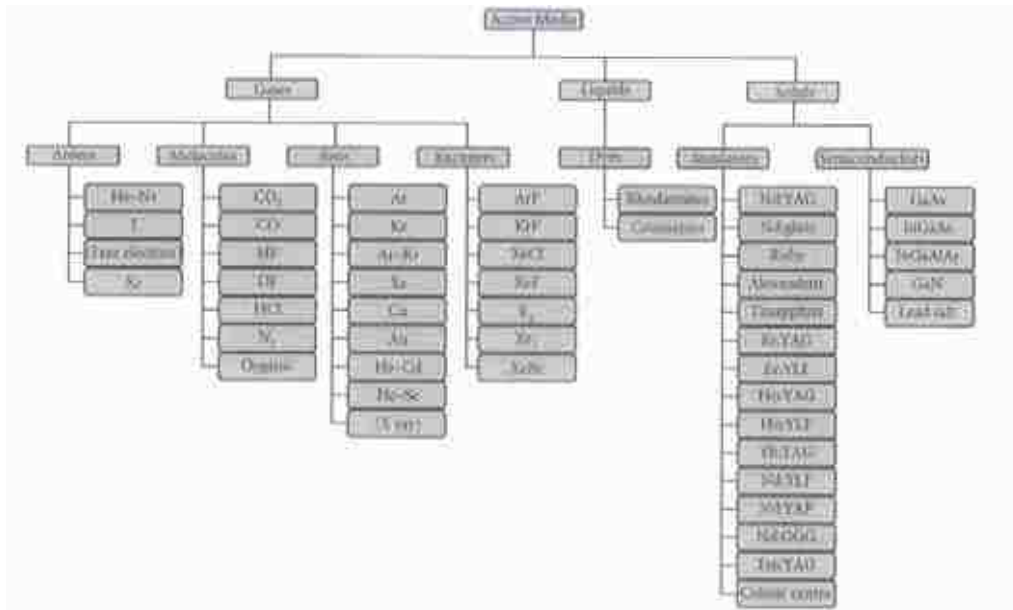


Figure 2: Laser types used in material process categorized by the type of active medium [9]

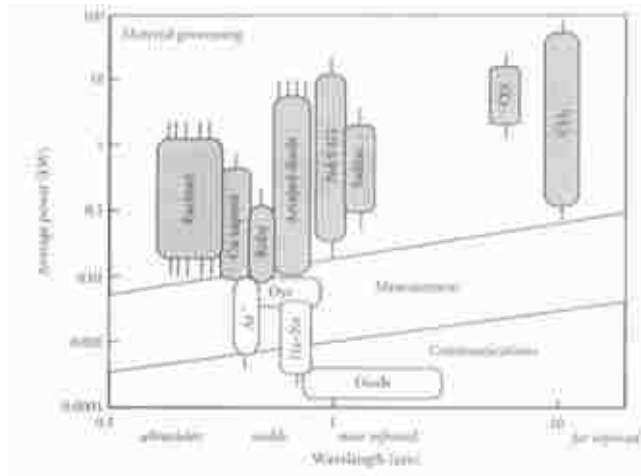


Figure 3: Average power vs. wavelength for commercial lasers [9]

A laser device works by light radiation being emitted from the transitions between energy levels in the lasing medium. For common incandescent white light radiation, electrons in the conduction band are excited, thus putting them in a metastable state. White light radiation is emitted in all directions with a wide range of frequencies when the electrons decay back to their stable state. Laser light radiation is different since it uses the process of stimulated emission whereby a photon collides with the lasing material to release additional photons. The processes of spontaneous emission, stimulated emission and absorption are illustrated in Figure 4. The photons emitted for laser light radiation have the same polarization, frequency and phase (temporal and spatial). This is the reason laser light has its unique properties (monochromatic, coherent, low divergence and high brightness).

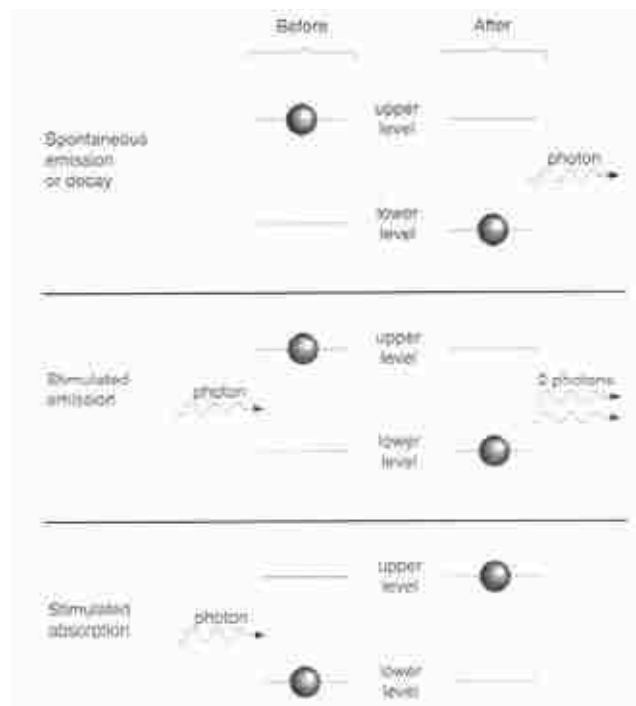


Figure 4: Radiation processes associated with the interaction of light with matter spontaneous emission, stimulated emission and absorption [10]

The laser device also amplifies the light as the stimulated emissions of radiation are internally reflected between mirrors on either side of the lasing medium. Figure 5 illustrates the photons traveling between two mirrors. The output mirror is only partially reflective, thus allowing the amplified light beam to be emitted from the laser.

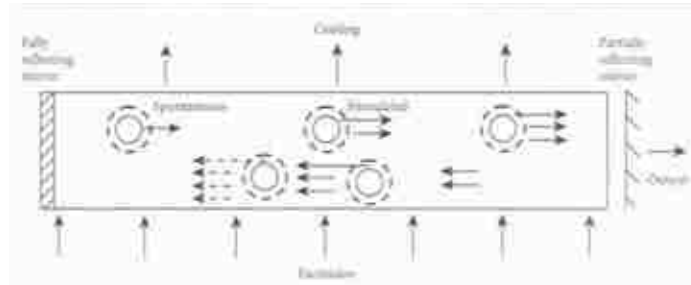


Figure 5: Amplification of light by stimulated emission of radiation [9]

2.3 Process Review- Plastics Welding with Lasers

Infrared (IR) and laser welding is a technique that utilizes energy from lasers and laser diodes to heat the joining materials. There are three basic techniques utilized for infrared/laser welding of plastics; i) surface heating, ii) IR/laser transmission welding and iii) IR/laser staking.

2.3.1 Surface Heating

Surface heating process is similar to hot plate welding in that the surfaces to be joined are heated directly by the IR/laser to produce a molten layer. The surfaces are then pressed together and allowed to cool, thus producing a weld; refer to Figure 6 for a schematic of this process.

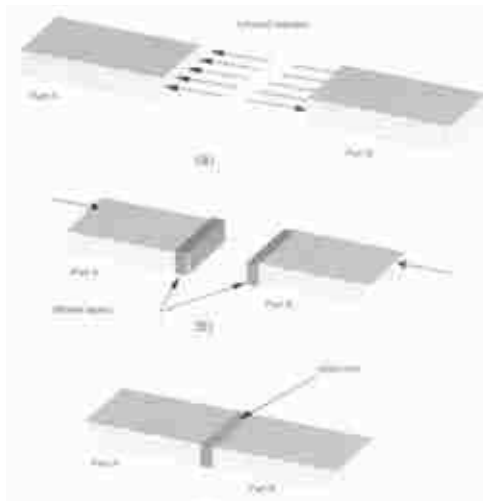


Figure 6: Surface heating using IR/laser welding [2]

2.3.2 Infrared/Laser Transmission Welding

Infrared/laser transmission welding employs one material that is transparent to the laser beam and one that is absorbent. The laser goes through the transparent material and the energy is absorbed and converted to heat, mainly near the interface of the two materials. The absorbent material being heated expands and transfers heat to the transparent material by conduction. The result is a melt pool bridging the interface, producing a weld, see Figure 7.

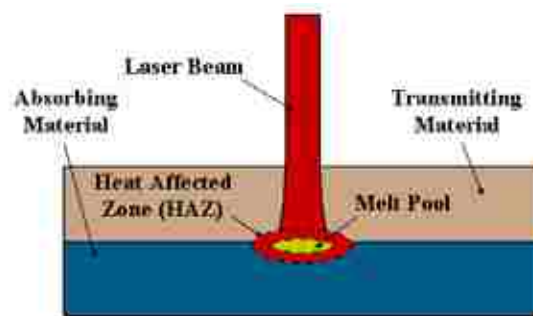


Figure 7: Infrared/laser transmission welding (LTW)

2.3.3 Infrared/Laser Staking

Similar to other staking techniques (ultrasonic and hot air cold staking), staking is used for joining materials that cannot be welded, such as a metal component to thermoplastic component. The laser beam heats the post and a forming head forms the post to a desired shape, joining the components.

2.3.4 Heating Using Transmitted Radiation

Infrared radiation can be supplied to the joining surface by three main methods, scanning/contour, continuous illumination, or mask welding [2]. During scanning the IR source is translated across the faying surface, Figure 8 (a). This process is easily programmable for welding various components. Continuous illumination uses the IR source to illuminate the entire faying surface to be welded by simultaneous or quasi-simultaneous methods, Figure 8 (c) and (d) respectively. Mask welding, Figure 8 (b), is similar to illumination except that a mask is used to block sections of the parts from the IR source. This method is highly suitable for complex and micro-structured areas.

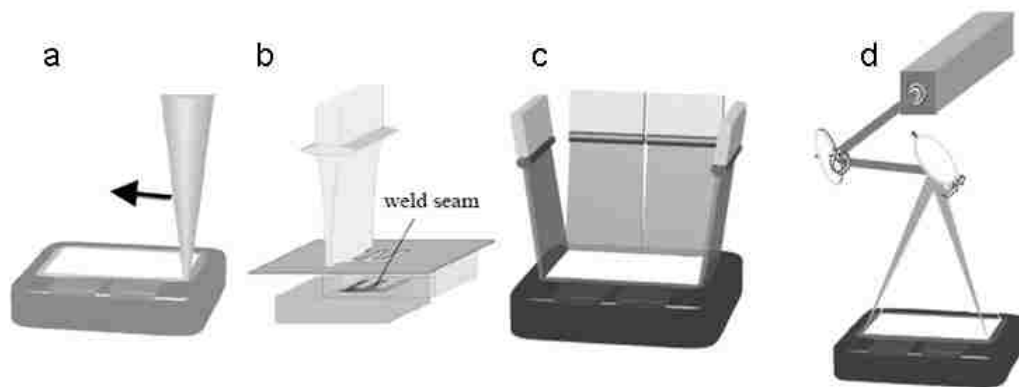


Figure 8: Methods of delivery of the laser beam to the joint interface: a) contour welding, b) mask welding, c) simultaneous welding (form of continuous illumination), d) quasi-simultaneous welding (form of continuous illumination) [11]

The electromagnetic radiation from the IR source interacts with the polymer whereby a fraction is reflected (R), a fraction is transmitted (T) and a fraction is absorbed (A) giving $100\% = R + T + A$, (Figure 9). $R = 100\% \frac{I_R}{I_O}$, $T = 100\% \frac{I_T}{I_O}$, $A = 100\% \frac{I_A}{I_O}$ where I_O is the intensity of the incident radiation, I_R is the intensity of light reflected. I_T is the intensity of light transmitted, and I_A is the intensity of light absorbed.

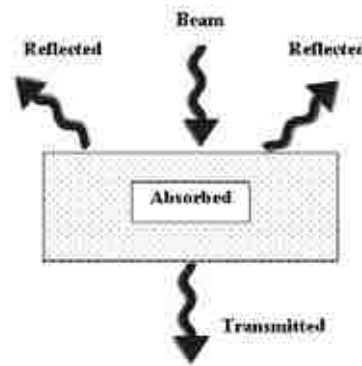
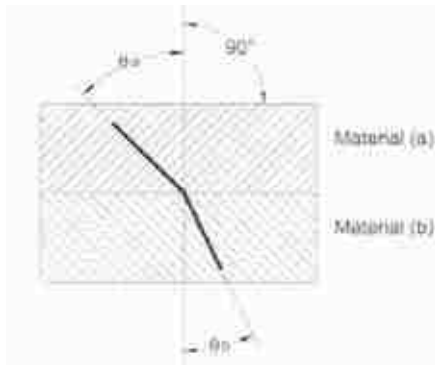


Figure 9: Interaction of radiation from laser beam with plastic, reflection, transmission and absorption

Most plastics do not reflect much light, therefore the fraction of reflection is typically low (between 2-8%), giving absorption and transmission the greater influence on the laser transmission welding process.

Transmission of the light/radiation is complex due to the refraction of light when traveling through two materials of differing indexes of refraction, see Figure 10. The amount of refraction can be determined by Snell's law, Equation 1 where n_a and n_b is the refraction index of material a and b respectively.

Figure 10: Refraction of light through two materials with differing index of refraction [2]



Equation 1: Snell's law [2]

$$\frac{\sin \theta_a}{\sin \theta_b} = \frac{n_a}{n_b}$$

For pure, unfilled polymeric materials the chemical structure defines the amount of light that can be transmitted and absorbed. When incident light encounters the polymer, the resonant absorption of infrared radiation excites the molecular bonds which then vibrate in particular modes. Table 2 gives summary of wavelengths at which common chemical bonds vibrate and the mode of vibration. The vibration of the molecular bond dissipates heat which raises the temperature of the material promoting melting.

Table 2: Vibration modes for chemical bonds during infrared radiation exposure [2]

Bond	Group	Mode	λ (μm)
C-H	CH_2 , CH_3	Stretching	3.3-3.4
C-H	$=\text{C}-\text{H}$	Stretching	3.0
C-H	$-\text{CH}_2-$	Bending	6.8
O=C	$>\text{C}=\text{O}$	Stretching	5.4-5.9
O-H	$-\text{O}-\text{H}$	Stretching	2.7-2.8

For transmission laser welding processes, the laser frequency is chosen to avoid having a wavelength near the main bonds' natural vibration frequencies. So the laser wavelengths are selected to be at infrared (IR) wavelengths with relatively high transmissibility.

Scattering may also occur, especially with crystalline materials, since each phase will refract and scatter the light/radiation. Additives, like glass fibres or mineral flour may cause absorption. Therefore during laser transmission welding, the thicker the sample the more energy is needed since more scatter will occur, decreasing the energy reaching the faying surface. The amount of scatter or the decrease in intensity due to absorption can be determined from Equation 2, Lambert Bouger's Law, where I_t is the intensity of light, α is the absorption coefficient, t is the thickness, and I_o is the intensity of radiation. This simple exponential equation is material dependent since the absorption coefficient is dependent on quality, color and additives present in the material such as glass fibres, talc, and/or inorganic dies.

Equation 2: Lambert Bouger's Law [2]

$$I_t = I_o e^{-\alpha t}$$

The light absorbed is dependent on the material chemical structure, crystallinity and type and quantity of additives. Note that the "transparent" material should absorb minimal radiation whereas the "absorbent" material should absorb nearly 100% of the radiation near the surface. Crystallinity affects the light absorbed since with higher crystallinity there is more scatter of the IR radiation thus producing more vibrations of the chemical bonds. Additives such as carbon black are beneficial in the absorbent material since it effectively acts as a blackbody, absorbing almost all wavelengths. Relatively low carbon black levels are needed to absorb nearly 100% of IR radiation. For example 0.03 wt% is needed for nearly 100% absorption within a depth of 0.5mm, and only 0.07 wt% for a nearly 100% absorption within a depth of 0.25mm [2].

Considering the case for contour welding, the heat source is concentrated to a small region and this source travels along the faying surface. Assuming point-source heating, moving at a constant velocity, for a semi-infinite material, Equation 3 along with Figure 11 can be utilized to determine the temperature distribution.

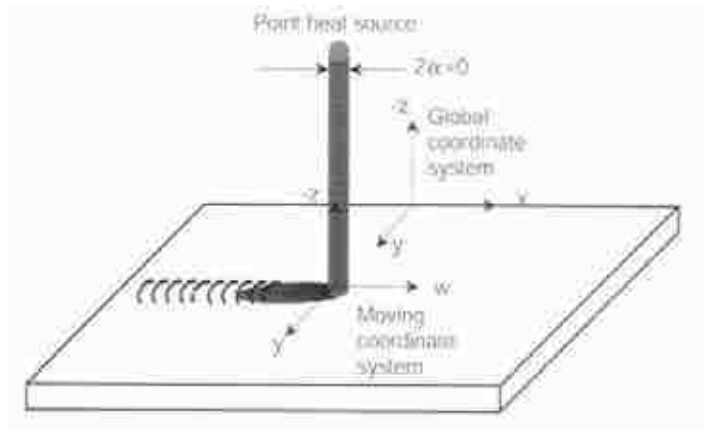


Figure 11: Moving heat source (Scan welding) [2]

Equation 3: Temperature distribution for moving heat source [2]

$$\theta(t) = \theta_i + \frac{P}{2\pi\lambda r(t)} \exp\left(\frac{-v}{2\kappa}(w(t) + r(t))\right)$$

Where: $w(t) = x - vt$, $r(t) = \sqrt{w(t)^2 + y^2 + z^2}$, v is the velocity, P is the power, $\theta(t)$ is the temperature, t is time, θ_i is the initial temperature of the solid, λ is the thermal conductivity, κ is the thermal diffusivity.

Infrared/laser welding is a flexible welding process which can reduce flash and eliminate meltdown distance (which is needed for other welding techniques such as ultrasonic welding), thus providing an aesthetically pleasing component. The disadvantages of

IR/laser welding are the need for continuous contact requiring tight dimensional control and the limitation on the thickness of material for the transparent component in laser transmission welding.

2.4 Porosity/Voids in Polymers

In the laser welding carried out for this thesis, a surprising level of voids was observed at and near the faying surface in the welded parts. It is therefore convenient to provide the reader with a review of the characteristics and sources of some types of voids in polymers.

Voids in polymers can be attributed to any of a number of reasons; non-uniform shrinkage to volatile vapours to degradation of the polymer. A list of some causes of voids in polymers is summarized below. Moisture is the most common cause of voids in polymers due to the hygroscopic nature of some polymer materials or of their additives [12].

Causes of voids in polymers [12]

- Poor filling of cavity during injection moulding
- Depolymerization of the polymer to produce volatiles (e.g. PS, POM, PMMA)
- Degradation of the polymer to produce volatiles (e.g. PVC)
- Water vapour evolved from moist resin during processing
- Evolution of water from dehydration of pigments during processing
- Entrapped humid air during manufacture (especially in composites)
- Excessive volume contraction of the polymer during cooling (shrinkage)
- *In situ* water evolution during polymerization
- Air encapsulation during moulding
- Non-optimum processing conditions (e.g. During injection- and rotomoulding)
- Carbon dioxide produced during polymerization (e.g. polyurethanes)

Welding of polymers needs to be strictly controlled to prevent the formation of voids/porosity at or near the welded region. The material may undergo degradation due to

high temperatures resulting in void formation. Figure 12 is an example of PVC welded by hot-gas welding. The temperature was too high, thus allowing for degradation and void formation.

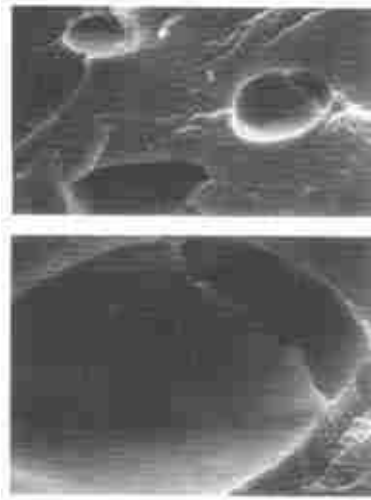


Figure 12: Voids present in PVC that has been hot-gas welded. The ellipsoidal shape of the voids is due to the deformation of the material by the pressure applied during welding [12]

Microstructural analysis of the voids can assist in determining the causes of the voids. Figure 13 is a tree diagram illustrating the characterization of voids based on their appearance.

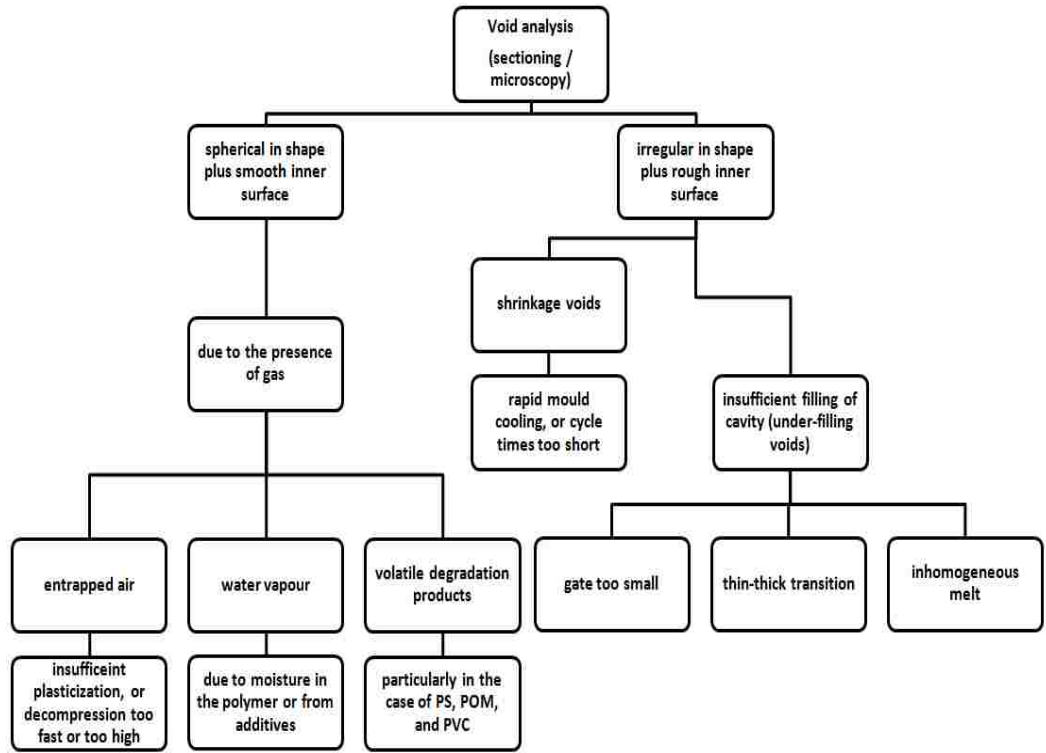


Figure 13: Tree diagram illustrating the characterization of voids based on their appearance [12]

2.5 Laser Transmission Welding – Literature Review

The mid 1980's to the early 1990's was the gestation period of interest and studies into the joining of plastics using lasers. The motives included the relatively low cost of lasers and laser diodes and their fixturing, and the increase demand for part quality [2]. Patents [13] and processes emerged adapting existing joining methods for laser welding purposes. Adapting the process of non-contact hot plate welding by modifying the heating phase, simple butt joints were utilized to determine the feasibility, and flexibility of the laser welding process.

Some original studies using simple contact butt joints set out to determine the effects of process parameter such as laser power, welding time and clamping pressure [14, 15]. Ou et al [14] observed weld strengths approaching those of the bulk material while welding

butt joints of high-density polyethylene (HDPE) and polypropylene (PP) using a CO₂ laser.

Studies utilizing laser transmission welding and specifically contour laser welding began in the late 1990's with respect to the physics of the process. Grimm [16] describes the process of through transmission laser welding and observed the effects of weld force and welding rates on the strength of the weld. Good weld strengths and aesthetics were obtained when welding PMMA to PC.

Kagan et al. [3, 4, 17-20] utilized laser transmission welding on different materials mainly studying nylons. His studies on the optical properties [18] of nylons included the effects of fillers, modifiers, reinforcing agents and pigments. These studies show a decrease in the laser transmission with the increase of glass fibre content. This decrease is attributed to the increase in light scattering due to the glass fibres. The addition of mineral fillers dramatically reduces the laser transmission which was attributed to the particle size differences and possibly the refractive index. It was also shown that very low levels of carbon black was needed (0.03-0.07 wt %) to obtain very low transmission values (<0.3%). Kocheny, with Kagan and Macur [20] studied the effects of moisture for laser transmission welding using nylon 6, filled and unfilled. The moisture content was varied between dry-as-moulded (DAM) and 7.5 wt%. Shear strengths equal or near to frictional and hot plate welding joint strengths were obtained under optimized welding conditions. It was concluded that moisture up to 4 wt% does not have a significant effect for through transmission laser welding of nylon 6. Kagan and Pinho [19], compared the

tensile strengths of T-type butt joints of nylons welded via frictional vibration welding or transmission laser welding. Results show laser transmission welding as a viable alternative joining method demonstrating tensile strengths equal or near to frictional vibration tensile strengths.

Optical properties of the materials are especially important for laser transmission welding. Grimm and Yeh [21] studied the transmission of coloured acrylonitrile-butadiene-styrene (ABS) and polyethylene (PE) with varying levels of carbon black. It was seen that heating primarily by surface absorption was obtained at carbon black level in excess of 0.03 wt%.

Vegte et al. [22] studied optical requirements and physical aspects of the welded interface. Materials studied included PC, PA6, PA46 and PBT, unfilled and filled with various reinforcing agents, mineral filler, stabilizers etc. Agreeing with previous studies glass fibre content, fillers and crystallinity reduces transmission of laser light.

In some cases optical properties can interfere with part aesthetics. The challenge lies with creating an assembly for laser welding one color visually but with components having different optical properties in the infrared region (being that one component is transparent while the other is opaque to the infrared radiation). The result for PA6 30%GF by Vegte et al. [22], is an absorbing side that contains carbon black, rendering the component black in the visible spectrum region and opaque in the infrared region. The transparent

component has pigments such that the material is black in the visible spectrum and transmissive in the near infrared region this is shown in Figure 14.

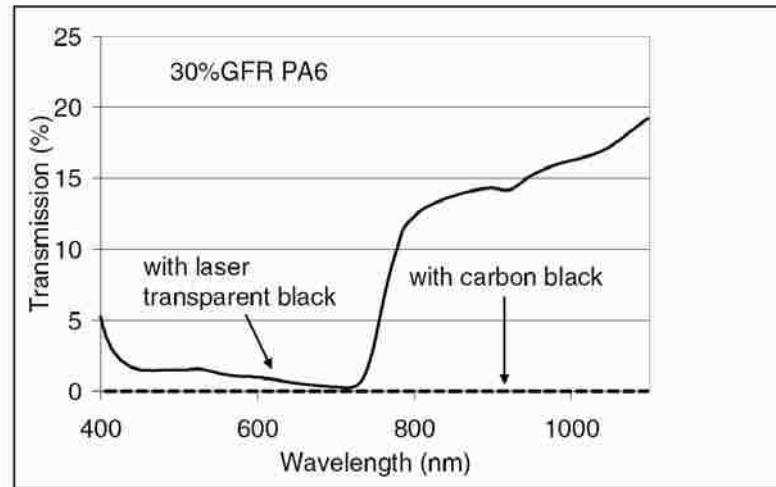


Figure 14: Transmission spectra for 30% GF PA6 [22]

Clearweld[®] is TWI's solution to manufacture aesthetically pleasing assemblies without the use of carbon black [9]. Clearweld[®] utilizes a visually colorless infrared absorbing medium between the adjoining parts (either painted/printed on one side, or as a film between the parts or encompassed in the bulk material). The welds produced are nearly invisible, making it well suited for clear products and also viable for coloured products.

Wang, Bates and Zak [23] studied the transmittance and reflectance of polypropylene (PP), polyamide 6 (PA6), and polycarbonate (PC) with different surface roughness, thickness and glass fibre content. It was shown that reflectance increases with increasing thickness of the sample for PA6, while transmittance decreases. The transmittance also decreases with the increase of glass fibre content. Lee and Ballou [24] studied laser

energy transmission (LET) measurements using nylon 6 with 30%GF. It was determined that local sample thickness can significantly affect the accuracy of measurement of LET. Also the exposure time varied the laser transmittance rate especially with thinner parts. It was recommended for industry wide standard procedure for measuring the LET.

2.5.1 Previous Measurements of Gap Bridging and Factors Affecting Transmission Laser Welding Tensile Strengths

Bates, Chen et al, have done many studies on the through transmission laser welding of plastics [25-27]. Especially relevant to Chen's present thesis was gap bridging studies wherein it was found that the weld strength decreases as the gap between adjoining parts increases. The gaps were provided by putting shims between the opposite ends of small plates. The laser beams were then passed across the plates, and when the molten zone on the lower absorbent material swelled enough to make contact with the transparent upper plate, welds were sometimes formed. Higher laser powers were needed to achieve maximum strengths for larger gaps since more material needed to be in the melt pool to bridge the gap. They found that increasing the power further resulted in higher temperatures and thus could eventually lead to polymer degradation. Also evaluated by this group were the influences of line energy, glass fibre content and part thickness using shear lap test samples of PA mXD6, again with shims between the samples being welded. For glass fibre contents of 0-60 wt% and part thicknesses of 0.5-2 mm, shear strengths comparable to the base material were measured. Maximum bridgeable gaps were found to be ~0.17 mm, and ~0.07 mm for carbon black contents of 0.025 wt%, and 1 wt%, respectively. Also, it is suggested that line energy can be used to correlate data for the

laser transmission welding material and speeds used in their studies, and possibly for other materials and parameters. Work was done by Prabhakaran, Bates and Baylis [28], using modified T-weld samples of nylon 6 welded with a diode laser, to investigate the effects of various welding parameters on the weld strength. The minimum line energy needed to generate meltdown was estimated to be between 2 and 3 J/mm.

Al-Wohhoush and Kamal [29] examined the joint tensile strength and the microstructure of samples of PC, PA-6 and PA-6 30%GF, laser welded by Bates group. These studies showed micro-flow and some fibre reorientation in the laser affected zone. It was suggested the weaker joints at high laser power could be attributed to the reduction of crystallinity and the fibre re-orientation.

Haberstroh and Luetzeter [30, 31] used PBT to study the effects of injection moulding parameters on the quality of LTW. It was found that optical properties vary, resulting in more or less transmission of laser light due to changes in mould and melt temperature as well as the injection speed. Furthermore, variation in the injection moulding parameters affected the crystalline zones and hence spherulite diameters creating either fine spherulite zones with high laser light transmission or coarse spherulite zones with lower transmittance. The lower transmittance is due to reflection and scattering at the interfaces with the crystalline areas. Therefore, it was recommended that any changes in the injection moulding parameters be relayed to the weld operator, so that modification to the laser transmission welding parameters can be made.

Laser welding of polymers produces high quality welds for a variety of material combinations, in some cases achieving weld strengths comparable to the bulk material. Laser welding has found a place in the industry reducing cost, improving quality and reducing environmental impact. There are many applications where laser welding is utilized and many more potential applications [5-7, 32].

2.6 Material Background- Nylons (Polyamides)

Nylon is the generic name for the thermoplastic family of polyamides (PA). The main-chain of polyamides/nylons consists of a repeating amide group shown in Figure 15. Although nylons are structurally related, each nylon is distinct, having significant differences in properties and processing behaviours.



Figure 15: Amide group [33]

Nylon's superior properties are due to the hydrogen bonding between molecular chains, and the flexibility of the carbon chains [33]. Nylons have low frictional properties, low melt viscosity, good toughness, good chemical resistance, good abrasion resistance, and at elevated temperatures offer superior load-bearing capability. Nylons and glass reinforced nylons are used in many applications including air intake manifolds, engine fan blades, un-lubricated gears, bearings, as well as fluid reservoirs.

Nylon 6 (PA6) is in the group of polyamides that is a melt-processable thermoplastic. The 6 in the name refers to the number of carbon atoms in the Caprolactam ring. Nylon 6 is produced by ring-opening polymerization, as per Figure 16. Caprolactam is heated at 533K in an inert atmosphere of nitrogen, where the ring breaks and undergoes polymerization.

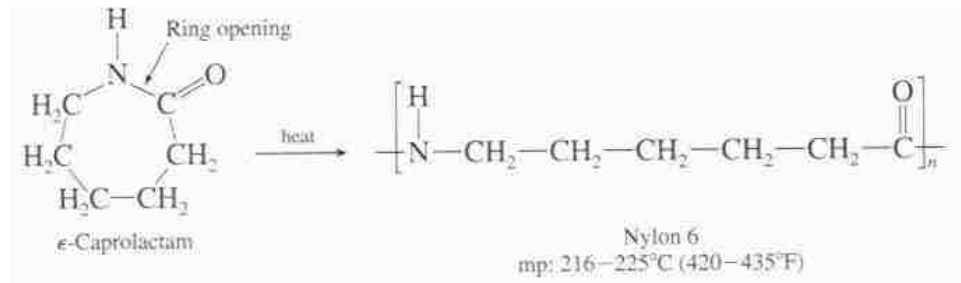


Figure 16: Ring-opening polymerization of nylon 6 [33]

A sometimes detrimental property of nylon 6 is that it is hygroscopic, that is to say nylon 6 will readily absorb moisture. The absorption of water molecules enables chain scission, thus breaking the polymer chains, reducing the strength and stiffness and increasing the flexibility and resilience. Care must be taken to dry nylon 6 before any melt processing.

Table 3: Properties of Nylon 6 (30% GF) [34]

Property	SI units	Imperial units
Density	1350-1420 kg/m ³	0.022-0.023 kg/in ³
Melting Temperature	228°C (440°F)	
Specific heat capacity	16-80 (10 ⁶ K)	
Tensile strength at break	165 MPa	24 ksi
Tensile modulus	8.62-10.0 GPa	1.25-1.45 (10 ⁶ psi)

Table 3 above gives some of the basic properties of nylon 6 (30% glass fibre or GF).

In the present thesis studies, nylon 6 with 30% GF is used with three concentrations of carbon black. The transparent material component (natural, denoted as N in this thesis) has no carbon black added. The material components that are opaque to the laser are black and denoted B in this thesis. There are two concentrations of carbon black. The first has the natural material with its standard commercial addition of carbon black as-commercially supplied by DSM, denoted S in this thesis. The second is a 50-50 blend of natural, and the natural plus carbon black materials (50% N + 50% S) this concentration is denoted S/2. The latter material allows some investigation in how gap bridging is affected by the carbon black level in the opaque component.

Chapter 3: The Creation, Characterization and Welding of

Manufactured Voids

3.1 The Concept of Manufactured Voids

The work [25-27] of the Bates group at Queen's University Kingston used shim plate spacers to create gaps between plates to be welded. They measured the values of welding parameters required to create the gap-bridging welds. In their study the gaps were essentially unbounded parallel to the plate surfaces. These conditions usefully represent severe warping conditions in the faying surface, but do not represent localized bounded dimples, divots, sink marks or gouges that may be present on the faying surfaces. For this reason, the manufactured void method was invented to create reproducible sets of voids on the faying surfaces of the flanges of hemispheric parts, previously used by Siemens/Mahle to test polymer weld joint geometries. The mould has a removable ring insert which can be modified to change the details of geometry of the faying surfaces on the flanges of the plastic parts. In the present variation, ten sub-inserts were fitted into the removable flange ring. Each sub-insert had a groove machined into it, and along the base of the groove were small plateaus, 50 to 150 microns in height which would create the voids on the flange surfaces of the injection moulded parts.

From previous studies [35] of laser welding shear lap samples, it was found that the weld puddle travelling along with the laser beam had a high pressure within it. The evidence was that when the beam reached the final edge of the sample a tongue of plastic was ejected out from the faying surface. This led to restating the gap problem from the Bates

study of bridging a gap, to one of a high pressure fluid flooding into an enclosed void on the faying surface. From this point of view, the question becomes one of whether different shapes of voids would fill differently, and would the loss of pressure measurably affect the overall weld strength.

The primary removable ring insert, shown in Figure 17 left has ten sub-inserts, each with 1 to 16 voids, arranged around the ring on this flange. CAD drawings of the moulded parts are shown in Figure 18 showing the gate location and the positions of the sub-inserts. Figure 17 right, is a photograph, lighted with highly oblique conditions, of one of the sub-inserts showing the groove and plateaus that will create the raised ring and voids.

Both the transparent specimens and the absorbent specimens are moulded using the same ring and sub-inserts, so that when they were fitted together, with the gates aligned for welding, sub-insert 1 on the transparent material is superimposed over sub-insert 10 on the opaque material. The void pattern on sub-insert one is matched to that of sub-insert 10, but they have different void depths. Similarly the arrowheads on sub-inserts 4 and 7 point in opposite directions on the mould so that they will match when fitted together. In total there are 66 voids on the moulded parts.

The differences in void depth between the matching sub-inserts allow twice as many voids to be produced by rotating the gates 15° from being aligned. That places the transparent moulded sub-inserts against the flat flange sections on the absorbent side. These voids would be shallower. This option proved to be unnecessary.

The void geometry was designed using CAD software. The void groove and plateaus, typically 50-200 μ m high were machined using a Militronic CNC machining center and very sharp carbide end mills.

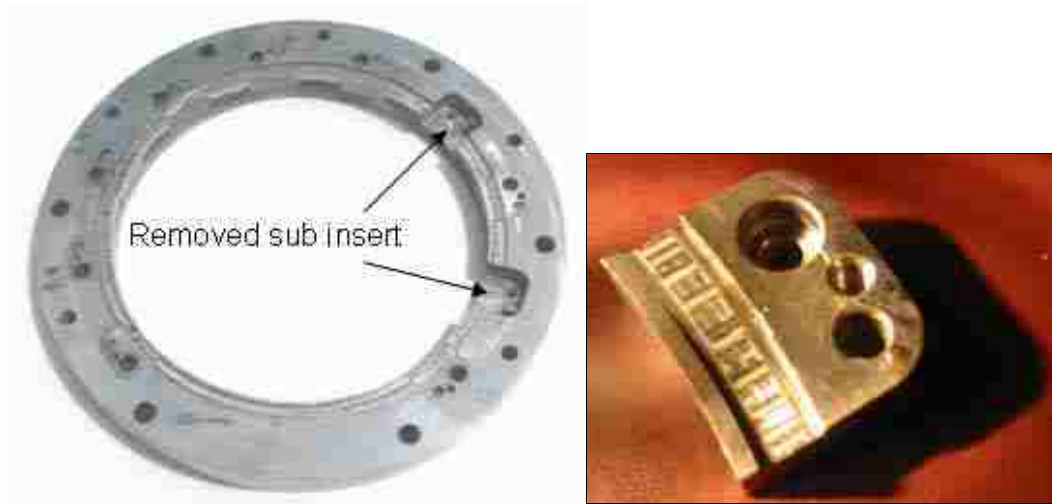


Figure 17: Left: Removable ring for Mahle injection mould for hemispherical parts. Right: Sub insert from removable ring insert for injection mould

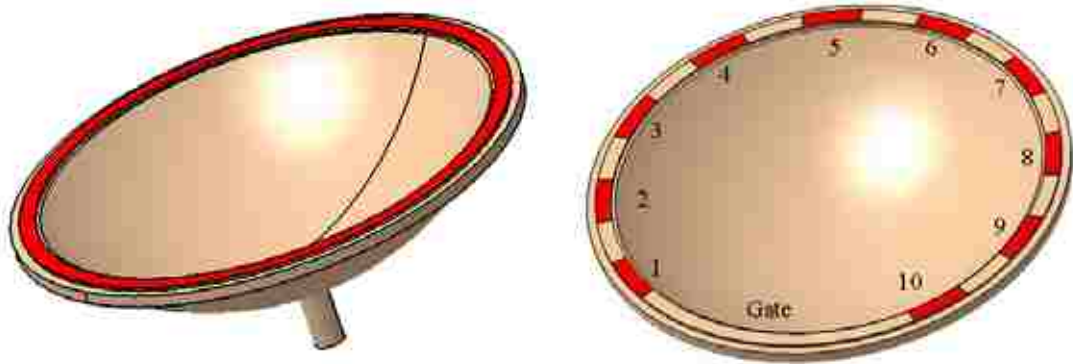


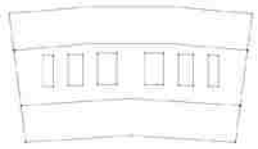














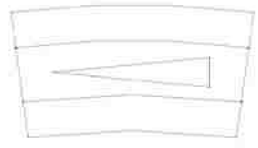


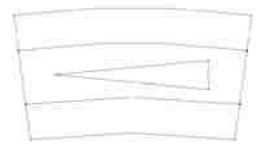

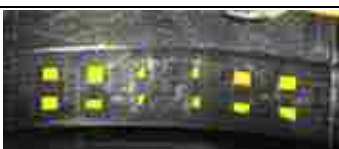
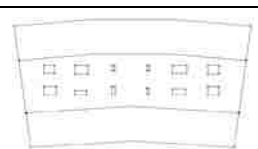

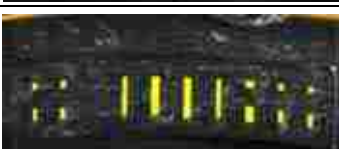


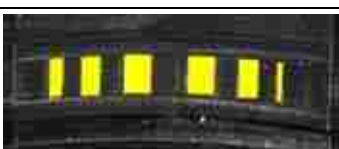



Figure 18: Left - Flange where reproducible voids are present on hemispherical component. Right - Each sub insert is labelled 1 through 10.

The geometry of the voids present in each insert is summarized in Table 4. The images shown are from the moulded parts not the sub-inserts of the mould.

Table 4: Insert geometry on the moulded parts (Stereographic microscope with oblique lighting)

#	Moulded Insert Area	Highlighted	Schematic
1			
2			
3			
4			
5			
6			
7			
8			
9			
10			

3.2 Moulding the Parts, and Characterization of the Voids

The moulding of the parts was completed using a 400 Ton Cincinnati injection moulding machine at the Mahle facility in Windsor. The material used is 30%, glass fibre filled nylon 6, which was provided by DSM. The absorbing material had the common standard commercial addition level of carbon black, but other parts were made that had a 50-50 mixture of the natural and the standard commercial carbon black level to give a reduced absorption coefficient. Once a stable moulding condition was reached, providing good definition of the void surfaces, then all the parts were moulded at that condition. It is important to note that the thickness of the ring flange material (neglecting the voids) penetrated with the laser is 4.4 mm.

3.2.1 Characterization of the Voids

A topographical image of each void after moulding but before welding was prepared using an optical profilometer with sub-micron resolution. These images allow for comparison of the geometry (especially the profile and the depth) of the voids before and after welding. An example of the optical profilometer micrographs is shown in Figure 19, the remaining images can be found in Appendix I.

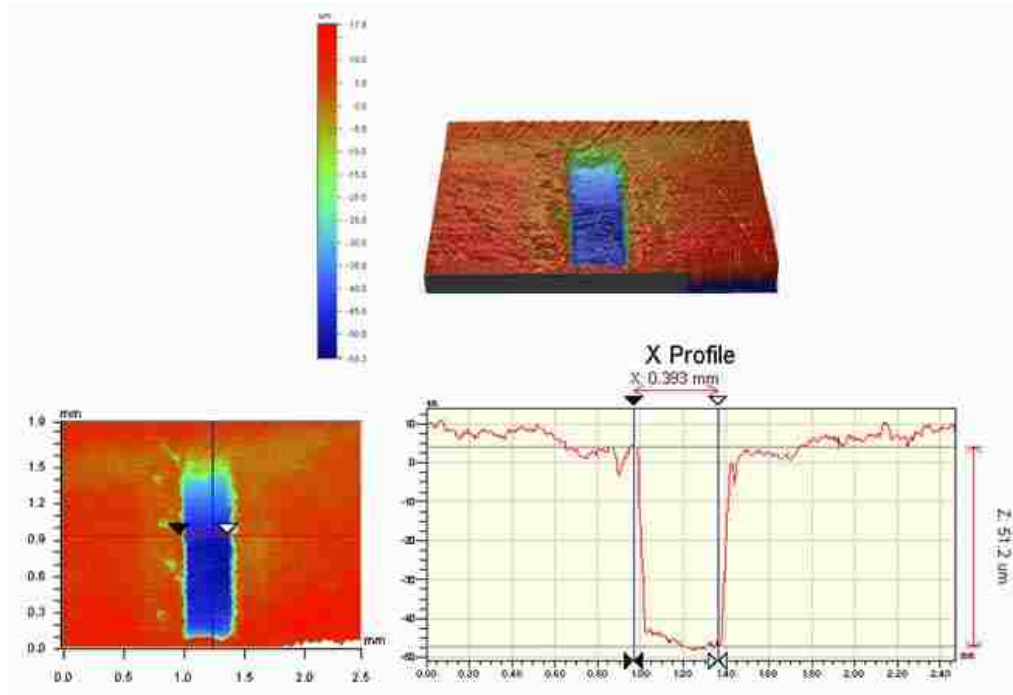


Figure 19: Topographical image of manufactured void showing profile and depth

3.3 Laser Welding of the Parts

The laser welder used for the current studies was a Nd:YAG laser. The wavelength of the laser is 1064 nm. The laser is located at Fraunhofer Center for Laser Technology in Plymouth Michigan. Figure 20 shows the experimental setup for laser welding. Noting that the specimen being welded has circular symmetry, a rotating table was used instead of programming the laser to translate around the circumference of the specimen. Therefore the robotic arm, once in position above the specimen need not move during the welding. Also the rotating table could also be easily programmed to rotate at different speeds. The working distance (distance from the laser output to the specimen surface) was set at 269mm. The specimen was clamped in the specimen holder to prevent movement of the parts during rotation. The toggle clamps are positioned between the inserts since the clamp handle shadow prevents the laser from reaching the part.

Therefore the areas shadowed by the clamps are not welded, and the areas occupied by the inserts are welded.



Figure 20: Equipment setup for the Nd:YAG laser at Fraunhofer Center for Laser Technology

A summary of the welding parameters used for these studies can be found in Table 5. The parameters were chosen so as to easily compare welding parameters; Settings A-B compares laser power, A-C compares amount of carbon black addition level, B-D compares the beam transverse speed, and C-E compares line speed effect at constant line energy.

The line energy is the laser power setting divided by the traverse speed, giving it units of J/mm. It is the amount of energy applied per unit length along the weld line, so if the

power setting and beam speed are increased by the same factor, then the energy will be deposited on a given part of the faying surface at a rate (W/mm/second) which is the same as the original rate, since $W=J/s$. But doubling both the power and speed applies this energy twice as quickly. The effect of heating a given small area faster is that during the time that the energy is being applied, it has less time to diffuse away by conduction, so the peak melt temperature is higher but the volume melted may be lower [35].

Table 5: Welding parameters (S denotes commercial grade, S/2 denotes 50-50 mixture of natural and commercial grade)

	Specimen Identification	Carbon black level	Power (W)	Speed (mm/min)	Line Energy Ratio (power/speed)
A	HG 25, 26, 27	S/2	180	1500	0.12
B	HG 28, 29, 30	S/2	270	1500	0.18
C	HG 8, 9, 10	S	180	1500	0.12
D	HG 34, 35, 36	S/2	270	1800	0.15
E	HG 2, 3, 4	S	240	2000	0.12

One of the welded samples for each parameter setting was used for sectioning and microstructural analysis, one sample was forcibly separated immediately after welding for fracture surface analysis and estimating general strength levels, and one sample was used for hydraulic burst testing. The procedure for each assessment method will be explained in further detail in the sections which follow.

Chapter 4: Welding - Quality Assessment Methods

4.1 Microstructural Analysis (Sectioning)

One method of characterization of the welded zones is through microstructural analysis. Initially a stacked specimen, Figure 21, is assembled which incorporates the welded sample and two cut ring flanges from un-welded hemispheres. The un-welded specimen rings are positioned to line up above and below the corresponding welded sub insert regions so that they give a clear reference location of the manufactured voids as the specimen is sectioned through.

The steps for assembling the stacked specimen is as follows, referring to Figure 21; take welded sample A, and two flanges cut from an un-welded hemisphere shown in B. Using epoxy, join the flanges to the welded sample, C, making sure the gates align. If the gates are aligned then the inserts on the un-welded samples should align with the corresponding insert on the welded sample. Once the epoxy has cured the stacked specimen can be cut, D, giving the stacked specimen for each insert, E. Lastly the stacked specimen is mounted in a PVC pipe using epoxy, F. Small diameter fiducial marker holes were drilled perpendicular to the flat face of the mounted stacked specimen, parallel to and at the faying surface marking the positions of the ends of the sub-inserts. These were an aid in lining up the micrographs from one sequential section to the next, and in locating the same manufactured void remnants on different sections of the same specimen.

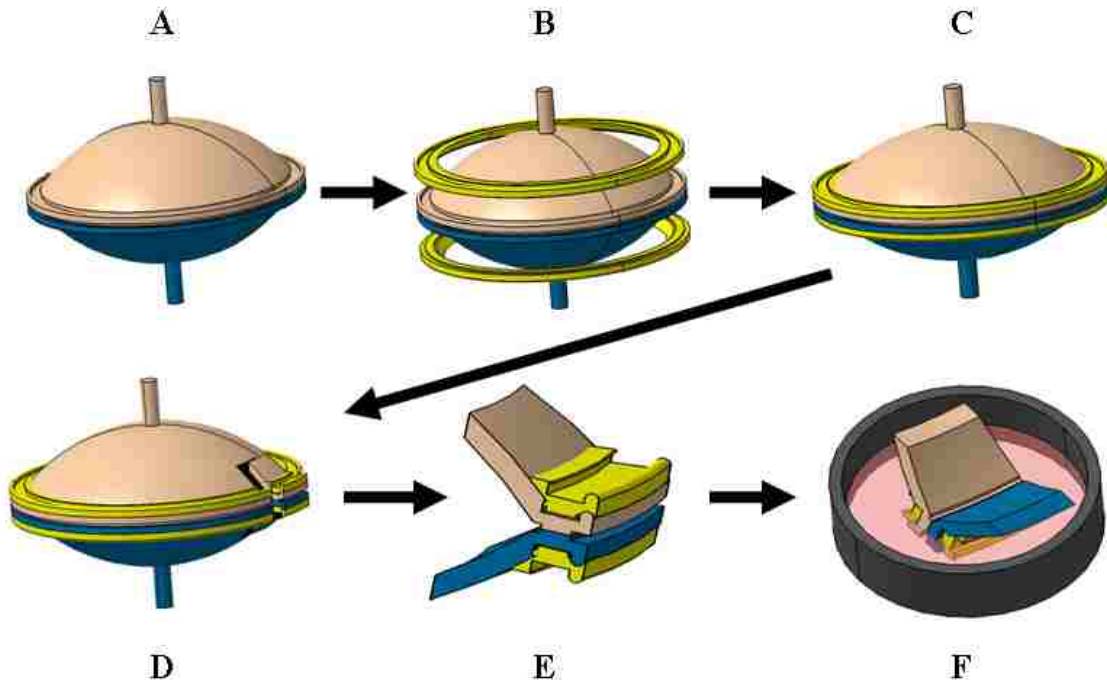


Figure 21: Steps for assembly of stacked specimen. A- Welded sample. B- Two flanges cut from an un-welded hemisphere (preassembly). C- Un-welded flanges glued to welded hemisphere. D- Stacked specimen for each insert is cut out. E- Stacked specimen for one insert. F- Stacked specimen is mounted in a PVC pipe using epoxy.

The mounted specimen can now be sectioned by polishing in increments of approximately 0.2 mm- 0.4 mm. The sections start from the outer circumference (0mm) of the flange and work towards the center (~6 or 7mm).



Figure 22: Line of sight for the microscope. (Perpendicular to the center axis, z, of the assembly)

This process was very time consuming, therefore for each welding condition only three specimens are used. One specimen is taken from the area near the gate where no manufactured voids appear. These samples are denoted “no insert” and give a baseline for the welding conditions. The remaining two specimens are from the section with insert 3 natural/transparent, insert 8 black/opaque, denoted as “3N-8B”, and from the section with insert 4 natural/transparent, 7 black/opaque, denoted as “4N-7B”. These inserts were chosen since they are representative of the majority of the remaining manufactured voids.

In addition, for each welding condition, images were taken along the weld line in an area with no manufactured voids, looking parallel to the direction of travel of the laser beam. Figure 23 shows circled the surface that is polished and microphotographed. These images are useful for showing the location of the laser beam with respect to the flange, as well as an indication of the energy intensity and porosity profile, the depth of laser beam penetration as well as any misalignment of the sample.

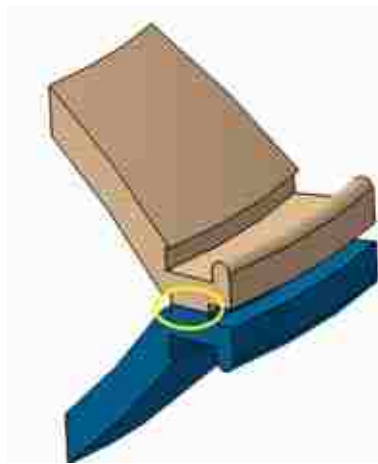


Figure 23: The location of laser beam with respect to the flange is obtained by images taken parallel to the direction of travel. Circled is the surface that is polished and microphotographed.

4.2 Fractured Surface Analysis

One sample for each condition was broken immediately after welding for fracture surface analysis. Steel wedges were inserted between the welded inserts to pry apart the components Figure 24. As stated previously the clamp handle shadow prevented the laser beam from reaching the part between the inserts, thus these areas were not welded, allowing easier insertion of the wedges. The wedges were then hammered into the joint to break the sample open without otherwise disturbing the fracture surfaces where the weld occurred. Most of the welds were very strong, requiring that the wedges be driven in with many hammer blows, frequently bending the tips of the steel wedges. The fracture finally occurred with a loud bang, and usually fractured only the welds adjacent to the wedges. This was an early indication of overheating, and also a predictor that the presence of voids was not deleterious to the weld strength.



Figure 24: Welded sample being separated for fracture surface analysis. Wedges are inserted between the welded inserts to “pry” apart the components. The clamps’ shadow prevented the laser beam from reaching the part between the inserts, thus these areas are not welded.

Later, using oblique lighting and a digital camera, images were taken of the fractured surfaces. The images were then analyzed to find;

- i) The amount of transfer determined by percentage of opaque material area visible on the transparent side,
- ii) The area of adhesion contact, determined by the percentage of area visibly fractured on the absorbing side and
- iii) If any manufactured voids were still visible.

4.3 Burst Test

The welding of the burst tested samples is slightly different than the microstructural and fracture samples. The samples are initially welded with the clamps in the clamped position. Since the clamps created a shadow and prevented these areas from being welded, and knowing that a hermetic seal is needed for burst testing, the samples had to be welded again with the clamps removed. Square pieces of steel acting as shields were placed over the sections which were welded by the first pass to prevent them from being welded a second time. Welding the same area twice was to be avoided since the purpose of the burst test is to estimate the effect of unwelded voids on the weld strength. A sample with the clamps removed and shield placed can be seen in Figure 25. This particular method would not be used in a commercial application. Instead a mask would be produced and precisely placed to shield previous welded areas, or a different clamping system would be developed where the laser beam can reach the entire faying surface.



Figure 25: Shields used for burst tested samples

The burst test involved drilling a hole in the stub section of the two hemispheres that are initially laser welded. The part is held underwater until the air is removed from the sample. The pressure was recorded as more water was pumped into the sample while the whole part is under water, until the sample fails. Failure was by leaking or bursting at the weld seam. Due to the geometry of the part and set up for the burst testing, the parts undergo a “peeling” force rather than a purely tensile force when under pressure. These forces act in the radial and z direction of the hemisphere; see Figure 26.

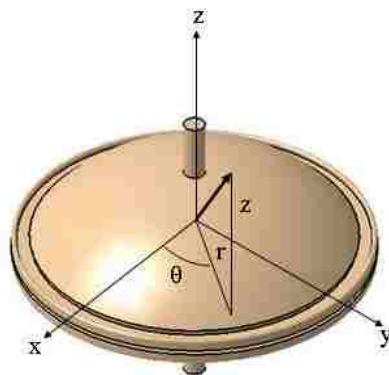


Figure 26: Axis system for burst tested samples

Chapter 5: Laser Transmission Welding Results – Burst Test

Burst testing involved placing the welded samples underwater and pumping water into it until the part fails. Failure was by leaking or bursting at the weld seam. The resulting burst pressures are shown in Table 6. Previous studies by Xu et. al [36], have shown that an ideal geometry for laser welds is to incorporate them into a wall parallel to the specimen axis, connecting the two flanges. These specimens were moulded in the same mould used for the present work, but with different ring inserts. This geometry is called the taper lock joint. This removes most of the peel component at the faying surface, and shifted the location of the failure away from the faying surface to the change of cross-section where the flange intersects the body of the hemisphere. The taper lock joint themselves did not fail. This reference [36] also gave data on vibration welds of similar geometry and material as the hemispheric components used in the present thesis research. The vibration welds had burst strengths of 360-680 kPa, and the peel component moved the failure to the faying surface. It is important to note that these vibration welds and the present laser welds both have a similar peel component of stress, since both welds are located on the raised rings on an external flange. When comparing the burst strengths of the vibration welds with the current laser transmission welds with manufactured voids, it can be seen that the laser transmission welds are stronger, even in some cases where leaking occurred before fracture.

Leak-before-break results were caused by slightly misplaced shields on the parts causing a very small section to not be welded. This provided the water with an easy escape route,

preventing the pressure from reaching the true burst value. The un-welded areas commonly went from the inside edge across to the outer edge of the flange, and so they also acted as a stress raiser. Therefore the burst stresses recorded for the samples that leaked before breaking probably do not represent the burst value for the same welding condition on a fully welded faying surface. This is especially true for the usual case where the break was confined to an area near the leak.

Table 6: Burst test results

Sample Identification	Carbon Black Level	Power (W)	Speed (mm/min)	Line Energy (J/mm)	Burst Pressure (psi)	Burst Pressure (kPa)	Failure	
E	HG-4	S	240	2000	7.2	119.68	825	Weld
	HG-7	S	210	2000	6.3	n/a	n/a	Leaked
C	HG-10	S	180	1500	7.2	61.43	424	Leaked
	HG-12	S	150	1500	6	126.4	871	Weld
	HG-17	S	150	1500	6	40	276	Leaked
	HG-18	S	150	1500	6	40	276	Leaked
A	HG-27	S/2	180	1500	7.2	86.52	597	Weld
B	HG-30	S/2	270	1500	10.8	131.92	910	Weld
	HG-33	S/2	225	1500	9	24	165	Leaked
D	HG-36	S/2	270	1800	9	89.4	616	Weld
	HG-39	S/2	180	1200	9	124.8	860	Weld

5.1 Influence of Variations in Welding Parameters on Burst Strengths

The idea of “manufactured voids” is original in the work described in this thesis. Because of the uncertainty of whether it would work at all, only a limited number of hemispheres were moulded, and the high leakage rates in the burst tests were not anticipated. The burst strength tests themselves have a significant variation amongst duplicate samples.

Therefore the data does not have sufficient duplicate burst strength values to make definitive claims in the section below. However some trends are evident, and especially when combined with the meticulous micrographic section studies, reveal interesting and important results.

Comparisons below of the peak temperature reached and size of the melt pool are based largely on the work of Watt et al, [37] and Haung et al [38]. The next few sections will compare different conditions to determine the affects of laser power, carbon black addition level, laser beam traverse speed and line speed effect at constant line energy.

5.1.1 Power - A (P180, S1500, CB S/2, LE7.2), vs. B (P270, S1500, CB S/2, LE10.8)

Condition B with the higher power shows a higher burst strength of 910 kPa when compared with condition A having a burst strength of 597 kPa. This difference is due to a lack of heating in A resulting in smaller melt pool and a lower peak temperature, hence poorer bonding between the two surfaces. These results show that increasing the laser power increases the burst strength.

5.1.2 Carbon Black Level - A (P180, S1500, CB S/2, LE7.2), vs. C (P180, S1500, CB S, LE7.2)

Condition A has a lower carbon black level than condition C, so it would be expected that the laser beam would penetrate deeper into A, producing a larger melt pool with a lower peak temperature. The burst test results show C has lower burst strength (424 kPa) than A

(597 kPa) but C leaked during the burst test. So, consider substituting for C the results for sample HG-12 (P150 S1500 CB S) where burst strength of 871 kPa was attained. Bearing in mind the effect of power level from the section above, it suggests that if sample C had not leaked, a strength level much higher than the 597 kPa found for sample A would have been obtained. This implies that peak temperature is more significant than the depth of the weld pool.

5.1.3 Beam Traverse Speed - B (P270, S1500, CB S/2, LE10.8), vs. D (P270, S1800, CB S/2, LE9)

B has burst strength of 910 kPa whereas D with the faster speed has lower burst strength, 616 kPa. The slower the part moves, the greater the amount of energy supplied to any given area along the faying surface. In other words, for a given area, the amount of time the power has to heat the surface is greater if the speed is lower. Given that B has a lower speed than D; B receives more energy allowing for more heating, a higher peak temperature and melt depth, and thus a higher strength. These results show that increasing the laser beam traverse speed decreases the burst strength of the weld.

5.1.4 Line Speed Effect at Constant Line Energy - C (P180, S1500, CB S, LE7.2) vs. E(P240, S2000, CB S, LE7.2)

Both C and E have the same line energy, although E has a higher laser power and a higher beam traverse speed. The burst test results show C having lower burst strength than E. But C leaked during the burst test. Again substituting HG-12 (P150, S1500, CB S,

LE7.2) for C, burst strength of 871 kPa is obtained which is similar to the 825 kPa from condition E. It is assumed that if sample C had not leaked, a higher strength would have been obtained giving similar results when comparing line speed effect at constant line energy. Work by Huang [38], has shown that using a higher speed and power at the same line energy produces higher strength welds. This is because a higher peak temperature is reached at the higher speed and power; the heat has less time to diffuse away from the weld zone by solid state conduction. For the present work on hemispheres, this effect may be lost in the inherent scatter of burst test results.

Chapter 6: Laser Transmission Welding Results - Fractured Surface

Analysis

Using oblique lighting and a digital camera, images were taken of the fractured surfaces of the samples split open immediately after welding. The images were then compared to determine the amount of transfer (determined using transparent half), the area of adhesion (determined using the absorbing half), and if the manufactured voids are still visible. Transfer is defined here as the amount (area fraction) of absorbent material transferred onto the transparent side of the faying surface within the boundaries of the sub-insert. This transfer is the result of the crack path veering into the absorbent material. Similarly the transfer of transparent material over to the absorbent fracture side means the crack ran through the transparent side at that part of its journey. Adhesion is defined here as the area fraction of the absorbent side of the fracture that shows visible fracture characteristics as opposed to the smooth as-moulded surface. The presence of the latter means that there was insufficient melting to form an adequate weld bond.

The digital images are used to measure the area of transfer and adhesion by object analysis (threshold) using computer software techniques. The steps are as follows, referring to Figure 27. The image is loaded into the software and calibrated. Next a freehand box is set around the area of interest. Only the area of the insert is examined, this area does not include the welded area beyond the insert, or the flash (faying surface material ejected radially). Finally a threshold technique is used to determine the area of transfer or adhesion.

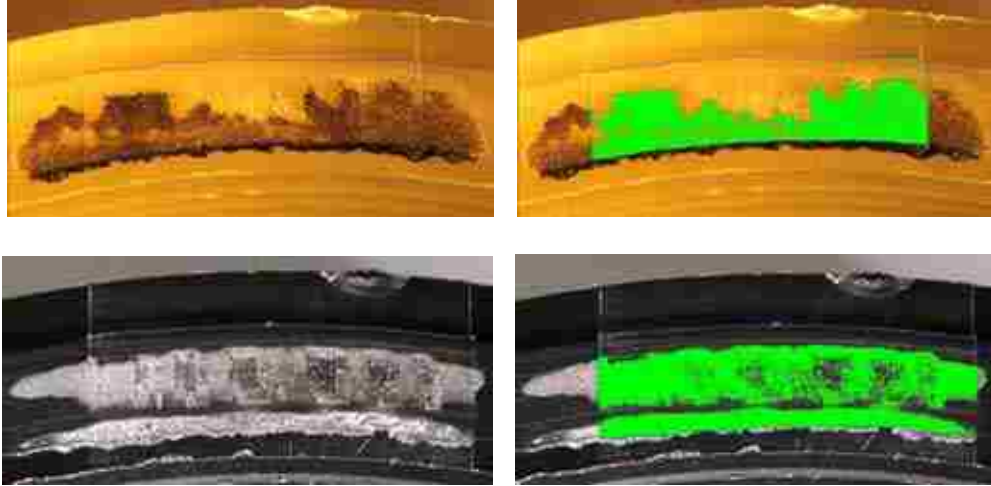


Figure 27: Image analysis using computer software techniques. Top- Before (left) and after (right) images of the transfer area defined by threshold technique. Bottom- Before (left) and after (right) images of the adhesion area defined by threshold technique.

Once all the areas have been determined, the two graphs shown in Figure 28 are compiled to show the percent of transfer and percent of adhesion, as well as a comparison of welding parameters. Table 7 through Table 12 are the images taken of the fracture surfaces.

The first letter of the sample designation for Table 7 through Table 12 refers to the welding conditions given in Table 6.

Table 7: Fracture surfaces A- HG 25




#	Transparent - N	Absorbent - B	#
1			10
2			9
3			8
4			7
5			6
6			5
7			4
8			3
9			2
10			1
L			R
R			L

Table 8: Fracture surfaces B- HG 28

#	Transparent - N	Absorbent - B	#
1			10
2			9
3			8
4			7
5			6
6			5
7			4
8			3
9			2
10			1
L			R
R			L

Table 9: Fracture surfaces C- HG 8 (Welded backwards, L and R - flat area left and right of gate respectively)
















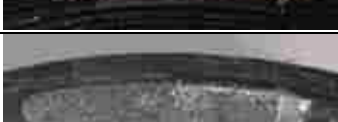








#	Transparent – N	Absorbent - B	#
1			4
2			3
3			2
4			1
5			L
6			R
7			10
8			9
9			8
10			7
L			5
R			6

Table 10: Fracture samples D- HG34






















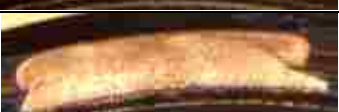


#	Transparent - N	Absorbent - B	#
1			10
2			9
3			8
4			7
5			6
6			5
7			4
8			3
9			2
10			1
L			R
R			L

Table 11: Fracture surfaces E- HG 2




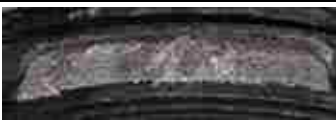
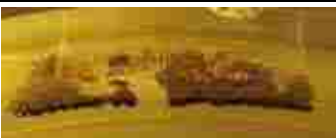





























#	Transparent - N	Absorbent - B	#
1			10
2			9
3			8
4			7
5			6
6			5
7			4
8			3
9			2
10			1
L			R
R			L

Table 12: Fracture surfaces- All

	Transparent - N	Absorbent - B
A- HG 25		
B- HG 28		
C- HG 8		
D- HG 34		
E- HG 2		

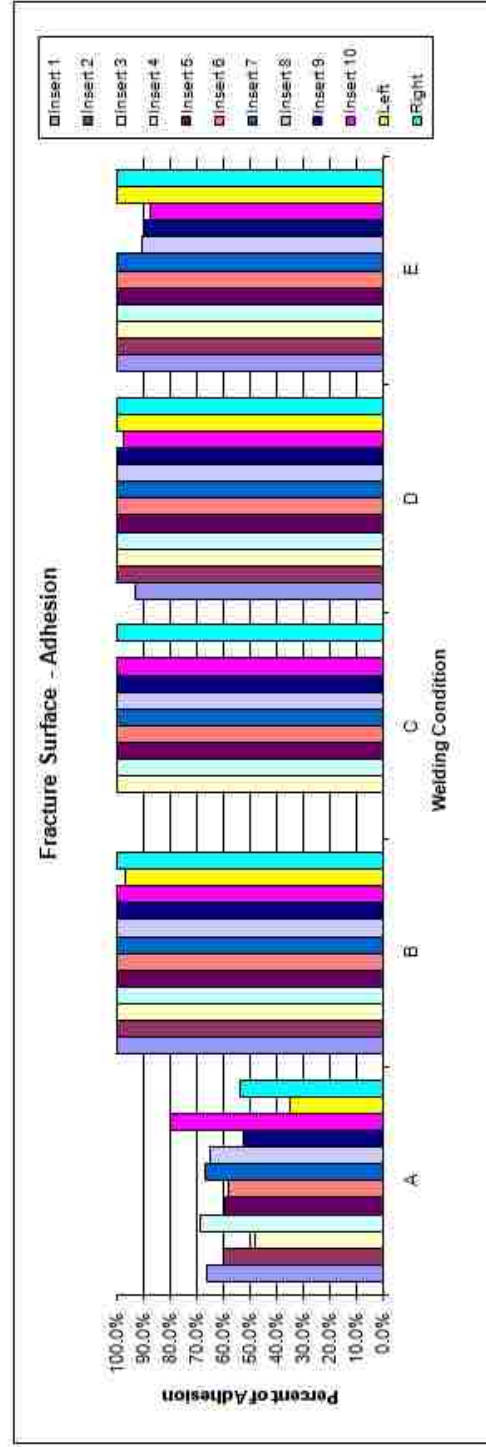
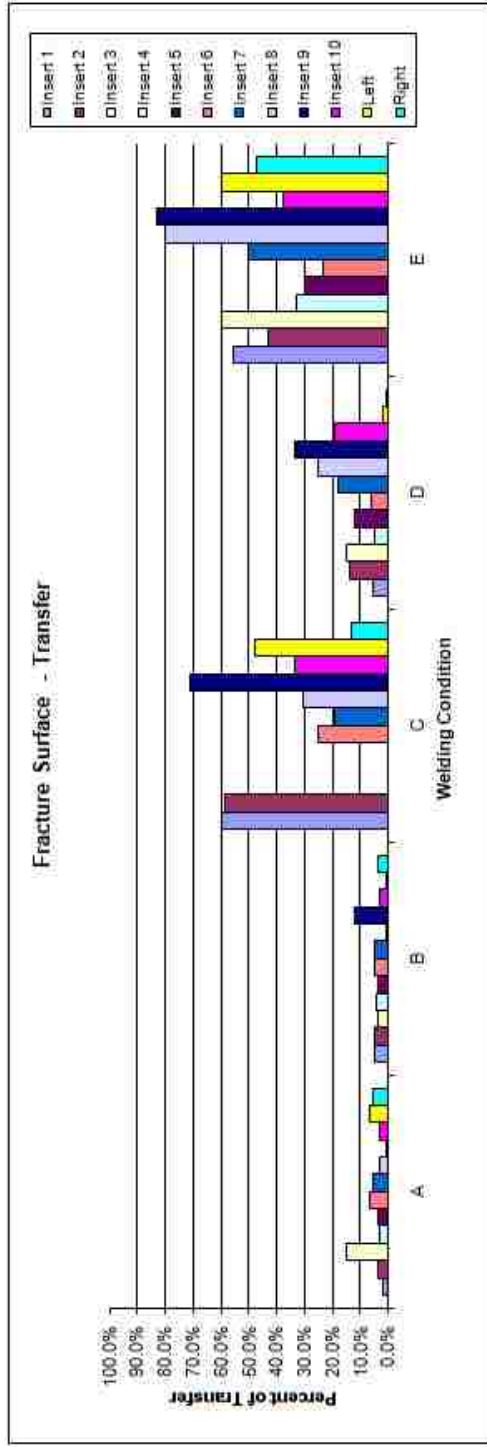


Figure 28: Fracture surface - Percent of transfer (top) and adhesion (bottom)

Conditions A and B show the lowest level of weld material transfer, followed by condition D, then C, leaving condition E with the greatest transfer. The adhesion is shown to be good for most conditions, with the exception of A and some inserts on C.

Each insert gives comparable results, compared to the other inserts, as the welding conditions are changed. Insert 7 tends to have the greatest transfer for most conditions. However, for welding condition C, the fracture surface has some areas where no weld occurred. This may be a consequence of a clamp unsecured during welding. When comparing welding parameters of the various conditions, insert areas of this type are neglected.

6.1 Power A (P180, S1500, CB S/2, LE7.2), vs. B (P270, S1500, CB S/2, LE10.8)

If the laser power is increased while the other process parameters are fixed, then one would expect to have a deeper weld pool with a higher maximum temperature. Despite the difference in power, the two conditions, A and B, have similar material transfer. Condition B, with the higher power, has a greater area of adhesion all around the faying surface. This higher adhesion, although not resulting in much transfer, does create a strong bond. Condition A has a much lower adhesion surface area than B. Also manufactured voids are still visible on the absorbing side of A, indicating insufficient heating. The lack of heating for A resulted in a lower melt volume and peak temperature, resulting in poorer bonding between the two surfaces.

6.2 Carbon Black Level - A (P180, S1500, CB S/2, LE7.2), vs. C (P180, S1500, CB S, LE7.2)

The lower carbon black level means the beam will penetrate deeper into the absorbing material, but the same energy will therefore be used to heat a larger volume, resulting in a lower maximum temperature in the melt. Condition A has a lower carbon black level than C, while their power and speed parameters are the same. This causes A to have a lower amount of material transfer and a lower adhesion surface area. The higher carbon black level in C results in a more concentrated absorption of the laser energy at the faying surface. Neglecting the inserts for C which did not weld (due to a clamp not being secured), the amount of transfer is much greater, suggesting a stronger weld. The adhesion area is lower for A, and the manufactured voids are still visible on the absorbing side of A, indicating an insufficient temperature rise. The result is poor bonding between the two surfaces.

6.3 Beam Traverse Speed - B (P270, S1500, CB S/2, LE10.8), vs. D (P270, S1800, CB S/2, LE9)

The faster the beam traverses along the weld line, the less the energy available for a given point along that line. So if the other parameters, laser power setting and carbon black content are held constant, increasing the speed will lower the melt volume and the peak temperature in the melt. When comparing B and D, it can be seen that the adhesion is similar. But D, with the higher speed, has a slightly higher amount of transfer than condition B. Although the transfer for B is lower, the burst strength is higher than D.

The slower the part moves under a fixed laser source, the greater the amount of energy supplied to the surface. In other words, for a given length, the amount of time the power has to heat the surface is greater if the speed is lower. Given that B has a lower speed than D, B has more time to heat the surface allowing for more melting, and a higher peak temperature, and thus a higher strength.

6.4 Line Speed Effect at Constant Line Energy - C (P180, S1500, CB S, LE7.2) vs. E(P240, S2000, CB S, LE7.2)

Line energy is the amount of energy per unit length along the weld line, calculated as the power divided by beam traverse speed. Condition C and E have the same line energy or rate at which power is supplied to the faying surface, but E has a higher power and beam traverse speed setting. Recall that the effect of the heating of a given small area faster, is that the energy has less time to diffuse away by conduction, so the peak melt temperature is higher but the volume melted is lower [35].

Neglecting the inserts which did not weld on sample C, the amount of transfer and the adhesion area is similar for C and E. Condition E, with the higher power and speed has a slightly higher percent of transfer overall, in addition to an apparently higher burst strength than C. However, C leaked before bursting, It is assumed that if this sample had not leaked, a higher strength would have been obtained, since in general a good bond was present.

Chapter 7: Laser Transmission Welding Results - Microstructural

Analysis

The remaining method of characterization of the welded zones was through microstructural analysis. The mounted specimen, sectioned by polishing in increments of approximately 0.2 mm- 0.4 mm was examined at each section using an inverted optical microscope. Micrographs allow direct comparison of the corresponding welded and un-welded sections. The objective is to find to what extent each of the welded voids healed, for the given welding parameters. This procedure also reveals the porosity caused by the welding process at the opaque near-surface and the rest of the weld pool zone.

The entire length of the weld cannot be micrographed at once; therefore multiple images are taken along the length and stitched together in a montage fashion using computer software. Figure 29, is an example of the stitched montage of micrographs, the profile of the un-welded and welded sections are highlighted for clarity.

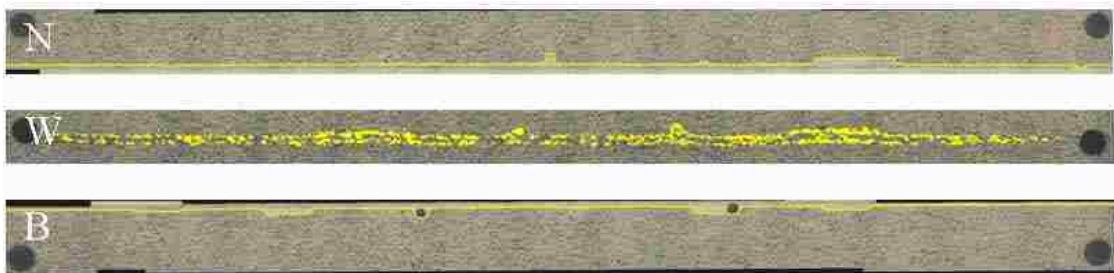


Figure 29: Micrographs of the healed voids and un-welded cross-sections from a stacked specimen. N- Un-welded natural/transparent material. W-weld line, upper section is transparent material and lower section is absorbent material. B- Un-welded black/absorbent material. (Micrographs of welding condition B)

Some cross-sections of the weld line show little healing of the voids, hence the manufactured voids are still visible; this is shown in Figure 30. Welding condition A

shows the majority of the manufactured voids unhealed throughout the sections of each of its inserts. Most of the other welding conditions show cross-sections with the manufactured voids healed, and a large degree of porosity present.

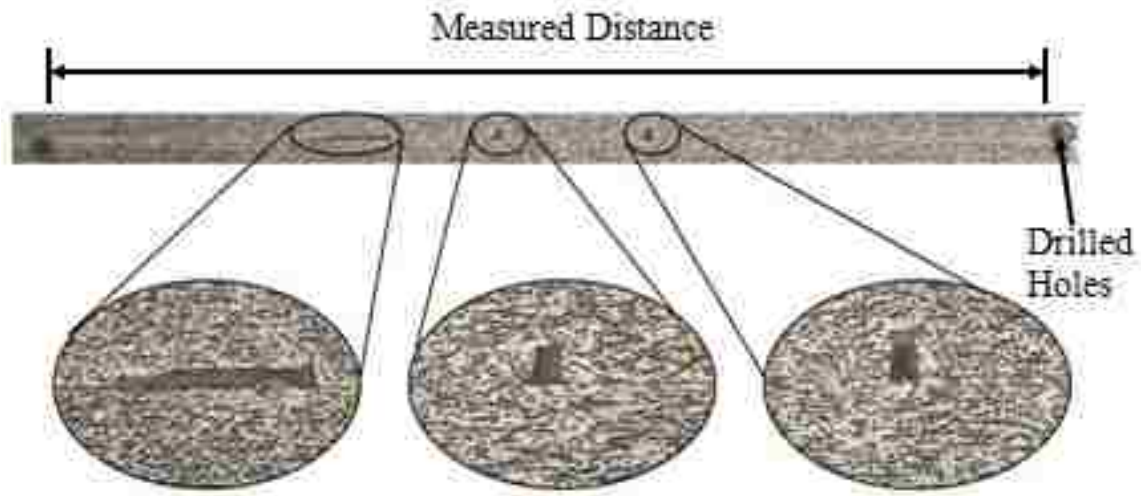


Figure 30: Montage of weld with voids that have not healed from welding (Micrographs of welding condition A)

Using computer software, the amount of porosity and unhealed voids was quantified as the sum of the areas (mm^2) of the pores on the cross-section per unit length (mm). The length was then determined by the distance between the holes drilled in the sample. This distance, shown in Figure 31, is the same for each section of a given insert but different for each insert. By normalizing the areas of the cross-section by the length between the holes, the porosity results for different welding conditions and inserts can be compared. Once the area per length of each section for a given sample has been determined, the data was compiled in a graph of area/length for a section versus the depth into the sample at which the section was taken.

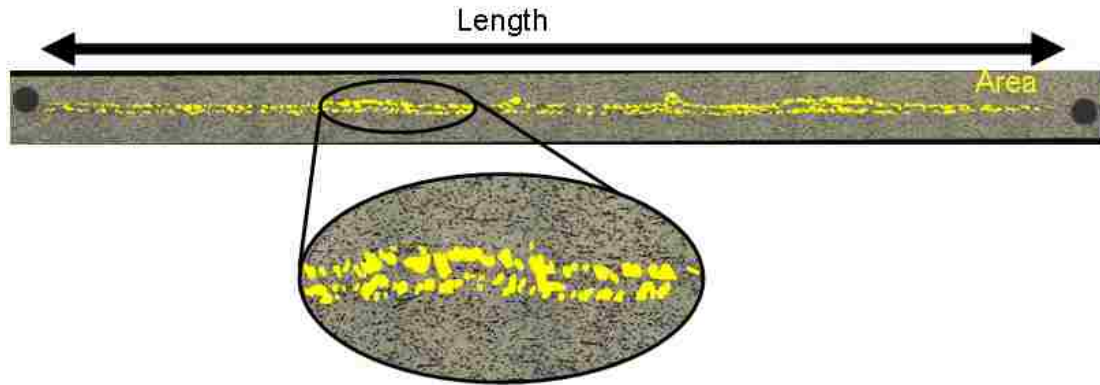


Figure 31: Porosity and unhealed voids is quantified as the average area (mm^2) of the pores on the cross section per unit length (mm)

An example of these graphs is shown in Figure 32. Each point on the graph represents one section through the sample, giving approximately 25 sections for insert 3N-8B and 4N-7B, and 13 sections for the no insert sample. The profile of the curve of best fit through the data was a result of the intensity profile of the Nd-YAG laser beam. The Nd-YAG laser beam intensity profile was Gaussian, thus giving a higher intensity at the center resulting in higher porosity. The remaining graphs can be found in Section 7.3.

An example of the montage micrographs for each welding condition is given in Figure 33 through Figure 35. The complete set of micrograph sections for each welding condition and insert can be found in Appendix II.

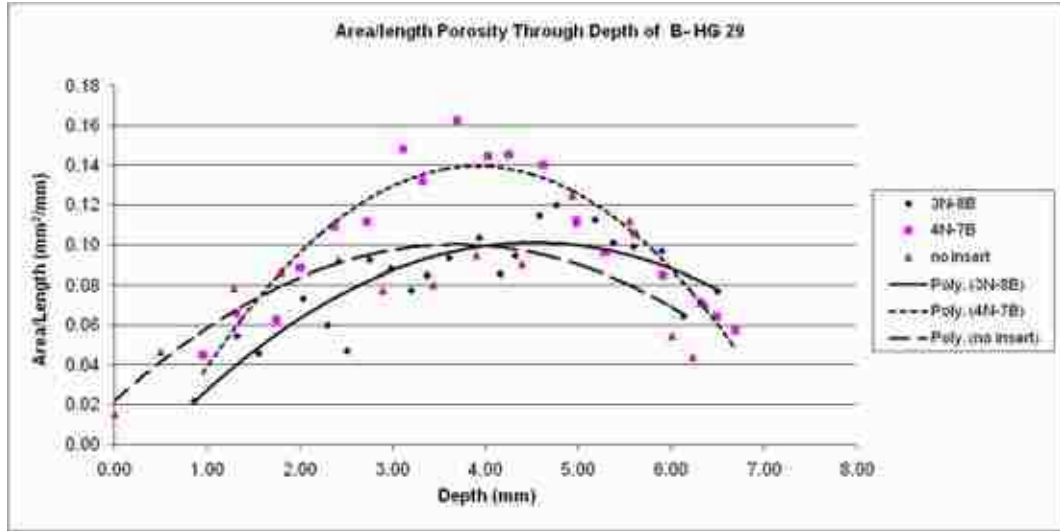


Figure 32: Area/length Porosity through Depth of B- HG 29

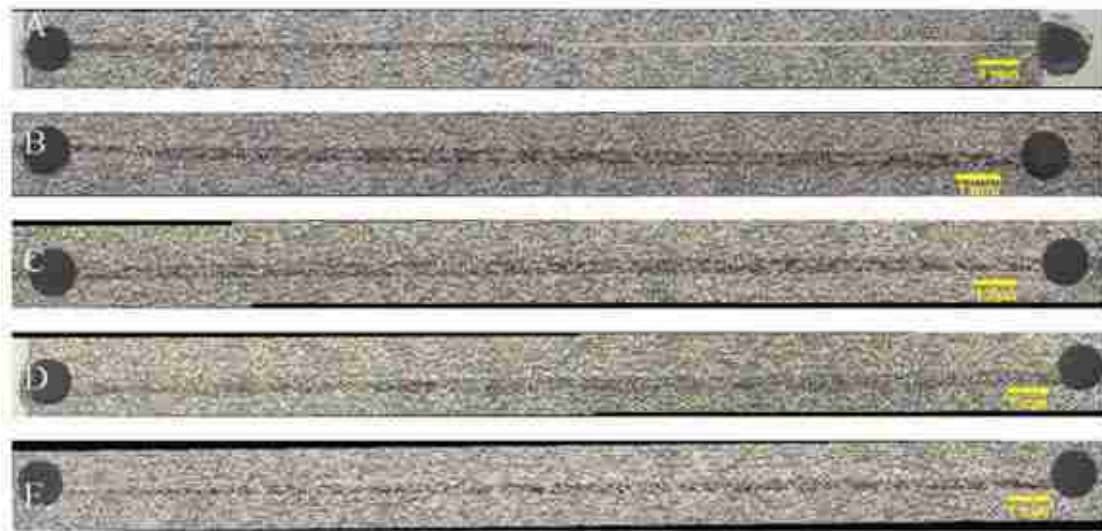


Figure 33: No Insert

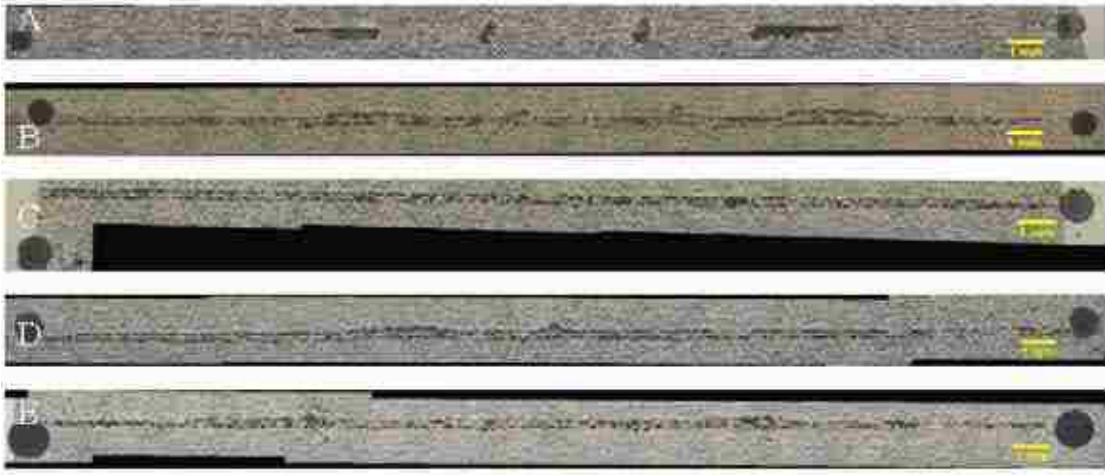


Figure 34: Insert 3N8B

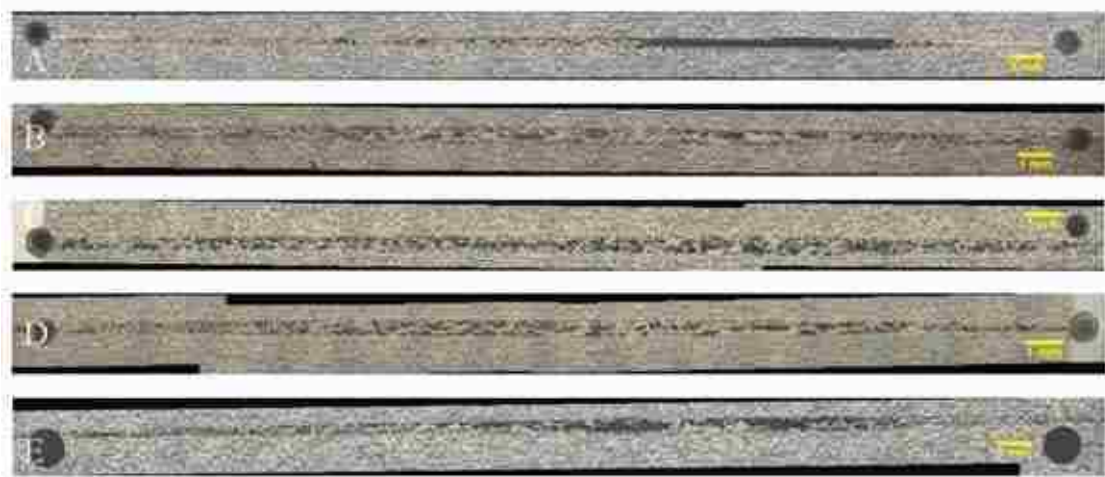


Figure 35: Insert 4N7B

7.1 Cross-sections Perpendicular to the Direction of the Laser Beam

The images taken across the weld line viewed parallel to the direction of travel of the laser beam can be found in Figure 36 through Figure 40 for each welding condition.

These images are useful for showing that the weld covers the entire span of the flange, except for the case of condition A. The images show a small amount of flash mostly on

the inside of the part. Also, an estimate of the minimum depth of penetration of the laser beam into the opaque material can be measured as the depth of the distance where porosity occurs in these figures.



Figure 36: A- HG 26 (Right is outer side of part, top is natural material)



Figure 37: B- HG 29 (Right is outer side of part, top is natural material)



Figure 38: C- HG 9 (Right is outer side of part, top is natural material)



Figure 39: D- HG 35 (Right is outer side of part, top is natural material)



Figure 40: E- HG 3 (Right is outer side of part, top is natural material)

Table 13: Depth of Penetration of Laser Beam

	Depth of Penetration (mm)
A	~0-0.08
B	~0.28-0.3
C	~0.2-0.35
D	~0.2-0.3
E	~0.15-0.2

7.2 Mechanisms for Porosity Formation

A study of the micrographs and the shape of the porosity/voids suggests a mechanism for porosity formation. The Tree Diagram of Figure 13 was used as the guide for the characterization of voids based on their appearance. The majority of the porosity voids can be categorized as shrinkage voids due to their irregular shape. Some voids appear spherical in shape leading to the belief these could be caused by other means, either by air encapsulation during welding or by water vapour or other volatiles. Each of these mechanisms for porosity formation will be explained in further detail.

7.2.1 Air Encapsulation During Welding

It is not hard to imagine air being encapsulated during welding Figure 41 since the manufactured voids themselves can hold a relatively large quantity of air between the adjoining surfaces. During welding as the polymer temperature rises, the softened or molten material expands to fill the manufactured voids. If the expansion of the material is insufficient or the air is unable to escape into the flash or otherwise, then upon cooling the trapped air remains creating porosities/voids at the faying surface.

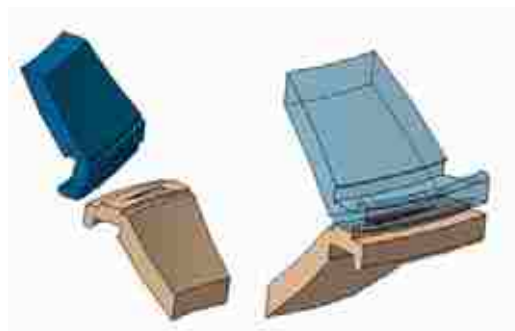


Figure 41: Manufactured voids and air encapsulation

7.2.2 Water Vapour Evolved from Moist Resin During Processing

Spherical voids may just as easily be caused by water vapour within the material. Although careful consideration was undertaken when processing the injection moulded hemispheric halves, proper storage before welding was not. As explained earlier in Section 2.6, the material for these studies is nylon 6, a hygroscopic material. In addition the additive used for the absorbing material, carbon black, is also a hygroscopic material. Given that the sample halves were stored in cardboard boxes in a common room, moisture from the air will have seeped into the material over time. The samples were not dried prior to welding, thus the moisture within the material would have created water vapour at the elevated temperatures of the welding process, thus forming porosities/voids.

7.2.3 Excessive Volume Contraction of the Polymer During Cooling (Shrinkage)

Excessive volume contraction could easily occur during the rapid cooling following the laser beam path, because the laser beam melts only the central region of the raised ring facing surface, meaning that there is no meltdown, and the distance between the flanges is not affected by the melting-freezing process. During contour laser transmission welding the laser beam traverses the length of the joint, typically at about 2 meters per minute, and at any point the melting and freezing process takes about 150 milliseconds [35]. In this short time plastic resin melts and expands, causing a compressive pressure. Ideally this causes expansion to fill the manufactured voids, and detrimentally it can possibly cause some flash to be expelled molten material from the weld zone. This flash is visible in Figure 36 through Figure 40, as well as the ragged edge on the bottom of weld zone on transparent side of Figure 27, and many of the other failure surfaces. As the

molten material cools, freezes and then further cools back to ambient temperature, it should cool back to the initial volume it had before heating, minus the flash. If the flanges remain the same distance apart, effectively there is too little material to completely fill the manufactured voids and maintain a continuous solid continuum between the two flanges. If a continuum could be maintained then it would be under a tensile hydrostatic stress to make up for the missing resin. But liquid plastic and even hot solid polymer has a limited tensile strength, though it has high ductility. For reasons that are not understood at the time of this writing, the voids appear to be nucleated by a cavitation process at the boundary between the solid polymer and the region where the viscoelastic soft material exists. It is known that high hydrostatic stresses are developed in the softer material where two materials having a large difference in elastic modulus are bonded together and are subjected to unidirectional tensile stresses [39]. These hydrostatic tensile stresses could nucleate the cavitation. As the polymer shrinks to the previous volume during cooling, it appears that the original manufactured void volume and the missing flash material volume is redistributed along the boundaries of the viscoelastic soft material as shrinkage porosity, refer to Figure 42.

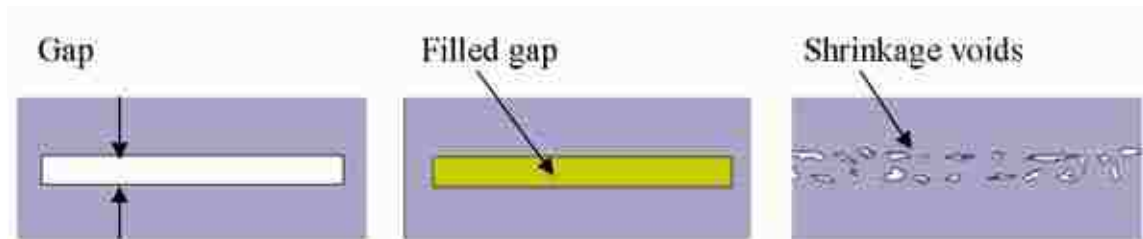


Figure 42: Porosity/void formation by shrinkage

It is unlikely that only one of these mechanisms for porosity formation is the cause of the large degree of porosity present. Instead it is assumed the porosity is due to a complex combination of all the causes; flash loss, air encapsulation, water vapour and shrinkage.

7.3 Graphical Data and Results

The following section includes the graphs obtained by porosity analysis of the cross sections for each welding condition. Also included are graphs used for a comparison of welding conditions and a discussion on results obtained by these graphs.

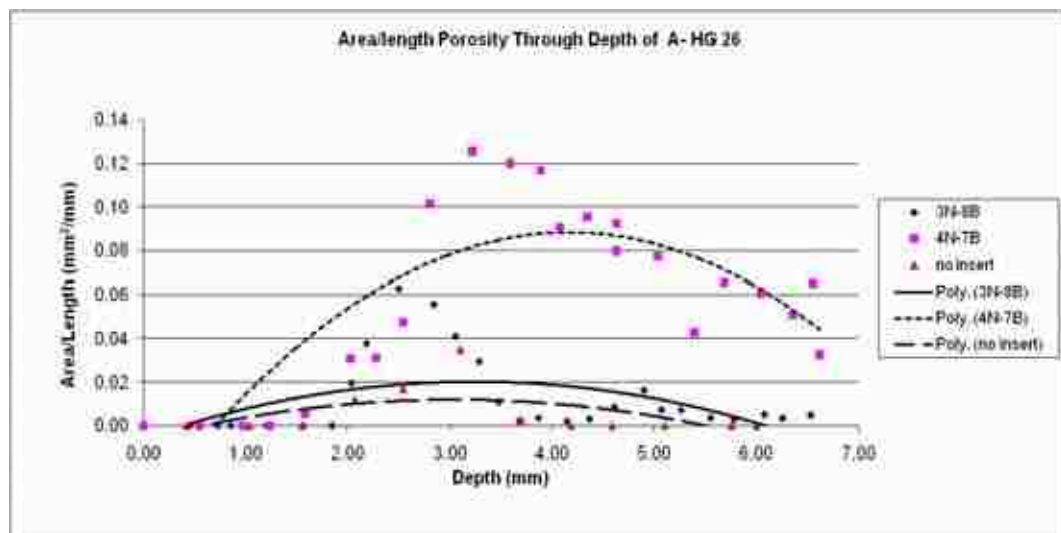


Figure 43: Area/length porosity through depth of A- HG 26

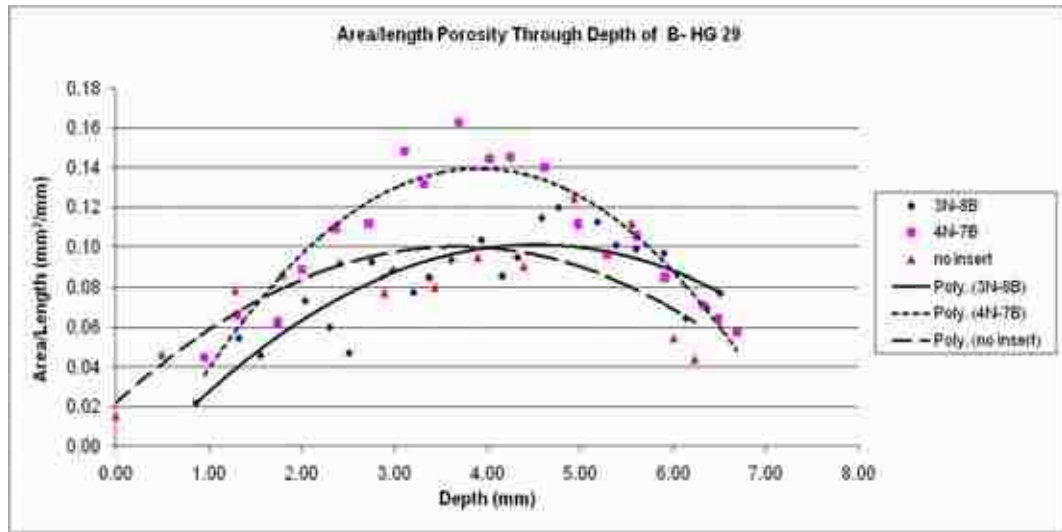


Figure 44: Area/length porosity through depth of B- HG 29

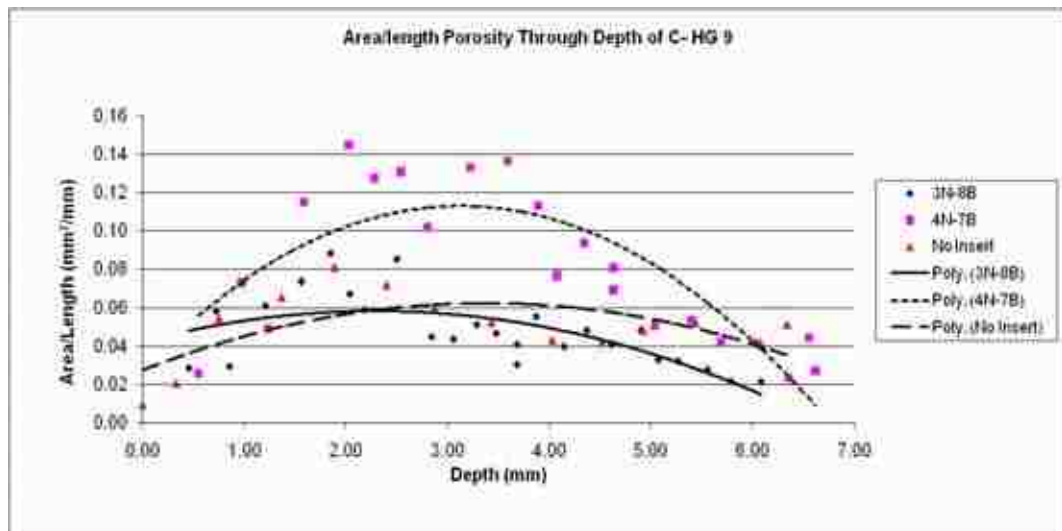


Figure 45: Area/length porosity through depth of C- HG 9

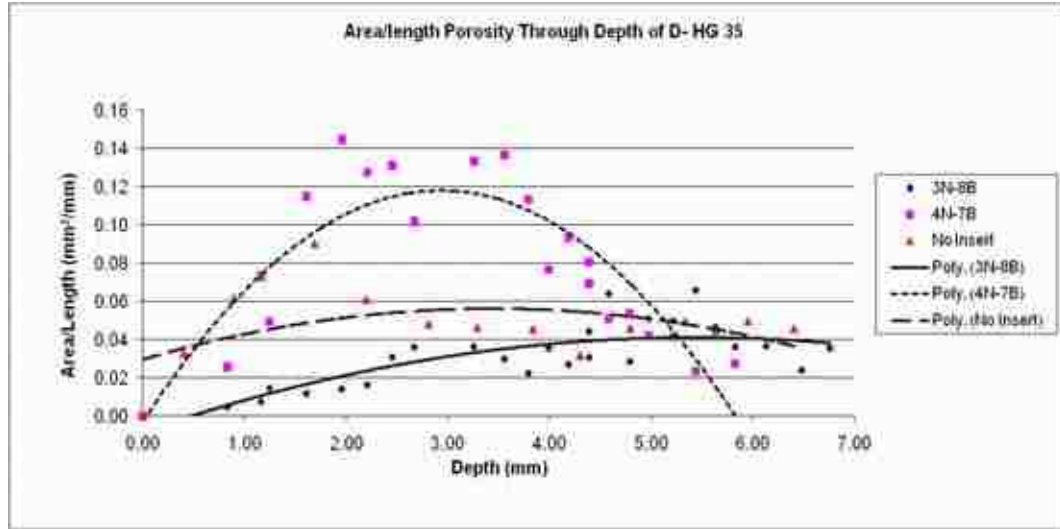


Figure 46: Area/length porosity through depth of D- HG 35

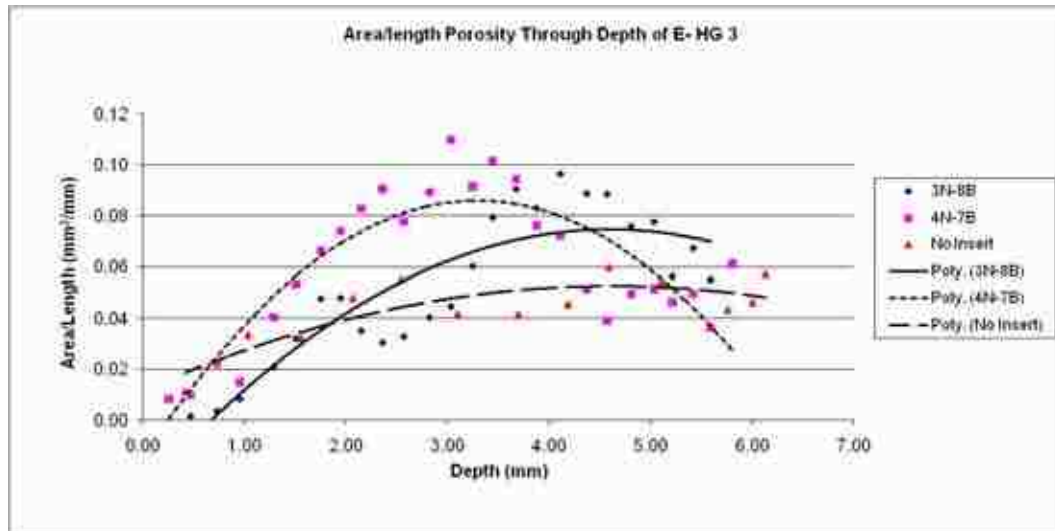


Figure 47: Area/length porosity through depth of E- HG 3

When comparing the porosity area/length for the different samples within the same welding condition, one can see from Figure 43 through Figure 47 that insert geometry affects the degree of porosity present in the samples. Insert 4N-7B (single arrowhead void) has the highest area/length porosity for each case, insert 3N-8B (2 rows of small rectangular voids) is next followed by the near the gate area (No insert) for conditions A, B and E, and for conditions C and D no insert is followed by insert 3N-8B.

The area/length porosity calculated for condition A, incorporates the porosity as well as the visible unhealed manufactured voids. Looking at the side profile micrograph in Figure 36, it appears that the weld width does not extend the width of the flange resulting in only the inside portion of the adjoining surfaces to be welded. For this reason the outer voids from insert 3N8B did not weld producing two distinct peaks for the graph in Figure 43. Although not as well defined in the graph, the void for 4N7B was also only partially welded, and can be seen in Appendix II along with the no-insert sections which also only partially welded.

The area/length porosity for conditions B through E does not have visible unhealed manufactured voids. However the profiles of the manufactured voids are visible in some micrographs in Appendix II, for example E-HG 3- 3N8B- section 7 depth 1.51mm.

7.3.1 Comparison of Welding Conditions

7.3.1.1 Power - A (P180, S1500, CB S/2, LE7.2), vs. B (P270, S1500, CB S/2, LE10.8)

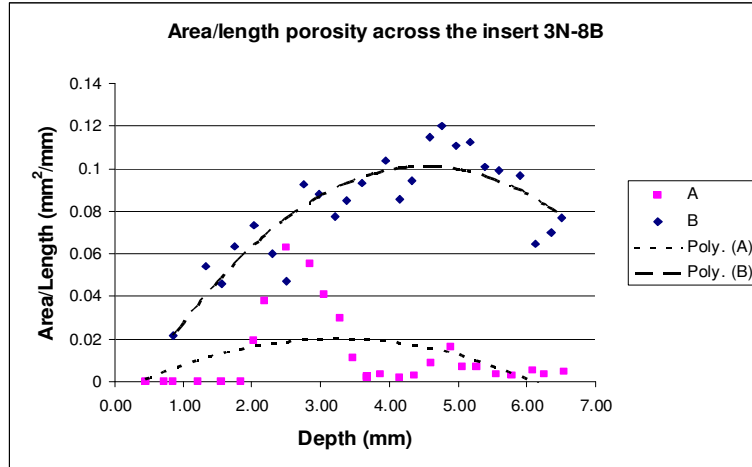


Figure 48: Insert 3N-8B, power level comparison, condition A and B

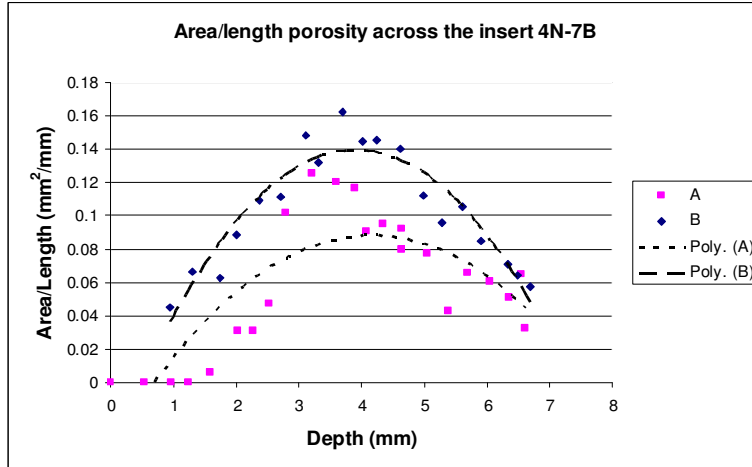


Figure 49: Insert 4N-7B, power level comparison, condition A and B

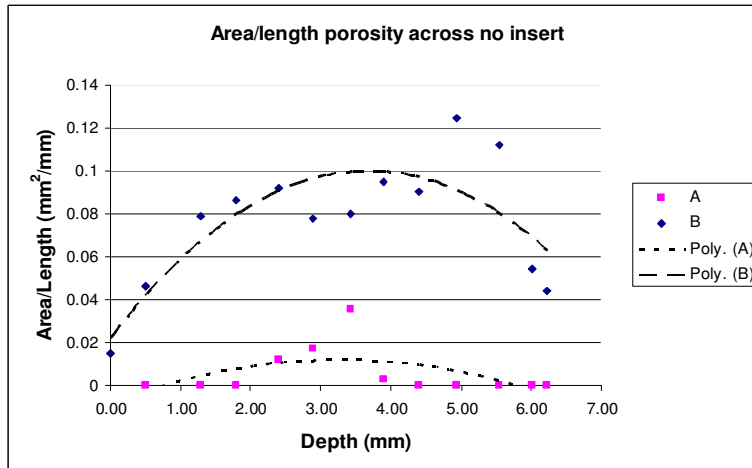


Figure 50: No insert, power level comparison, condition A and B

As stated before, if the power is increased while the other process parameters fixed, then we would expect to have a deeper weld pool with a higher maximum temperature. Condition B, with the higher power has a higher level of porosity than condition A for each sample 3N8B, 4N7B, and No insert. These results are typically to what would be expected. With the higher maximum temperature and deeper weld pool, a more sufficient melting is accomplished for condition B, resulting in a higher degree of porosity. Looking at the micrographs for condition A, Appendix II, the manufactured voids are still visible indicating inadequate melting and mixing of the materials along the faying surface. The micrographs for condition B, Appendix II, show moderate pore sized evenly dispersed throughout the length for each section of the inserts. The high level of porosity present does not have a detrimental effect on the burst strengths of the weld, since both condition A and condition B show appreciable results in burst strength.

7.3.1.2 Carbon Black Level - A (P180, S1500, CB S/2, LE7.2), vs. C (P180, S1500, CB S, LE7.2)

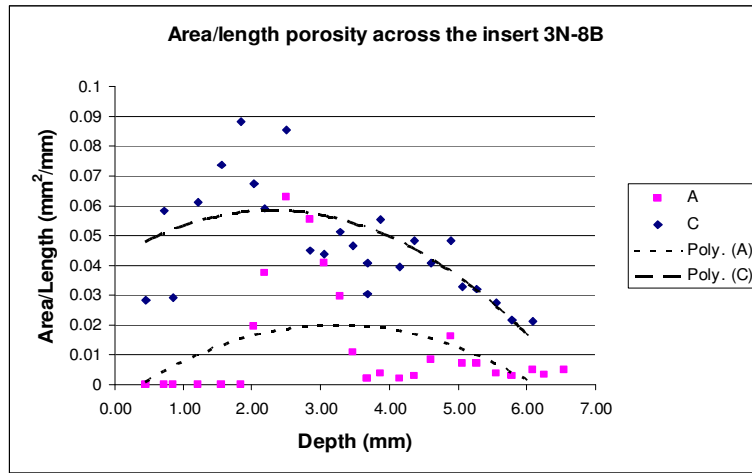


Figure 51: Insert 3N-8B, carbon black level comparison, condition A and C

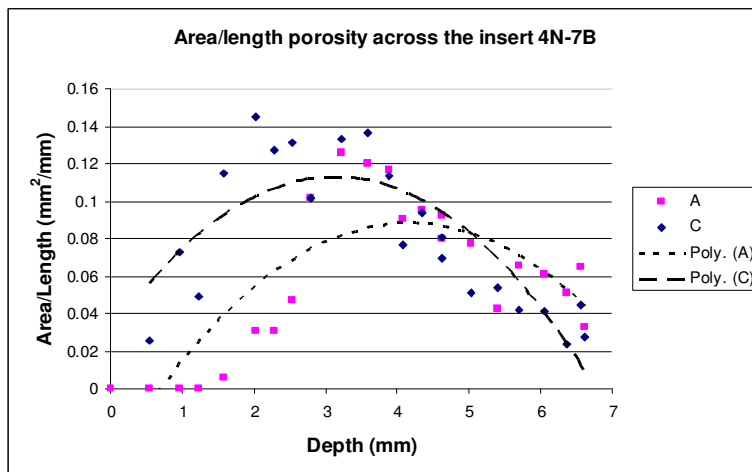


Figure 52: Insert 4N-7B, carbon black level comparison, condition A and C

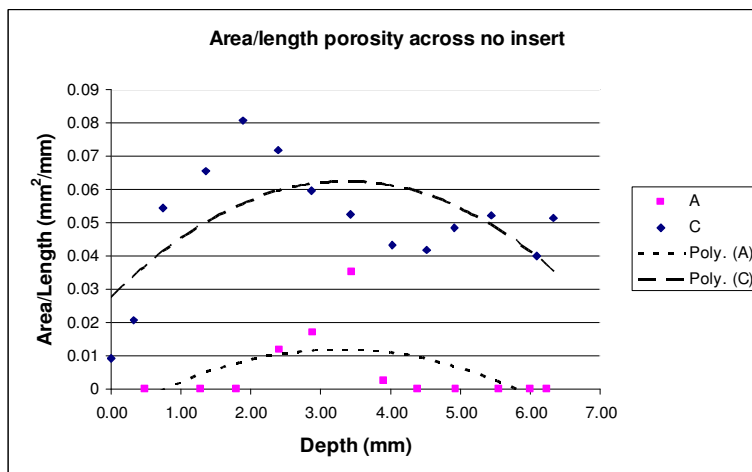


Figure 53: No insert, carbon black level comparison, condition A and C

Condition A has a lower carbon black level than C, while their laser power and beam traverse speed parameters are the same. The lower carbon black level in A allows for deeper penetration of the laser beam in the absorbing material. Given that the power and speed are the same for A and C, the same amount of energy is supplied. The energy in A is dispersed in a larger volume since the penetration is deeper, hence the maximum temperature of the melt will be lower. Looking at the micrographs for condition A, Appendix II, the manufactured voids are still visible indicating inadequate melting and mixing of the materials along the faying surface. Comparing condition A micrographs with condition C micrographs, C shows moderate pore sized evenly dispersed throughout the length and for each section of the inserts. The graphs in Figure 51 through Figure 53 show the anticipated results of C having higher porosity than A for each of the given inserts.

7.3.1.3 Beam Traverse Speed - B (P270, S1500, CB S/2, LE10.8), vs. D (P270, S1800, CB S/2, LE9)

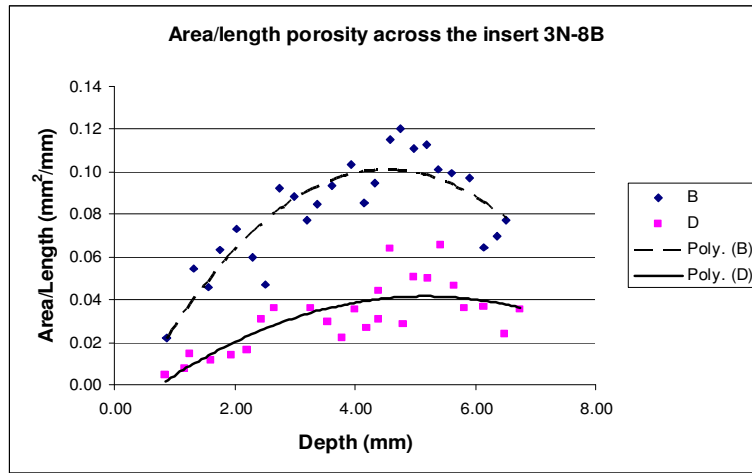


Figure 54: Insert 3N-8B, beam traverse speed comparison, condition B and D

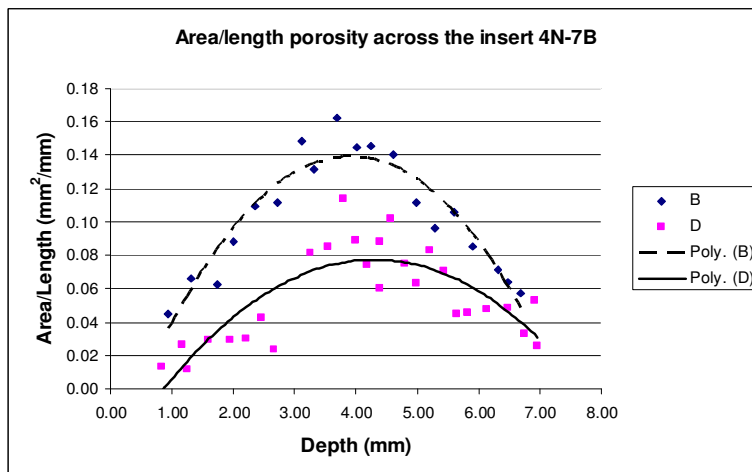


Figure 55: Insert 4N-7B, beam traverse speed comparison, condition B and D

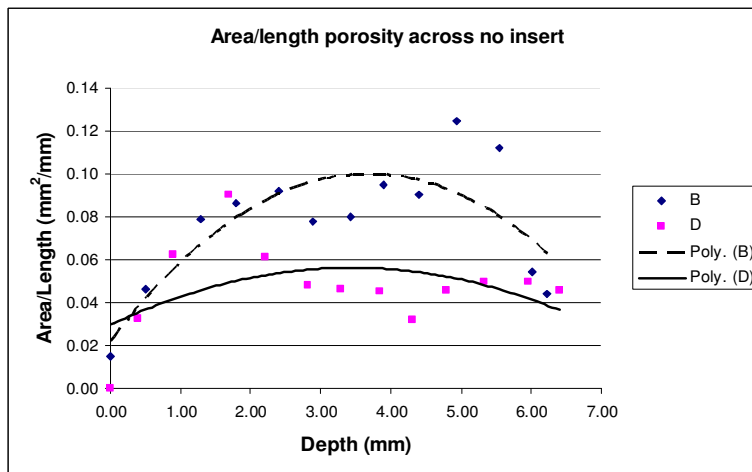


Figure 56: No insert, beam traverse speed comparison, condition B and D

As previously stated, the slower the beams traverse speed, the greater the amount of energy supplied to a given point along the line of travel. Condition B has a lower speed than condition D, while the laser power and carbon black content is held constant. The lower speed for condition B allows for greater energy supplied to the weld line resulting in a higher melt volume and higher maximum temperature in the melt. From the graphs in Figure 54 through Figure 56, of the three insert geometries, condition B has greater area/length porosity than condition D, which is expected.

7.3.1.4 Line Speed Effect at Constant Line Energy - C (P180, S1500, CB S, LE7.2) vs. E(P240, S2000, CB S, LE7.2)

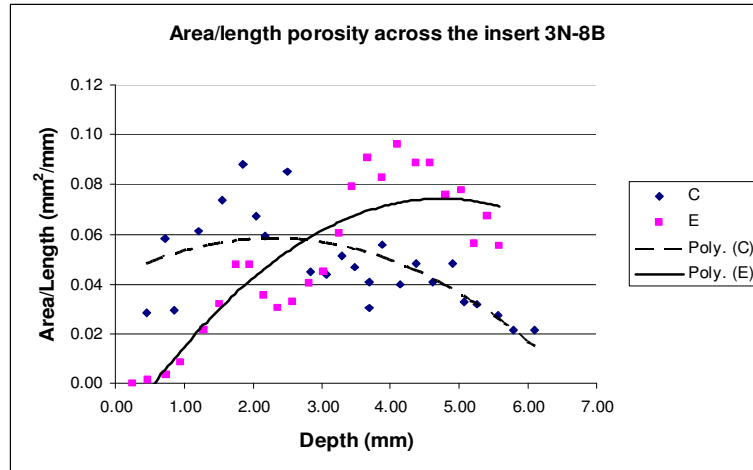


Figure 57: Insert 3N-8B, line speed effect, condition C and E

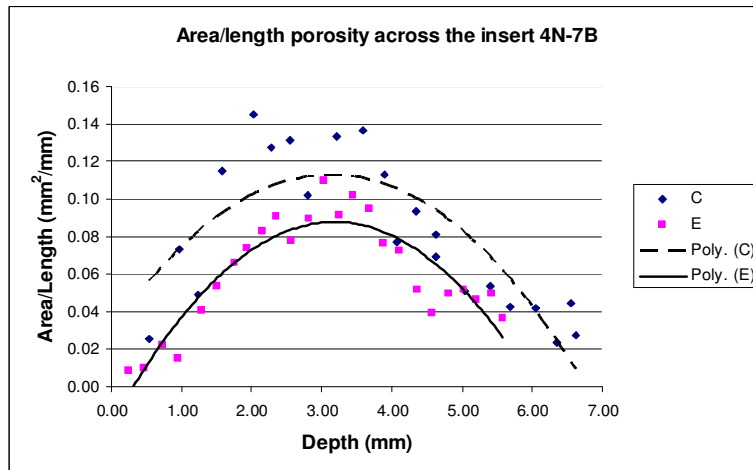


Figure 58: Insert 4N-7B, line speed effect, condition C and E

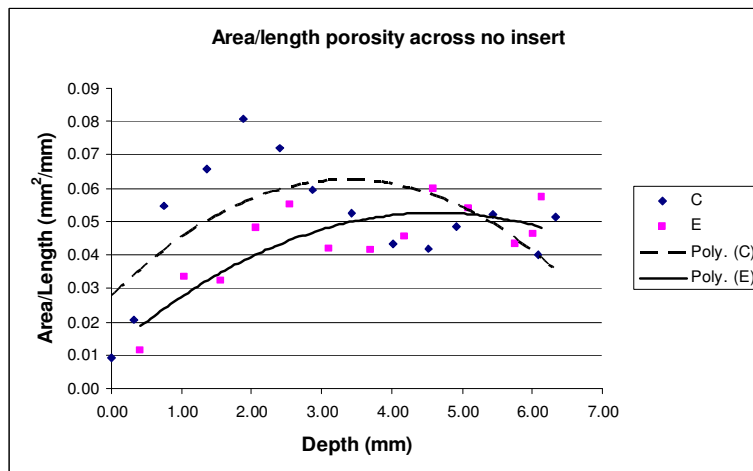


Figure 59: No insert, line speed effect, condition C and E

As stated before line energy is laser power divided by traverse speed. Condition C and condition E have the same line energy and carbon black level. The power and speed of E are higher than C. Although the amount of energy per unit length is the same, the higher power and speed of condition E will heat a given area faster, so the energy will have less time to diffuse away by conduction, thus resulting in a higher peak temperature and possibly a lower melt volume [35]. The area/length porosity of C and E shown in Figure 57 through Figure 59 is similar for each insert geometry, suggesting that increasing the speed and power by 33% at this line energy has only minor affects.

Chapter 8: Discussion and Interpretation of Results

The superior strength of the current laser welds compared with standard vibration welds, (introduction to Chapter 5) can be partially attributed to the random arrangement of the glass fibres after laser welding. During vibration welding the fibre orientation is parallel to the direction of the movement of the parts. This direction is perpendicular to the tensile force exerted during the burst test. Since the glass fibres only strengthen for loads primarily in their length direction, there is no benefit if the orientation is perpendicular to the major tensile force. During transmission laser welding the glass fibres maintain a random orientation at the weld line, enabling the glass fibres to share some of the tensile force exerted during burst testing. This is confirmed by burst testing results and the loud banging noise emitted during the separation by wedges of the fracture surface analysis samples indicating a large release of stored elastic energy.

Overall the results show that even with a large degree of porosity the welds produced by laser transmission welding are stronger than vibration welds. Contrary to popular belief the large degree of porosity did not have detrimental effects on the strength of the welds.

8.1 Overall Assessment of Each Welding Parameter

Let us now examine in detail the effect of the welding parameters.

8.1.1 Power (Conditions A-B)

Welding conditions A and B were compared to determine the effects of laser power. A and B had a speed of 1500 mm/min and both had the carbon black level of S/2. A has a laser power of 180 W and B has a laser power of 270 W. Given that the power is increased while the other process parameters fixed, we would expect B to have a deeper weld pool with a higher maximum temperature. The results of the fracture samples does show that B had a greater area of adhesion all around the faying surface. The higher power and maximum temperature allowed for greater conduction of heat to the transparent material promoting melting and mixing of both the transparent and absorbent materials. The lack of heating in A resulted in poor bonding between the faying surface, noticeable in the low levels of adhesion and the fact that the manufactured voids are still visible on the absorbing side of A. The manufactured voids are also clearly visible in the micrographed sections for condition A since they did not heal during welding. In contrast the micrographs for condition B show moderately sized pores evenly dispersed throughout the length for each section of the inserts. The burst results show B having burst strength pressure of 910 kPa where A has burst strength pressure of 597 kPa. Therefore, these results show that increasing the laser power also increases bonding at the faying surface allowing for higher burst strengths.

8.1.2 Carbon Black Level (Conditions A-C)

Condition A and C had the same laser power, 180 W, and the same speed, 1500 mm/min. The carbon black addition level in C is higher than A. The higher level of carbon black in C promotes heating at the surface since the material will more readily absorb the laser

energy. The laser beam will penetrate deeper in A and the energy will be more dispersed in a larger volume, instead of concentrated in the case of C. Since the same amount of energy is being used to heat a larger volume for A, the transfer and adhesion values are lower on the fracture surfaces as a result of insufficient temperature rise and poor bonding. This poor bonding is also present in the micrographs of A since the manufactured voids did not heal and are still visible. The micrographs for C shows moderately sized pores evenly dispersed throughout the length and for each section of the inserts. The porosity of C is also higher than A, which is what is to be expected since the energy was more concentrated, and actually healed the manufactured voids. Assuming the burst test results of HG-12 are similar to those that would be obtained if C had not leaked, then a burst strength of C would be higher than A, being ~871 kPa and 597 kPa respectively. These results show that increasing the carbon black concentration produces a stronger weld when the power is held constant.

8.1.3 Laser Beam Traverse Speed (Conditions B-D)

Conditions B and D have the same concentration of carbon black, same laser power setting of 270 W, but have different beam traverse speeds. B has a speed of 1500 mm/min and D has a speed of 1800 mm/min. The slower the part moves under a fixed laser source, the greater the amount of energy supplied to the surface, this is apparent when looking at the line energies, 10.8 J/mm for B and 9 J/mm for D. The higher amounts of energy supplied to the faying surface in B allows for a higher peak temperature, more melting and greater bonding. The burst strength for B, 910 kPa, is hence higher than D, 616 kPa. The fracture surfaces for B and D show similar results for both transfer and

adhesion. The micrographs for B and D both show moderately sized pore evenly dispersed throughout the length and for each section of the inserts. Although the micrographs are similar the calculated area/length porosity across the depth is different, with B higher for each insert.

8.1.4 Line Speed Effect at Constant Line Energy (Conditions C-E)

As stated previously line energy is laser power divided by traverse speed. Condition C and condition E have the same line energy and carbon black level. The power and speed of E are higher than C. Although the amount of energy per unit length is the same, the higher power and speed of condition E will heat a given area faster, but the energy will have less time to diffuse away by conduction, thus resulting in a higher peak temperature and lower melt volume [35]. The generated heat cannot diffuse away sufficiently fast and apparently causes a saturation effect. The micrographs of C and E are similar in both appearance and calculated area/length porosity vs. depth. Fractured surface analysis also reveals similar results as C and E had comparable transfer and adhesion areas. Assuming the burst test results of HG-12 are similar to those that would be obtained if C had not leaked, then burst strength of C and E would be ~871 kPa and 825 kPa respectively. These results suggest that samples with the same line energy but moderately different power levels will have similar welds.

Chapter 9: Conclusions and Future Work

9.1 Conclusions

The following is a summary of the conclusions based on the results of the present study:

1. Conventional wisdom states that porosity in plastics (or any other material) reduces the mechanical properties. This is especially thought to be true when the porosity is present as sheets of pores lying perpendicular to the principal direction of loading. If these are in a highly stressed region, premature failure is expected. Porosity present at a weld line should weaken the joint, and open cell porosity would make it difficult to create a hermetic seal [8]. The micrographs in the present study show a large degree of closed cell porosity, present in sheets parallel to the faying surface. The level of porosity, similar to early stage crazing, suggests the weld would be weak. In fact the burst test show high values of burst pressures, indicating a very strong bond is present even with the presence of porosity.
2. Laser transmission welding has the potential of obtaining strong welds, exceeding those of linear vibration welds of similar geometry. The increased strength of the laser welds can be attributed to the glass fibres being in a more random orientation after welding. During vibration welding the fibre in the faying surface rotate so that they lie in that surface. This orientation is perpendicular to the tensile force exerted during the burst test. Since the glass fibres only add strength when loaded in their length direction, there is no benefit if the orientation is perpendicular. In fact, because of their high stiffness compared with the polymer,

they act as stress raisers. During transmission laser welding the glass fibres maintain a more random orientation at the weld line, enabling the glass fibres to share some of the tensile force exerted during burst testing.

3. The burst strengths of transmission laser welded nylon6 30%GF parts was found to increase as laser power increased, or carbon black addition increased, or if the beams traverse speed decreased within the range of those values used in these tests.
4. Line energy is a ratio defined as the laser power divided by beam traverse speed. Line speed effect at constant line energy was compared using two conditions with the same line energy, but a 4/3 difference in the speed and power setting. Despite results of previous studies [35] indicating the higher power and speed condition will heat a given area faster and have less time to diffuse the energy, thus resulting in higher peak temperature and lower melt volume, the current study did not show significant difference between the two conditions studied. Therefore, these results suggest that samples with the same line energy but moderately different speed and power levels will have similar welds.

9.2 Recommendations for Future Work

The following is suggestions for further research based on the present study:

1. The current research is limited to a small statistical sample size due to various reasons as previously discussed. The burst strength tests themselves have a significant variation amongst duplicate samples. It is therefore recommended to complete more burst tests with the samples with manufactured voids and under the same welding parameters as A through E. Additional burst testing will allow for a more statistically significant analysis.
2. Gaps between adjoining surfaces prior to welding are a common occurrence due to warping. The gaps may span the entire width of the weld. It is therefore recommended to redesign the manufactured voids to have voids which span across the entire sub insert from outside edge to inside edge. Because of the multiple parts of the mould, only the sub-inserts would need to be manufactured to create this design change. The idea of this further work would be to determine if a hermetic seal is possible with gaps spanning the width prior to welding. The gaps may be designed with different depths and sizes, and assessment may be completed in a similar fashion as the present study.
3. The research should be extended to neat nylon6 to examine the role played by the glass fibres. Note that this could be done without the sub-inserts, using just the ring inserts made for vibration testing.

4. The research should be extended on dry as-moulded glass filled nylon to examine the effects of absorbed water.

5. The methods used in this research may be extended for research of other polymer materials, and of combinations of different polymers.

References

1. Stokes, V.K., *Joining Methods for Plastics and Plastic Composites: An Overview*. Polymer Engineering and Science, 1989. **29**(No. 19): p. 1310-1324.
2. Grewell, D.A., A. Benatar, and J.B. Park, *Plastics and Composites Welding Handbook*. 2003, Cincinnati: Hanser Gardener Publications, Inc.
3. Kagan, V.A., *Innovations in Laser Welding Technology: State of the Art Joining of Thermoplastics and Advances with colored Nylon for Automotive Applications*, in *SAE 2002 World Congress*. 2002, SAE International: Technical Paper 2002-01-0716.
4. Kagan, V.A., *Innovations in Laser Welding of Thermoplastics: This Advanced Technology is Ready to be Commercialized*, in *2002 SAE International Body Engineering Conference and Automotive & Transportation Technology Conference*. 2002, SAE International: Technical Paper- 2002-01-2011.
5. Giordano, G. and H. Inman, *Laser Welding Heats Up*. *Plastics Engineering*, 2009(September 2009): p. 28-30.
6. Mapleston, P., *Plastics Welding - The Choices Widen*. *Plastics Engineering*, 2008(April 2008): p. 10-16.
7. Hänsch, D. *Laser Transmission Welding of Electro-Pneumatic Valves*. in *ANTEC*. 2007: SPE.
8. Rotheiser, J., *Joining of Plastics. Handbook for Designers and Engineers*. 1999, Cincinnati, Ohio, USA: Hanser Gardner.
9. Ion, J.C., *Laser Processing of Engineering Materials - Principles, Procedure and Industrial Application*. 2005, Oxford: Elsevier Butterworth-Heinemann.
10. Silfvast, W.T., *Laser Fundamentals*. 2nd ed. 2004, Cambridge: Cambridge University Press.
11. Mayboudi, L.S., *Heat transfer modelling and thermal imaging experiments in laser transmission welding of thermoplastics*. 2008, Queen's University (Canada): Canada.
12. Scheirs, J., *Compositional and Failure Analysis of Polymers*. 2000, West Sussex, England: John Wiley & Sons, Ltd.
13. Nakamata, H., *Process for joining different kinds of synthetic resins*, in *United States Patent (4636609)*, Toyota, Editor. 1985, Toyota Jidosha Kabushiki Kaisha: Japan.
14. Ou, B.S., A. Benatar, and C.W. Albright, *Laser Welding of Polyethylene and Polypropylene Plates*, in *ANTEC*. 1992, SPE. p. 1764-1767.
15. Potente, H. and J. Korte, *Laser Butt Welding of Semi-Crystalline Thermoplastics*, in *ANTEC*. 1996, SPE.
16. Grimm, R.A., *Through Transmission Infrared Welding of Polymers*, in *ANTEC*. 1996, SPE.
17. Kagan, V., R. Bray, and A. Chambers, *Forward to Better Understanding of Optical Characterization and Development of Colored Polyamides for the Infra-Red/Laser Welding: Part I - Efficiency of Polyamides for Infra-Red Welding*. *Journal of Reinforced Plastics and Composites*, 2003. **22**(6): p. 533.

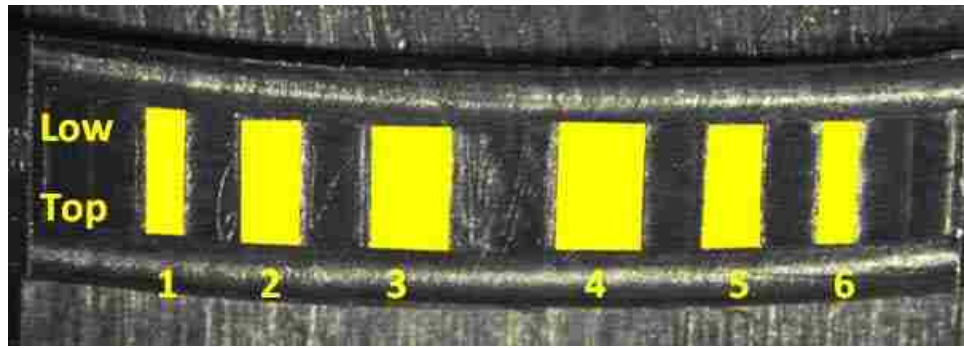
18. Kagan, V.A., R.G. Bray, and W.P. Kuhn, *Laser Transmission Welding of Semi-Crystalline Thermoplastics - Part I: Optical Characterization of Nylon Based Plastics*. Journal of Reinforced Plastics and Composites, 2002. **21**(12): p. 1101.
19. Kagan, V.A. and G.P. Pinho, *Laser Transmission Welding of Semi-crystalline Thermoplastics - Part II: Analysis of Mechanical Performance of Welded Nylon*. Journal of Reinforced Plastics and Composites, 2004. **23**(1): p. 95-107.
20. Kocheny, S.A., V.A. Kagan, and J. Macur. *Through-Transmission Laser Welding of Nylon - Breaking the Moisture Barrier*. in ANTEC. 2004: SPE.
21. Grimm, R.A. and H. Yeh, *Infrared Welding of Thermoplastics. Colored Pigments and Carbon Black Levels on Transmission of Infrared Radiation*, in ANTEC. 1998, SPE. p. 1026-1029.
22. Vegte, E.v.d., et al., *Engineering Plastics for Laser Welding*, in ANTEC. 2007, SPE. p. 1894-1899.
23. Wang, C.Y., P.J. Bates, and G. Zak, *Optical Properties Characterization of Thermoplastics used in Laser Transmission Welding: Transmittance and Reflectance*, in ANTEC. 2009, SPE. p. 1278-1282.
24. Lee, C. and R. Ballou, *Laser Energy Transmission (LET) Measurements of 30% Glass Reinforced Nylon 6*, in ANTEC. 2007, SPE. p. 1900-1904.
25. Bates, P.J., et al., *Influence of Part Thickness, Glass Fibre Content and Line Energy on Laser Transmission Welding of Polyamide mXD6*, in ANTEC. 2007, SPE. p. 2783-2787.
26. Chen, M., G. Zak, and P.J. Bates, *Prediction of Gap Bridging in Laser Transmission Welding of Amorphous Polymers*, in ANTEC. 2008, SPE. p. 1839-1843.
27. Chen, M., et al., *Gap Bridging in Laser Transmission Welding of PA6*, in ANTEC. 2007, SPE. p. 2788-2792.
28. Prabhakaran, R., et al. *Laser Transmission Welding of Unreinforced Nylon 6*. in ANTEC. 2004: SPE.
29. Al-Wohoush, M.H. and M.R. Kamal, *The Microstructure and Quality of Laser-Welded Joints*, in ANTEC. 2008, SPE. p. 1844-1848.
30. Haberstroh, E. and R. Luetzeler, *3D-Laser Transmission Welding*, in ANTEC. 2003, SPE. p. 1099-1104.
31. Haberstroh, E. and R. Luetzeler. *Laser Transmission Welding of Semi-Crystalline Plastics*. in ANTEC. 2006: SPE.
32. Kirkland, T.R., *Practical Joint Design for Laser Welding of Thermoplastics*, in ANTEC. 2004, SPE. p. 1236-1240.
33. Smith, W.F., *Foundations of Materials Science and Engineering*. Third ed. 2004, New York: McGraw-Hill.
34. ASM_International, *Engineered Material Handbook*. Engineering Plastics. Vol. 2. 1988, Metals Park, OH: ASM International.
35. Huang, Y., *Experimental and Numerical Study of Through-Transmission Laser Welding of Elastomers to Polypropylene*, in *Mechanical, Automotive and Materials Engineering*. 2004, University of Windsor: Windsor. p. 129.
36. Xu, S.X., et al. *On the Design of a Strong Contour Laser Weld Joint Geometry for Closed Hollow Chambers*. in ANTEC. 2006: SPE.

37. Watt, D., et al., *Measuring the Depth of Penetration of the Laser Beam in the Absorbing Material for Through-Transmission Welding Processes*, in ANTEC. 2006, SPE: Charlotte, North Carolina. p. 2305-2309.
38. Huang, Y., et al., *A Numerical Study of Scanning Through-Transmission Laser Welding*, in ANTEC. 2006, SPE: Charlotte, North Carolina. p. 2310-2314.
39. Watt, D.F., X.Q. Xu, and D.J. Lloyd, *Effects of Particle Morphology and Spacing on the Strain Fields in a Plastically Deforming Matrix*. Acta Materialia, 1996. **44**(2): p. 789-799.

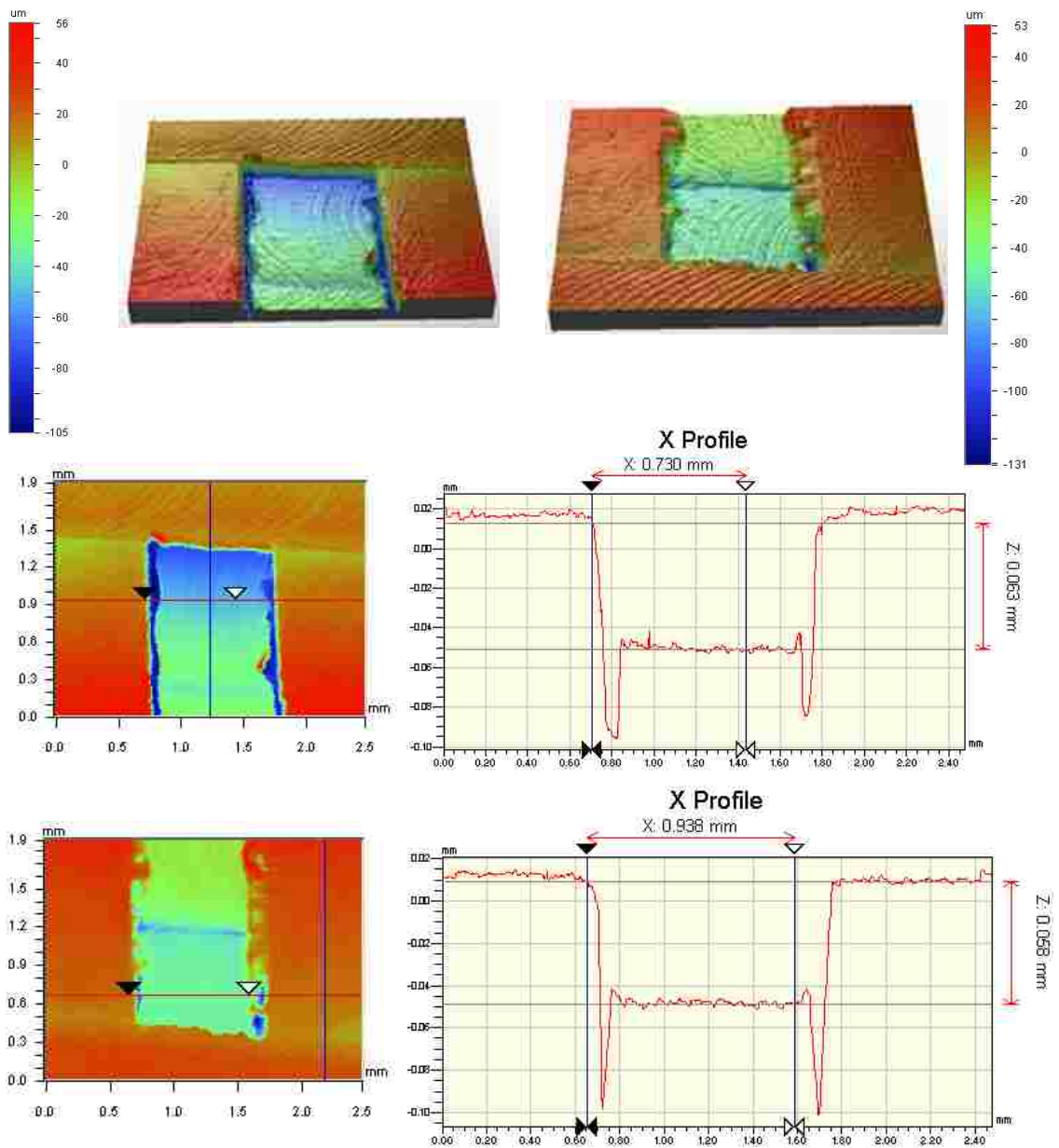
Appendix I : Optical Profilometer Data and Micrographs

Optical profilometer data was gathered by Ming Chen and Dr. Alpas, of the University of Windsor.

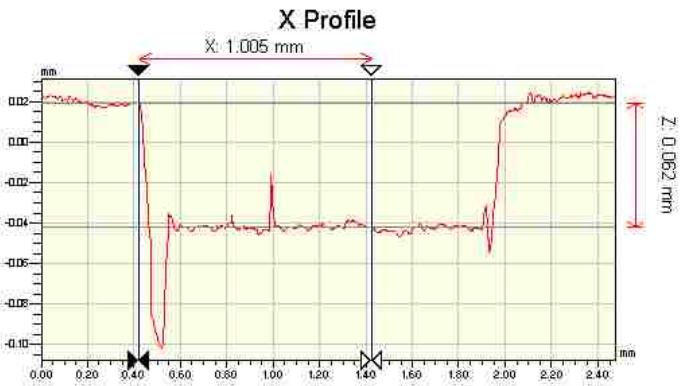
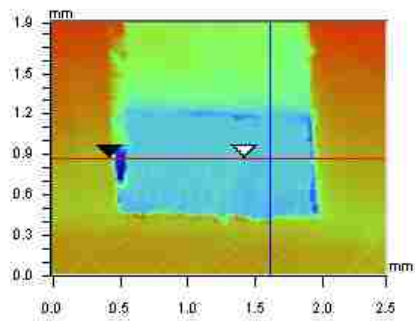
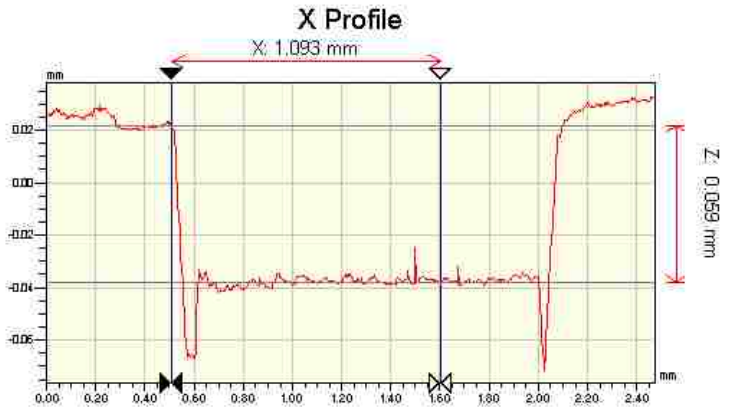
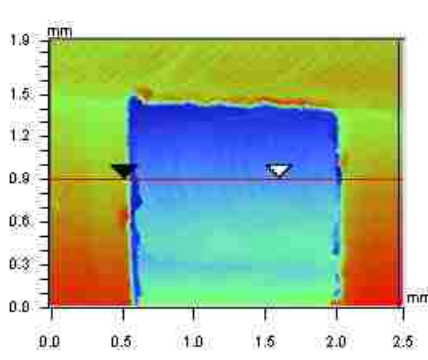
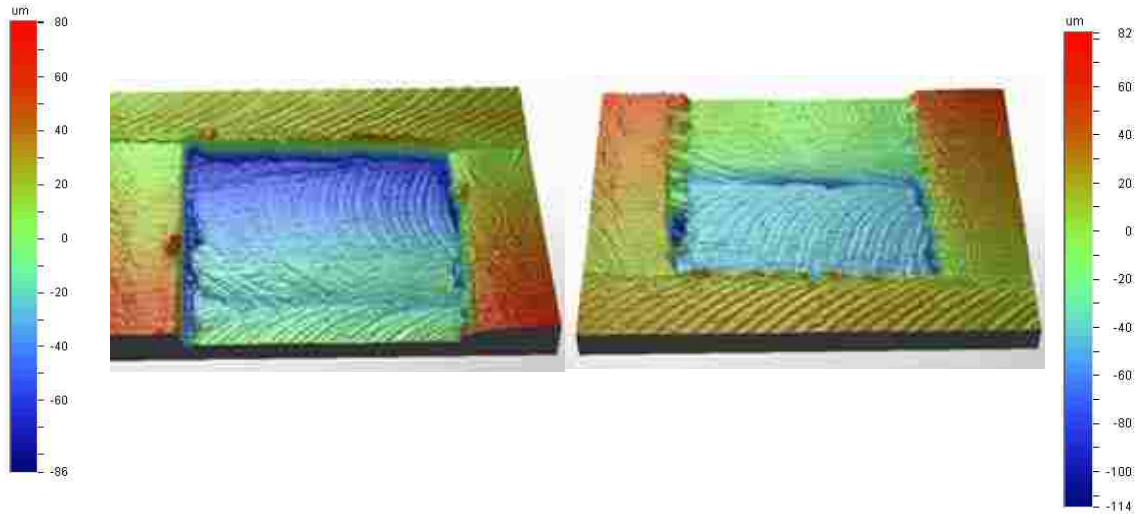
Insert 1



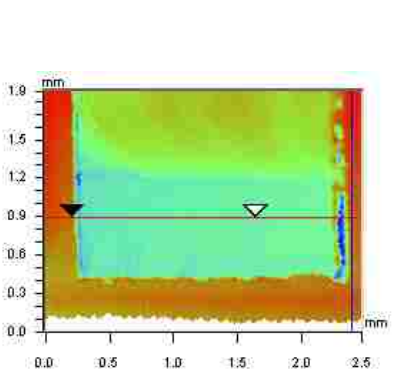
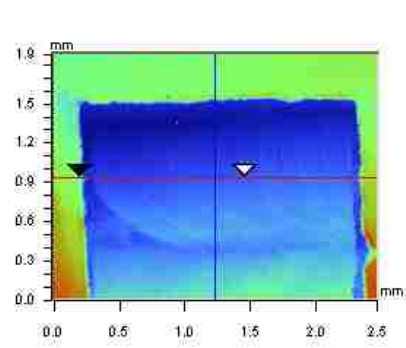
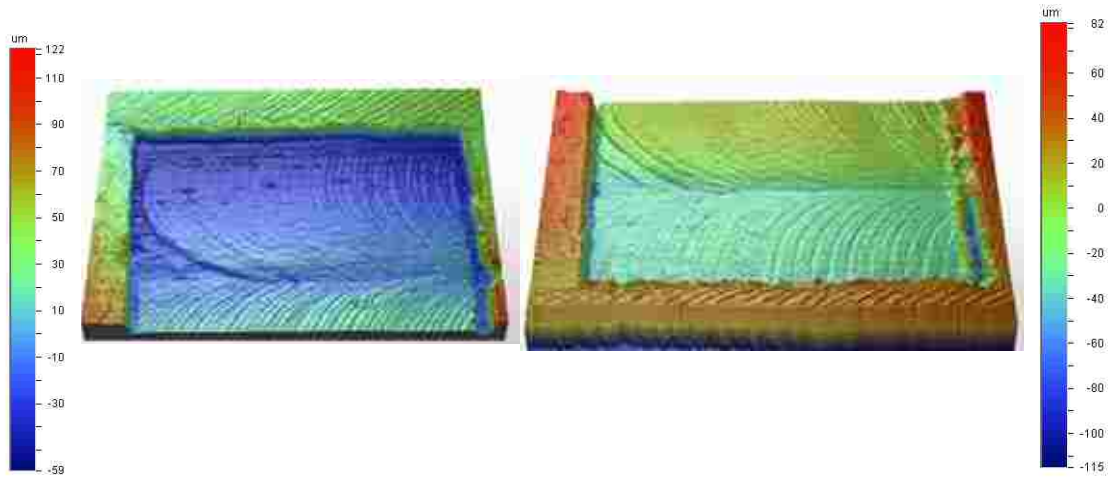
Insert 1- Void 1



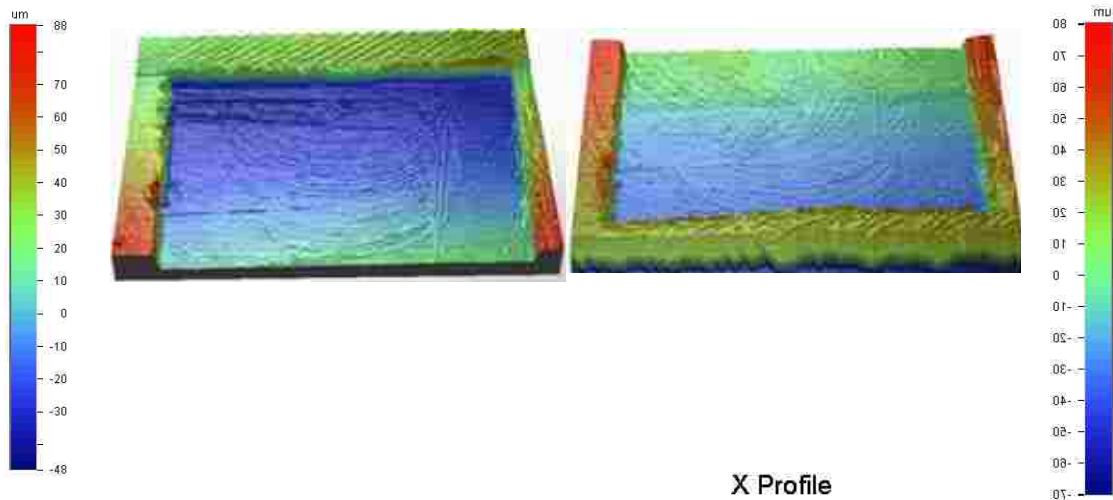
Insert 1- Void 2



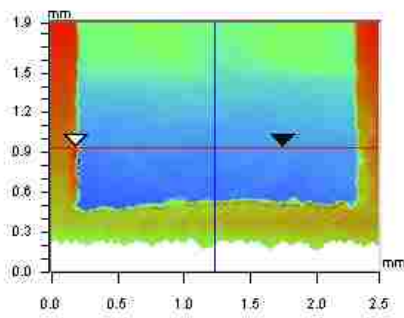
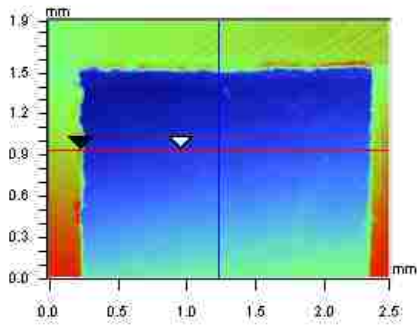
Insert 1- Void 3



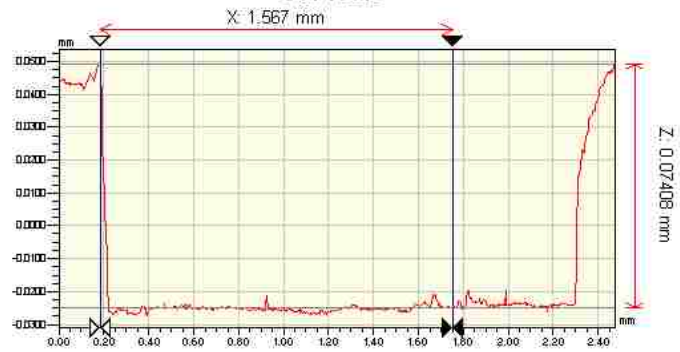
Insert 1- Void 4



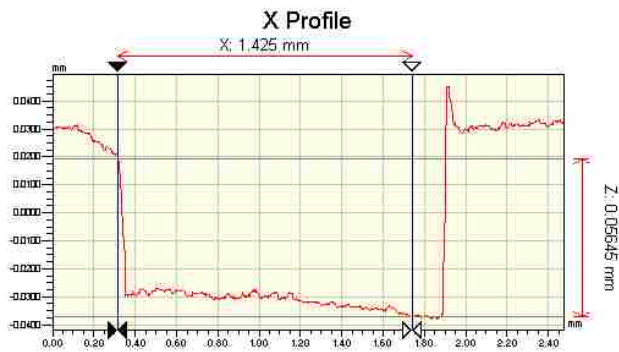
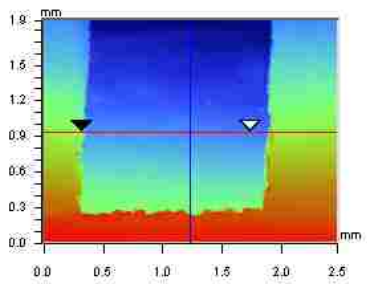
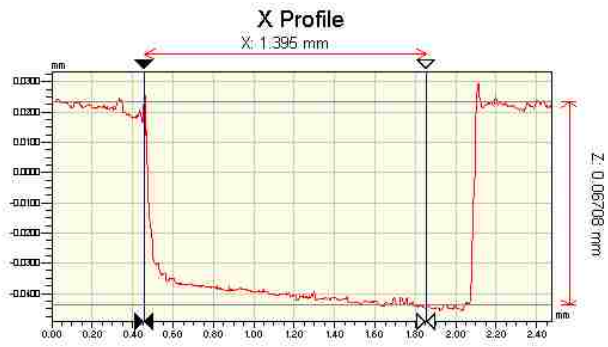
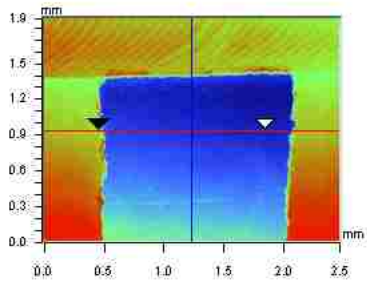
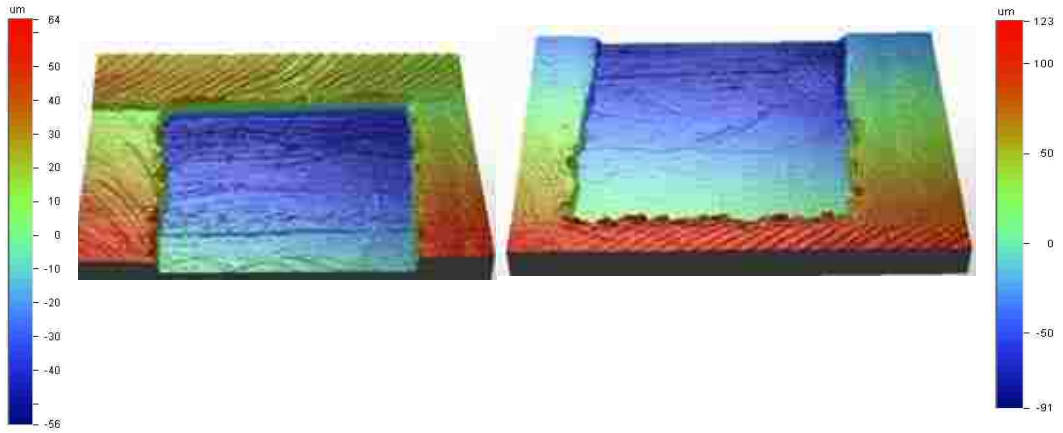
X Profile



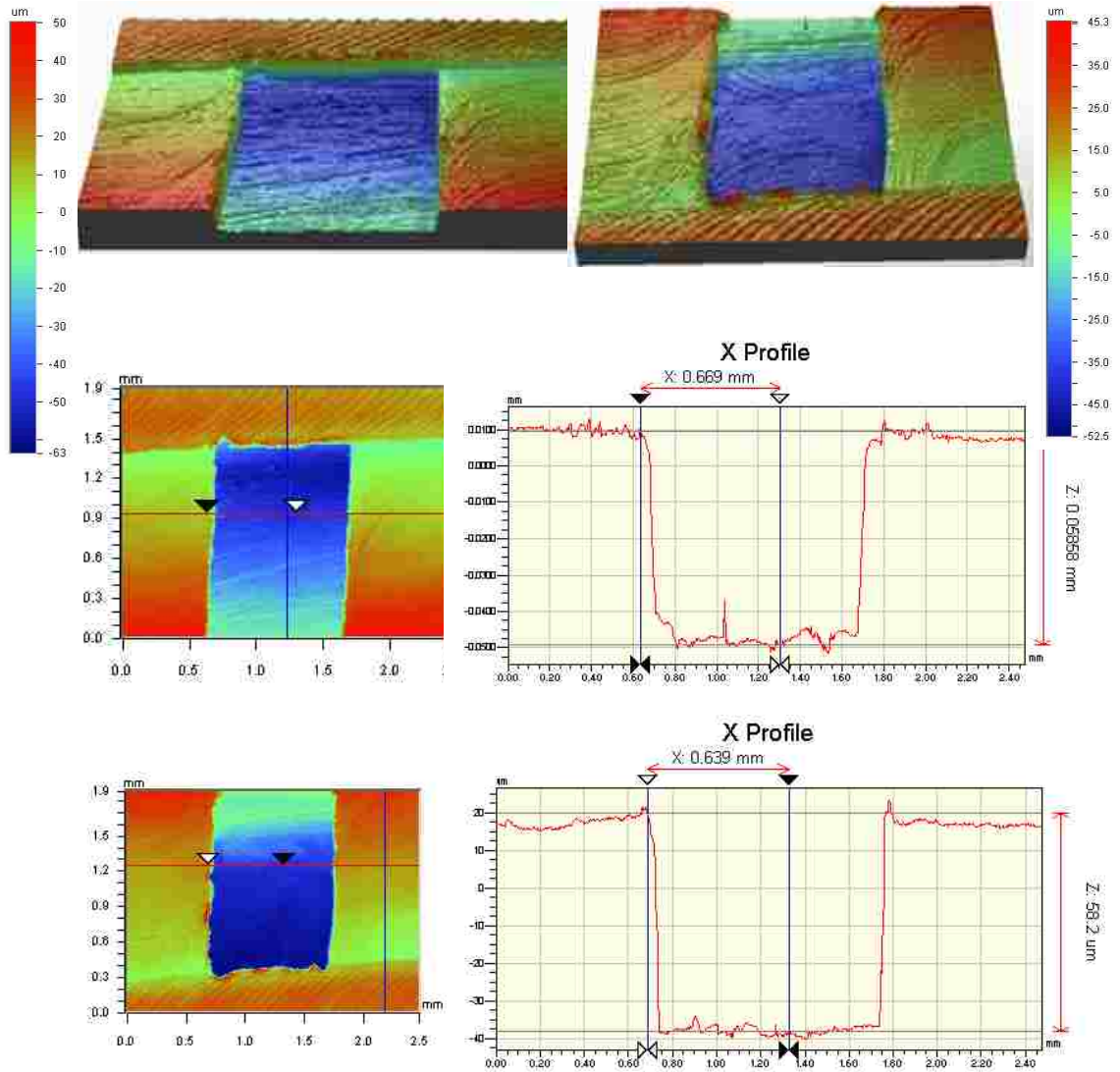
X Profile



Insert 1- Void 5



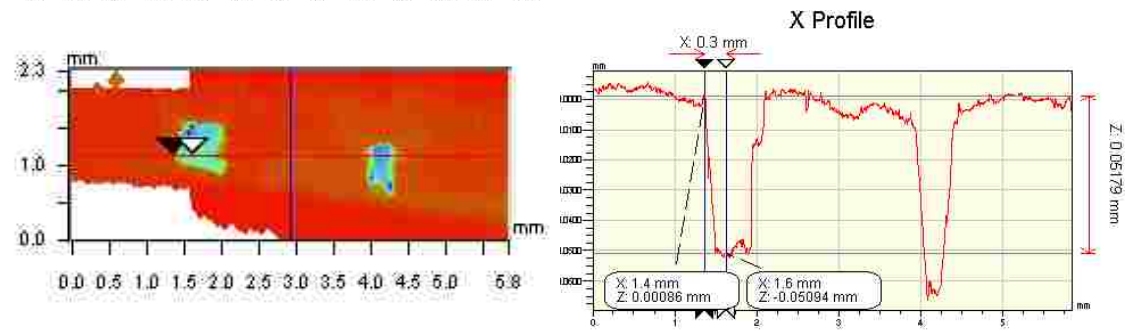
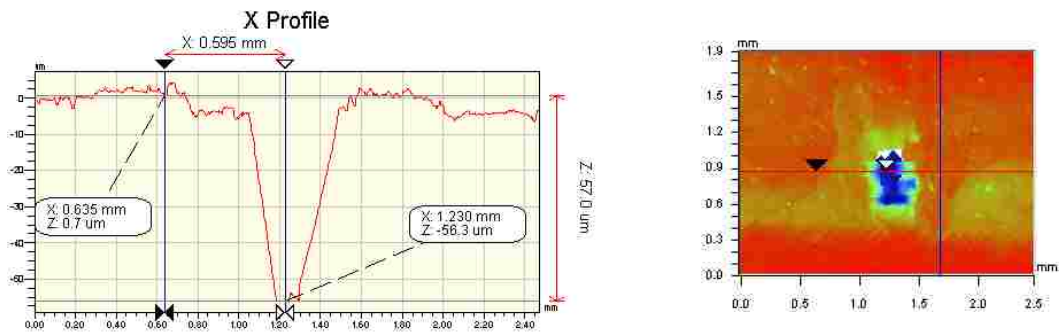
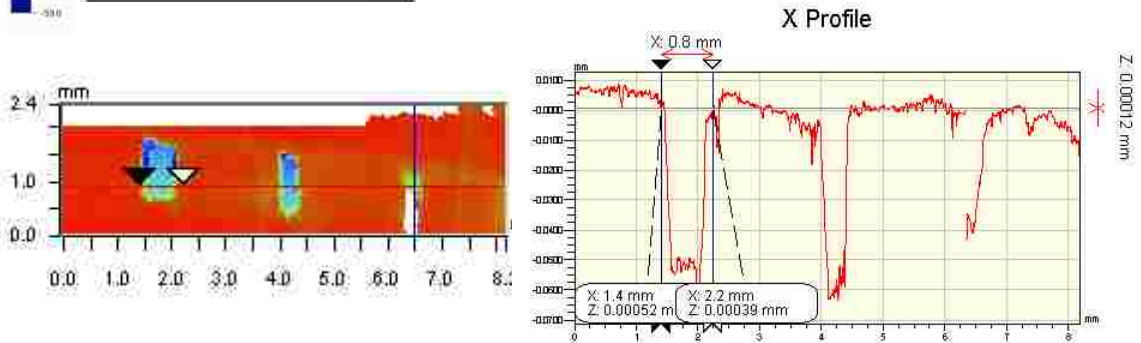
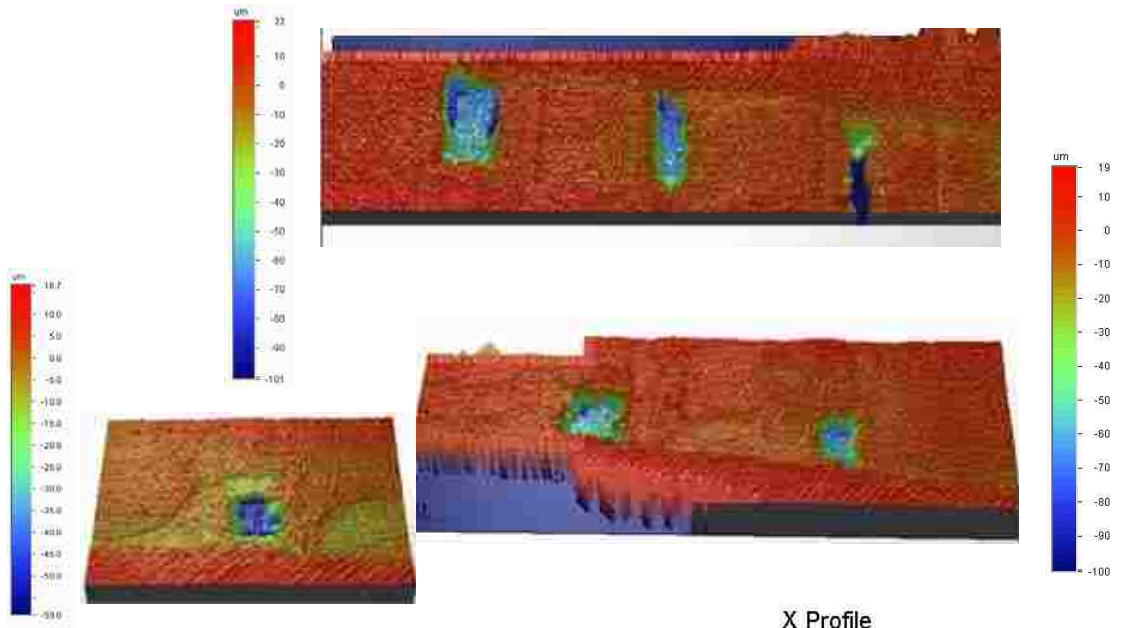
Insert 1- Void 6



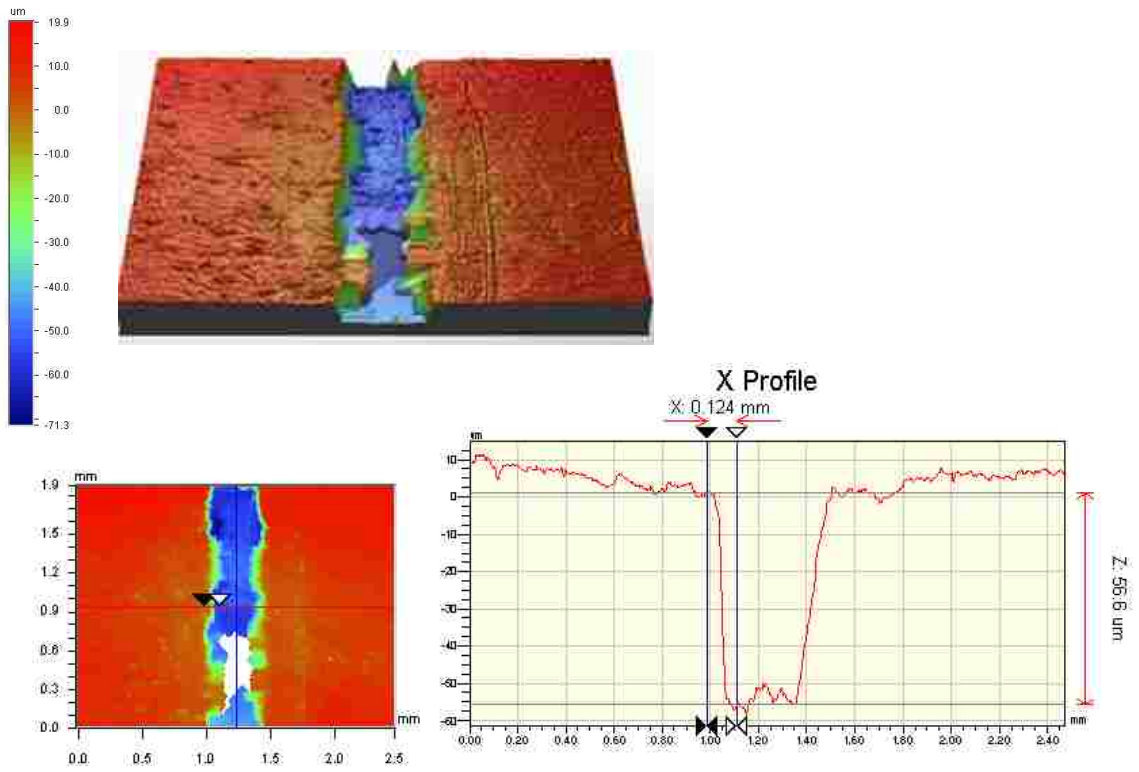
Insert 2



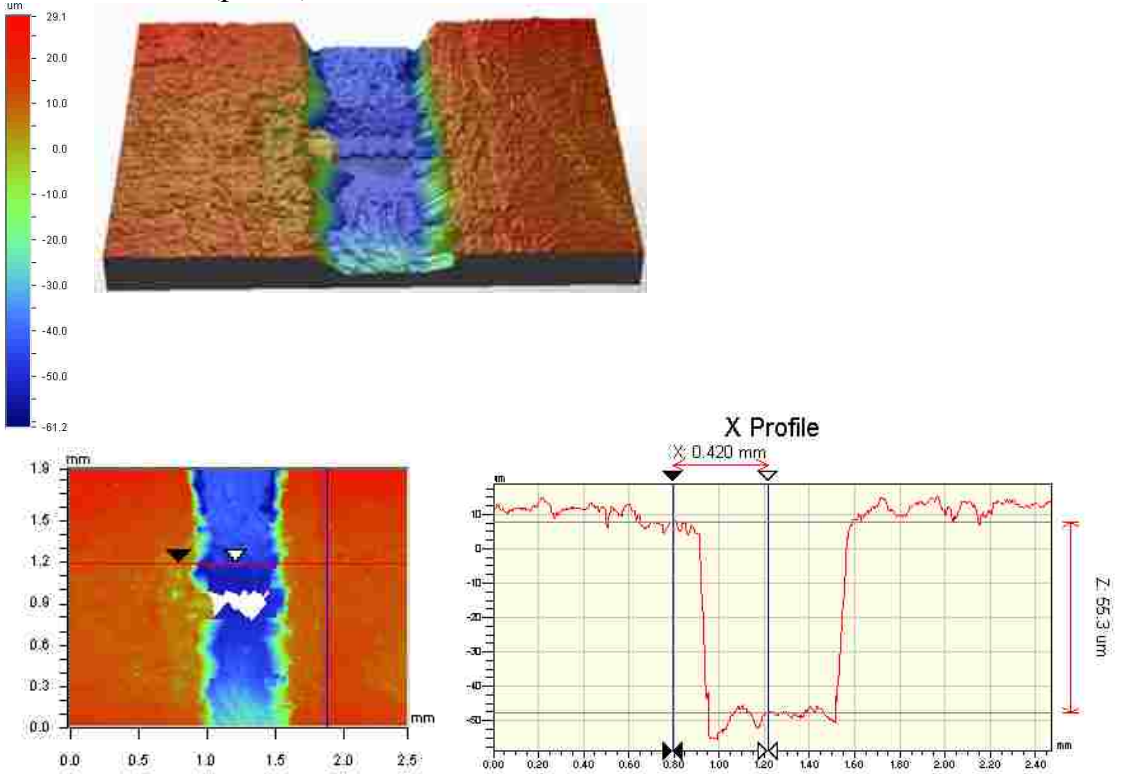
Insert 2 – Void 1, 2, 3 “Top and Low”



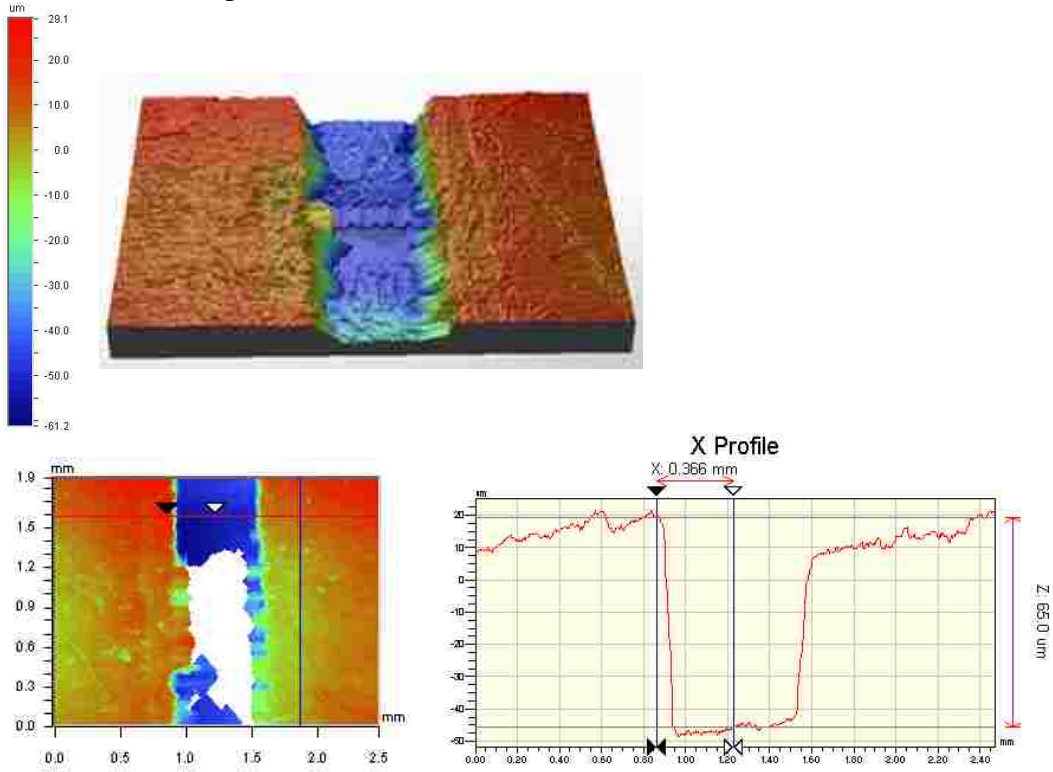
Insert 2 – Void 4 (partial)



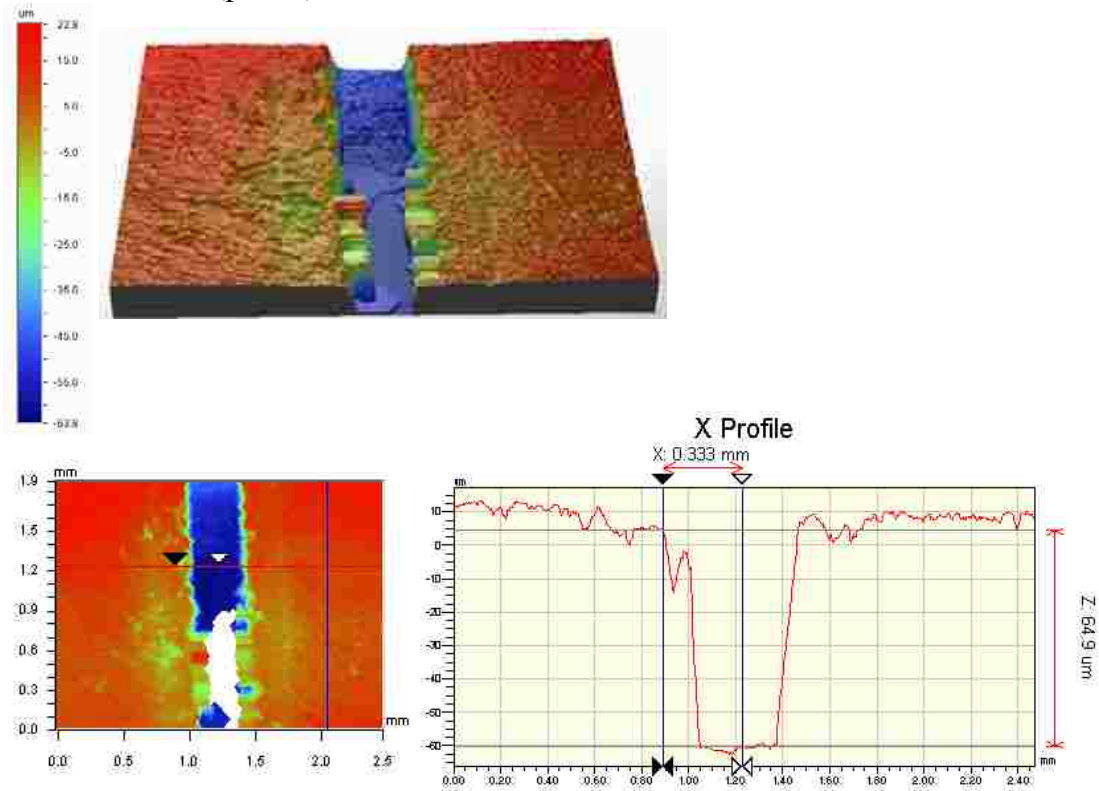
Insert 2- Void 5 (partial)



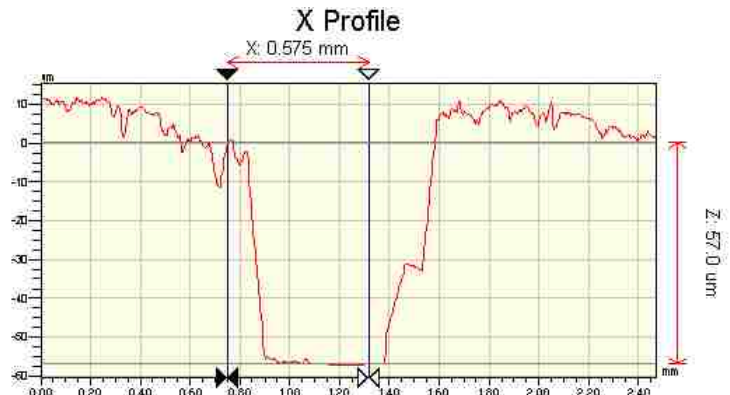
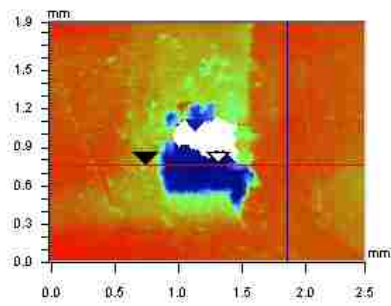
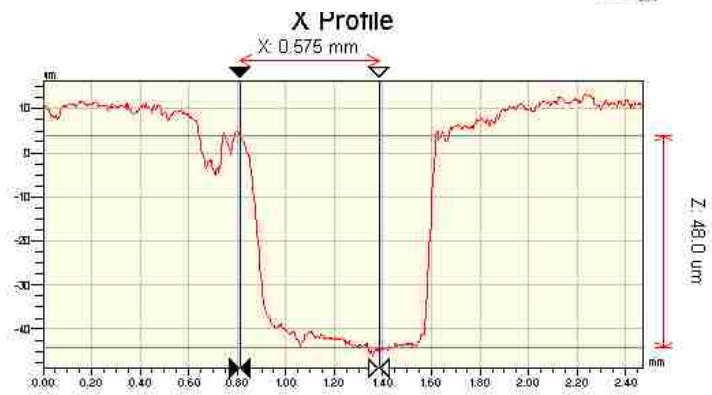
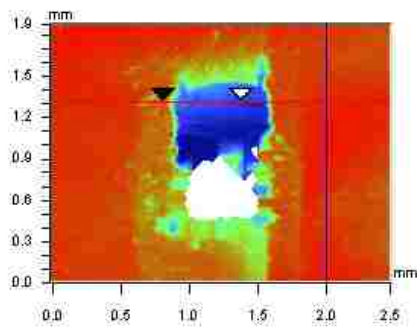
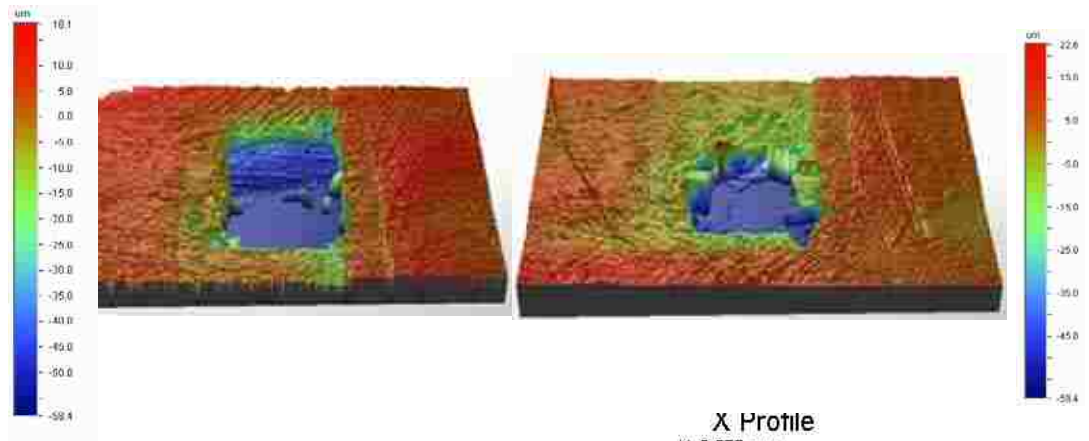
Insert 2- Void 6 (partial)



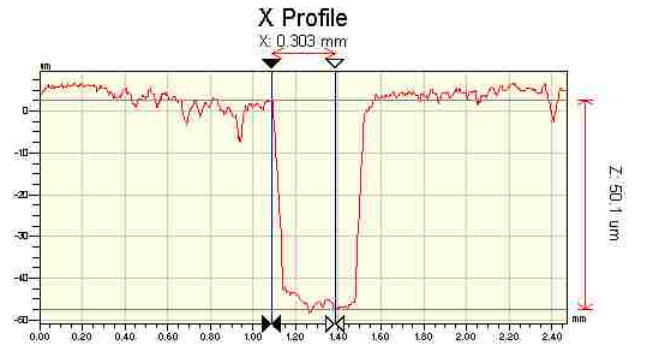
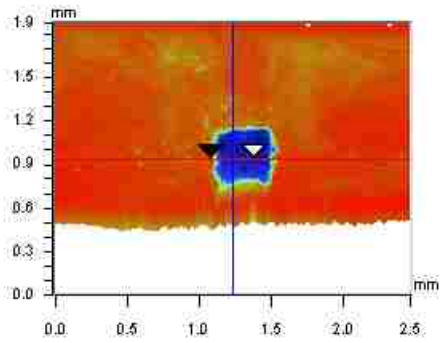
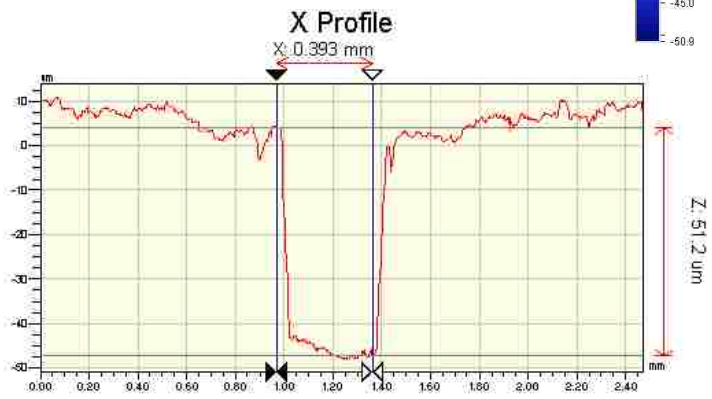
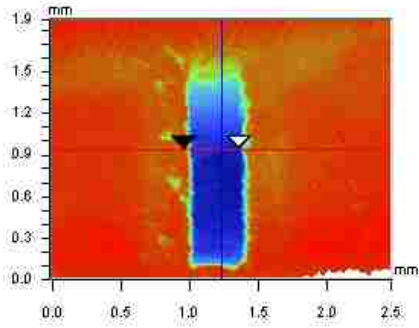
Insert 2- Void 7 (partial)



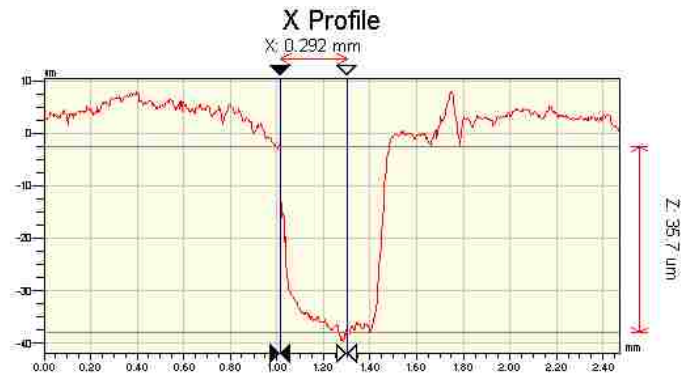
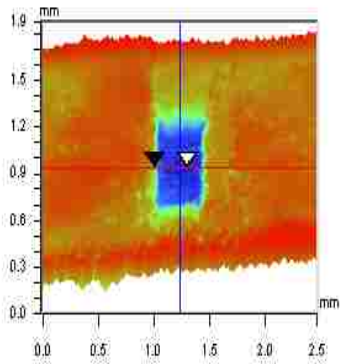
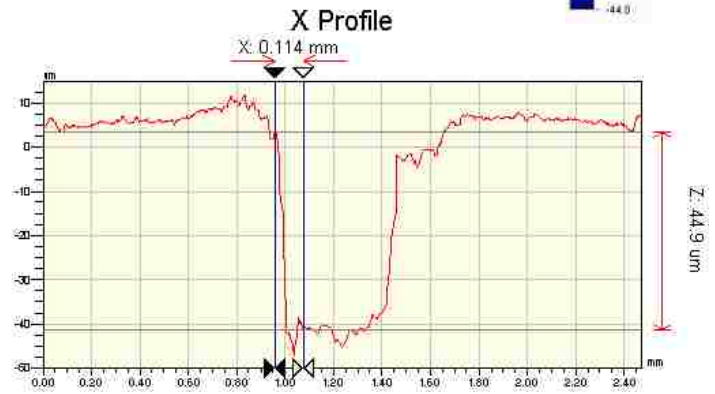
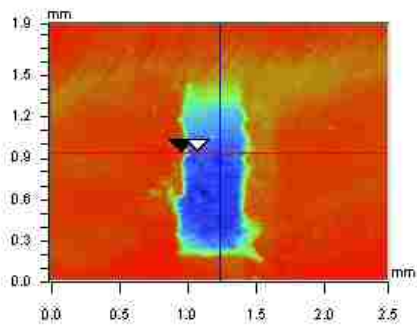
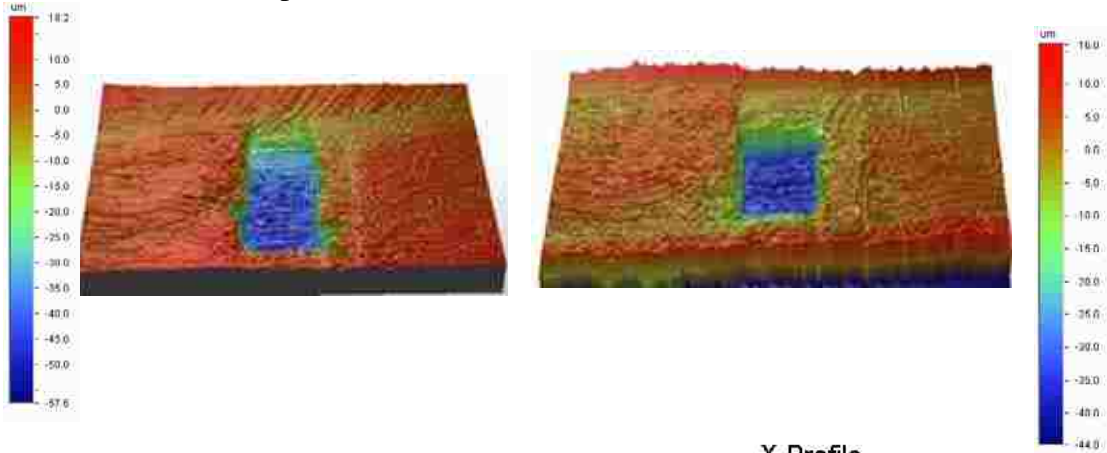
Insert 2- Void 8 “Top and Low”



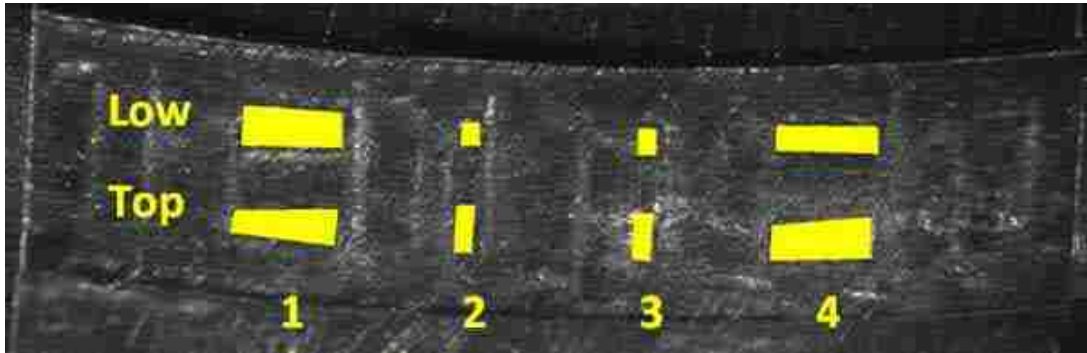
Void 9 "Top and Low"



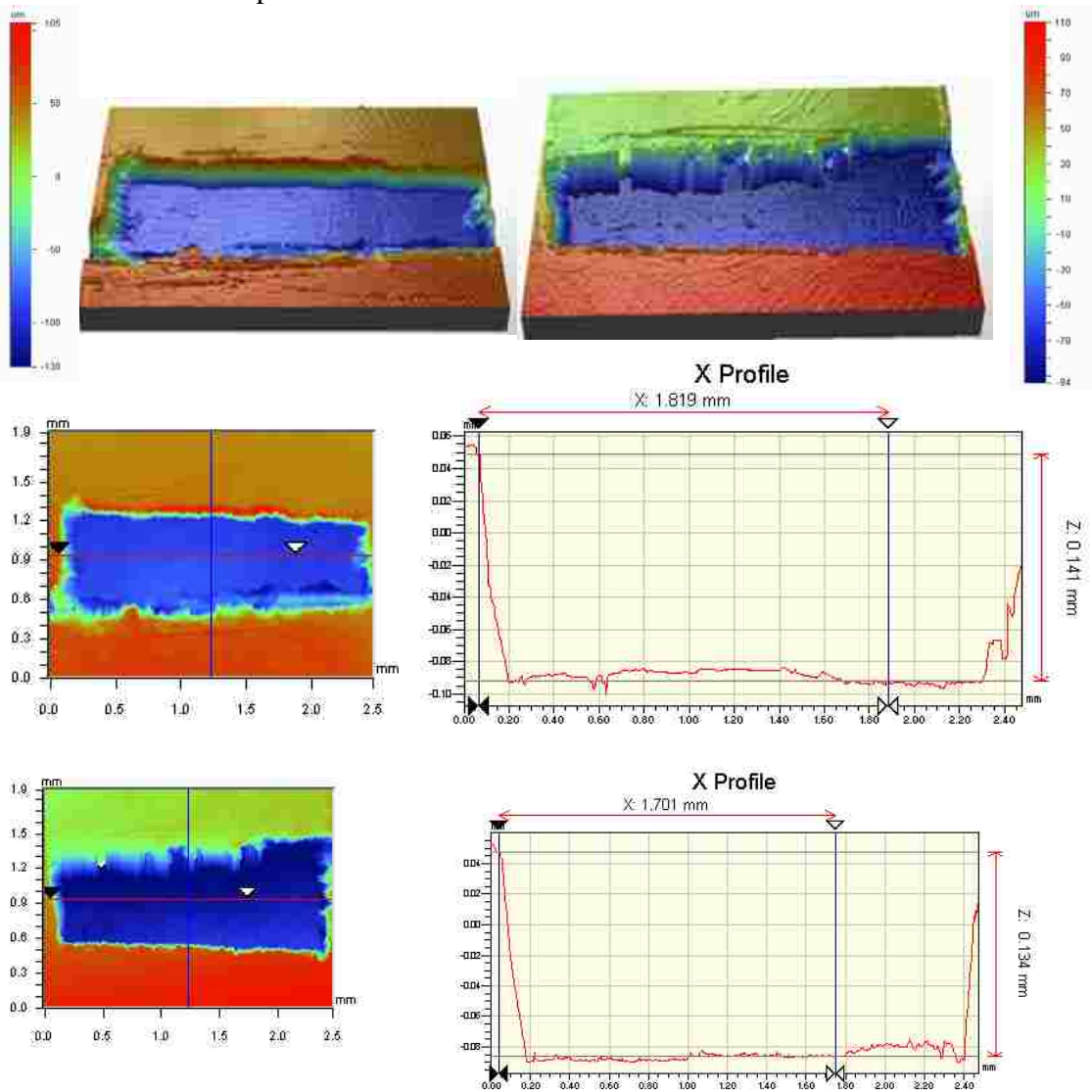
Insert 2- Void 10 “Top and Low”



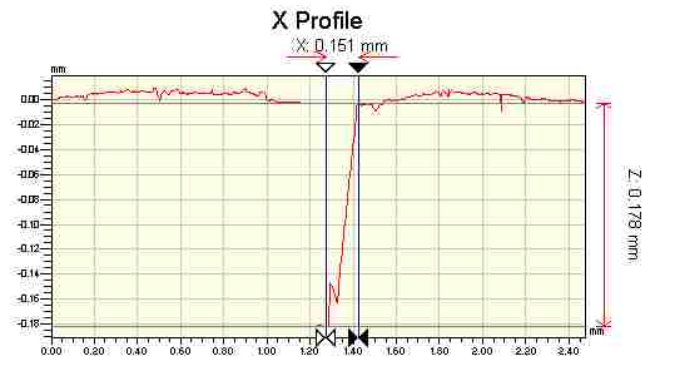
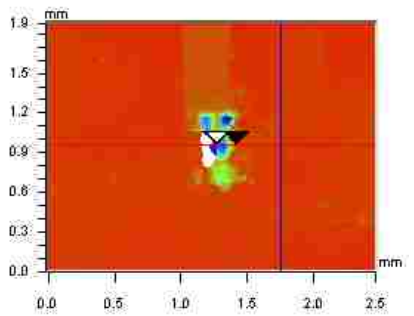
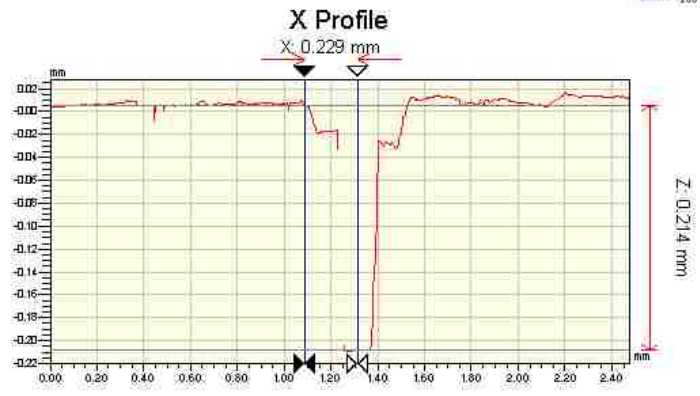
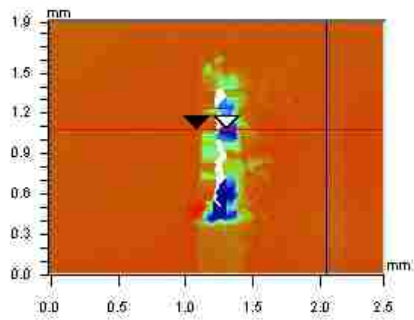
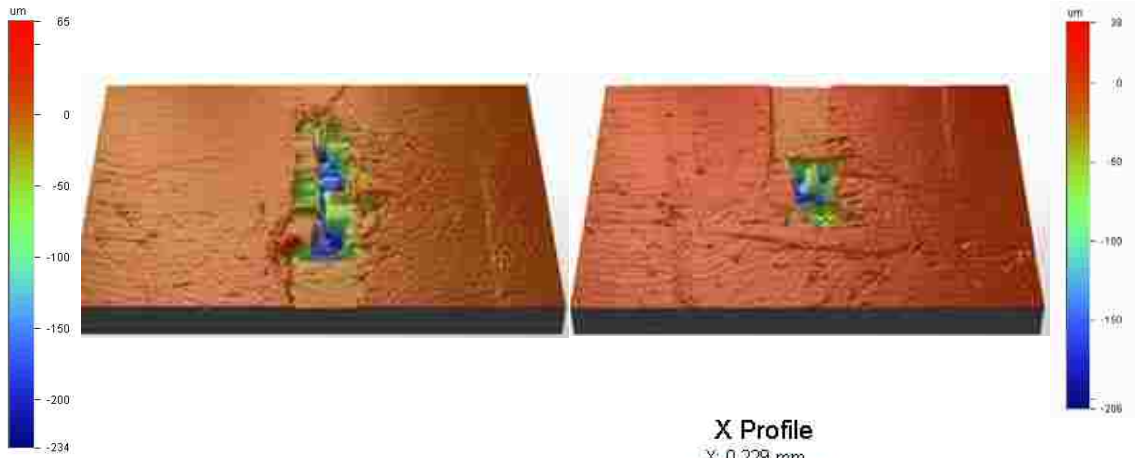
Insert 3



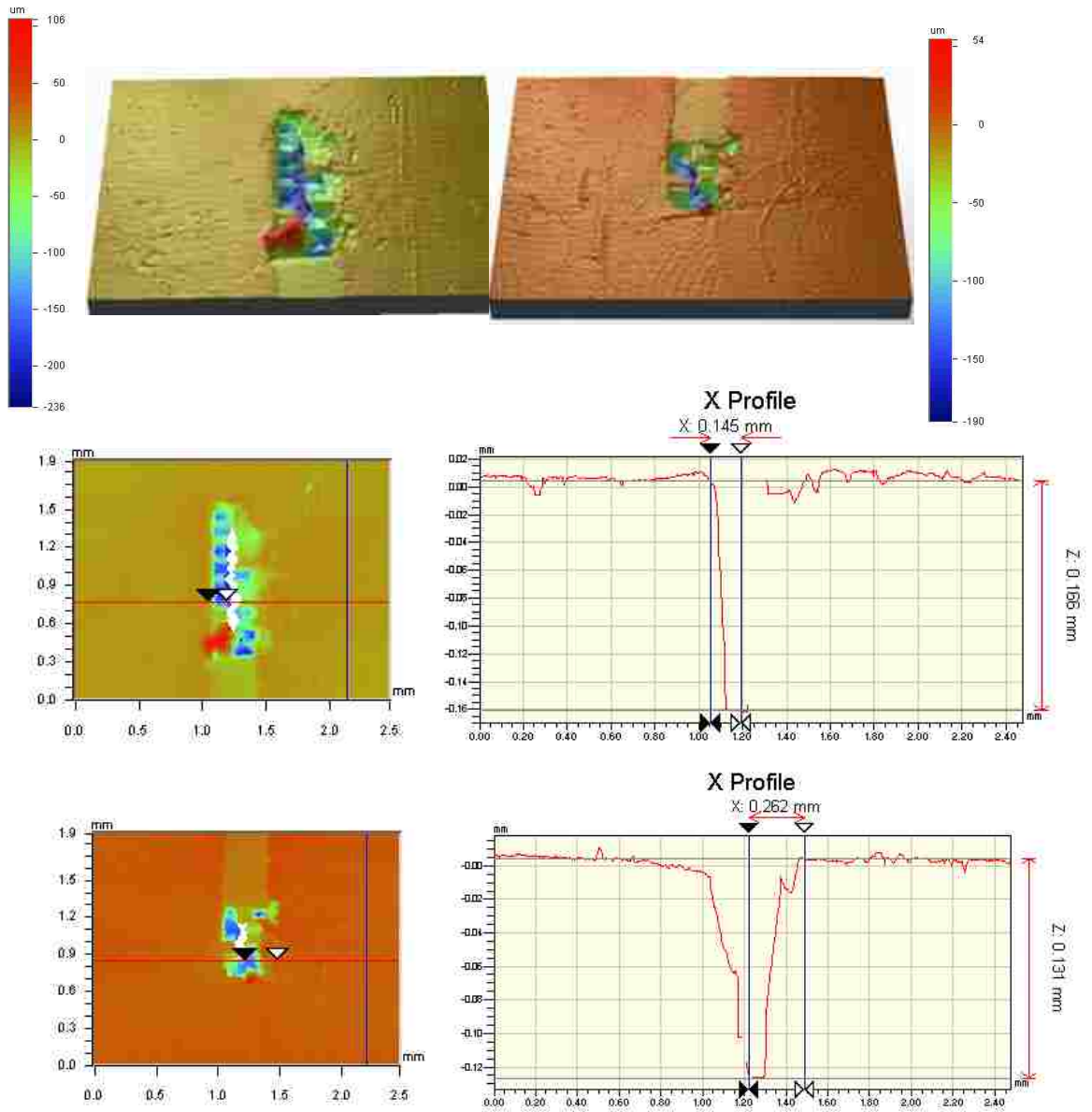
Insert 3- Void 1 “Top and Low”



Insert 3- Void 2 “Top and Low”

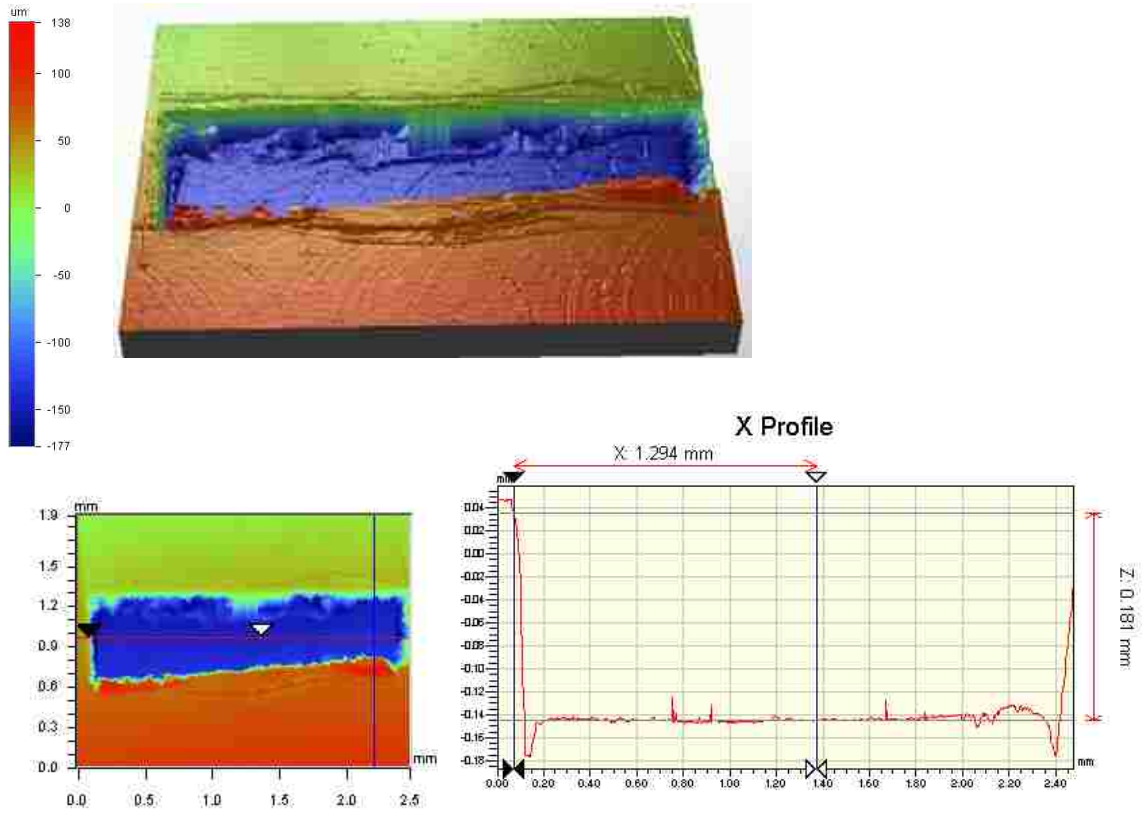


Insert 3- Void 3 “Top and Low”

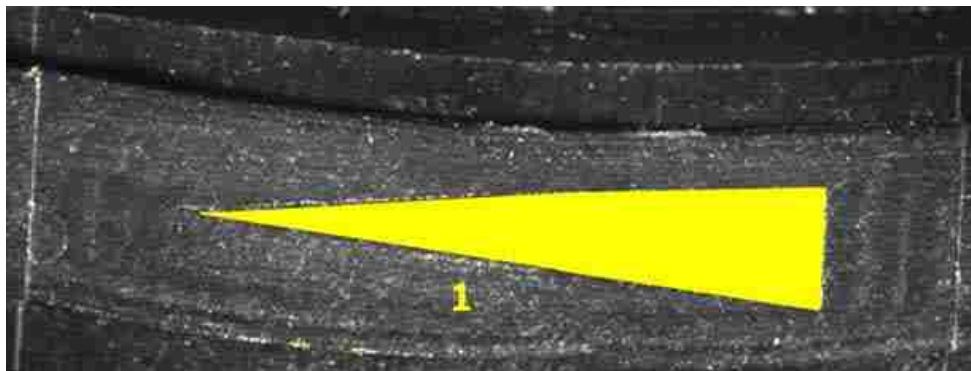


Insert 3- Void 4 “top” N/A

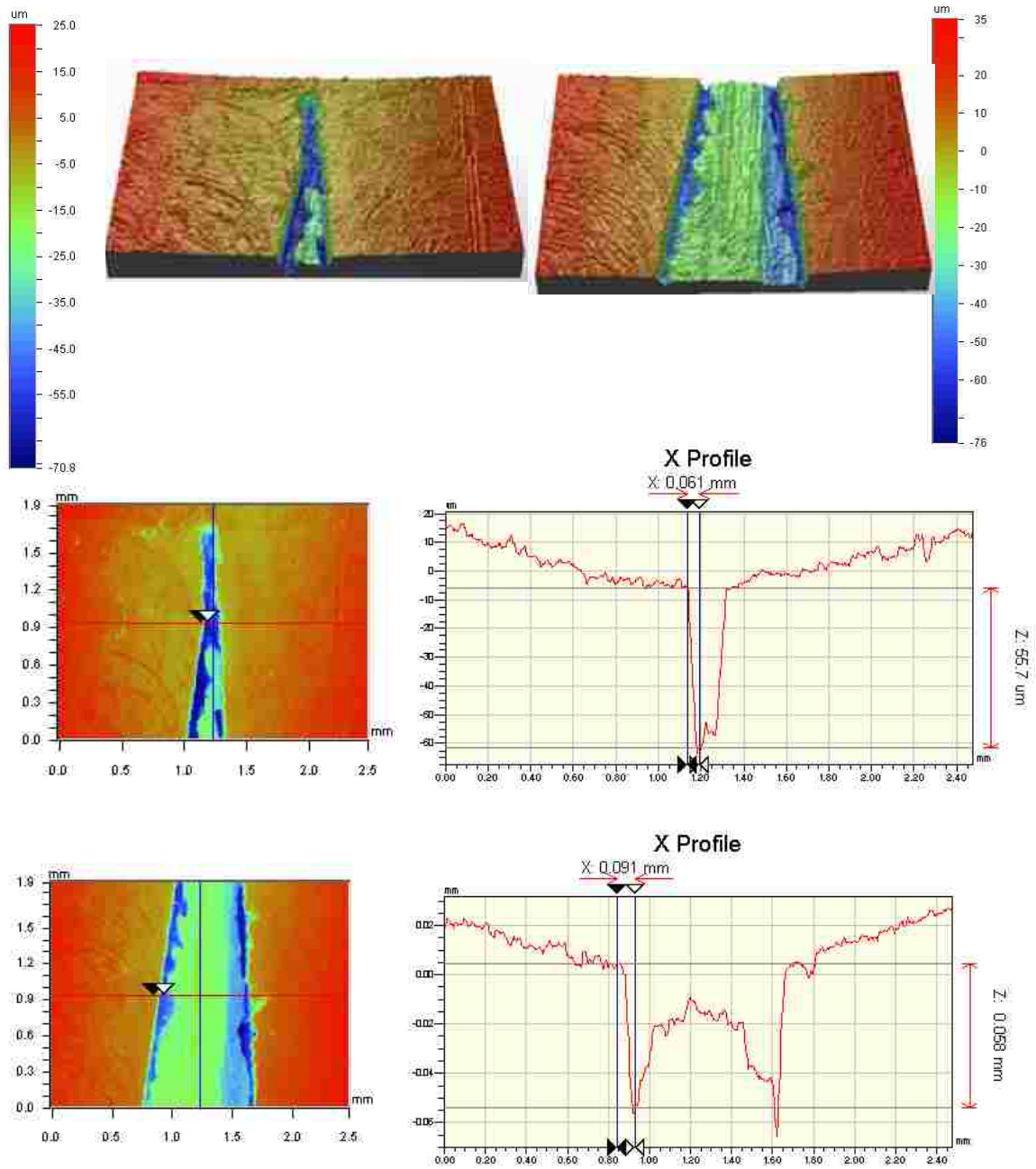
Insert 3- Void 4 “Low”



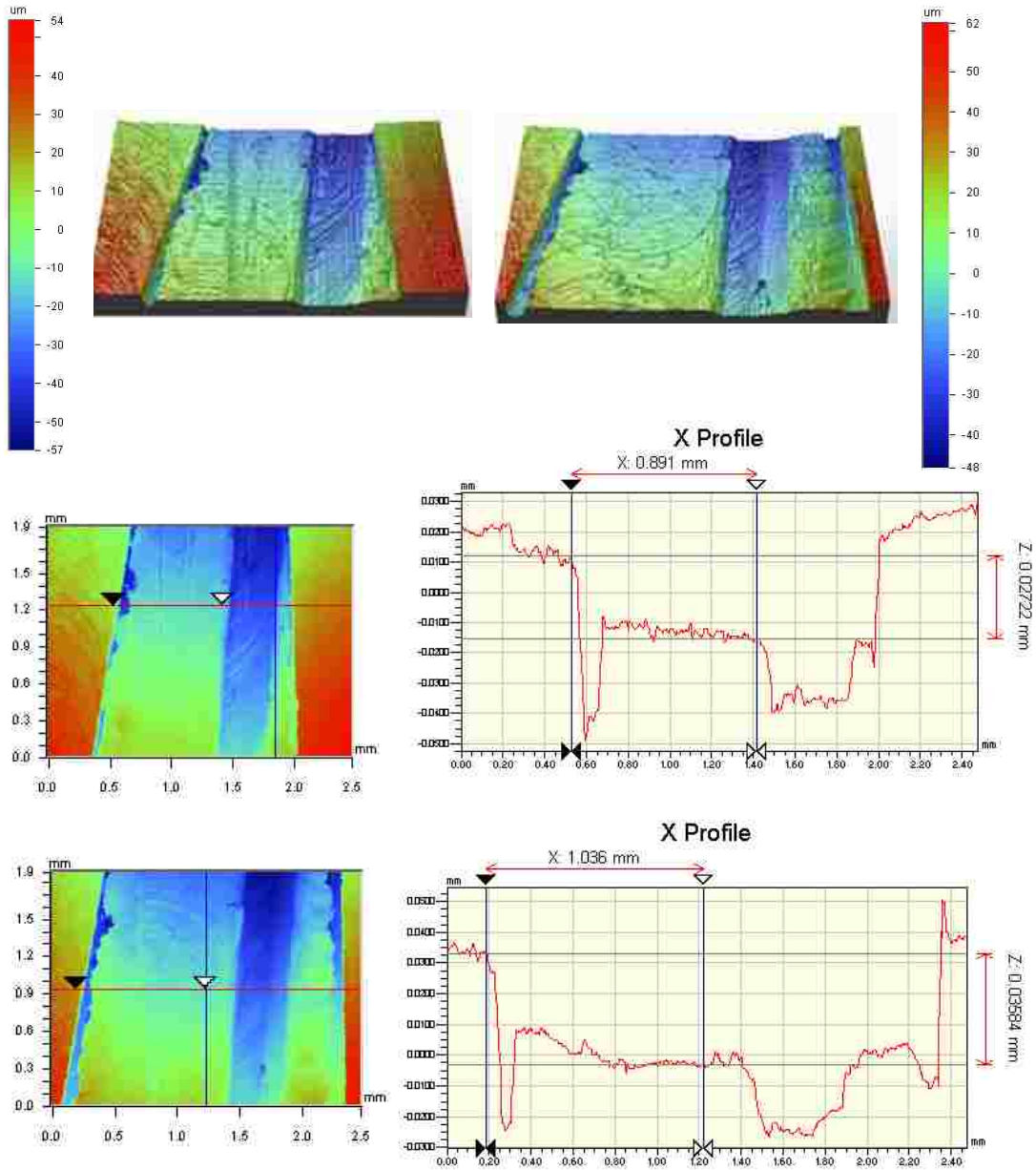
Insert 4



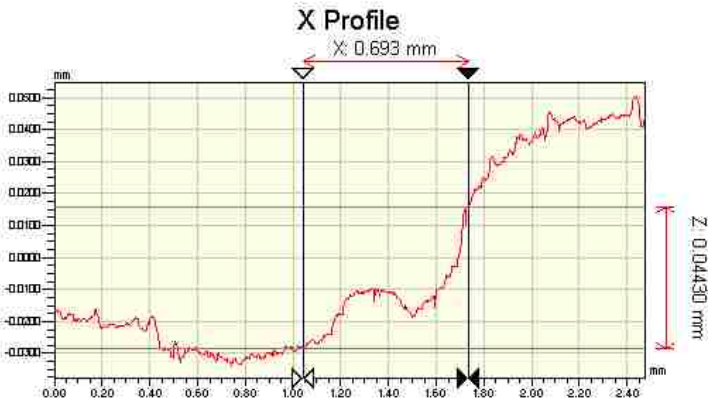
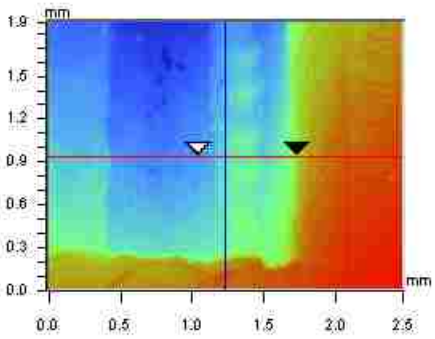
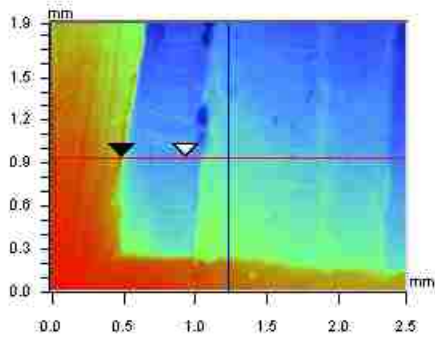
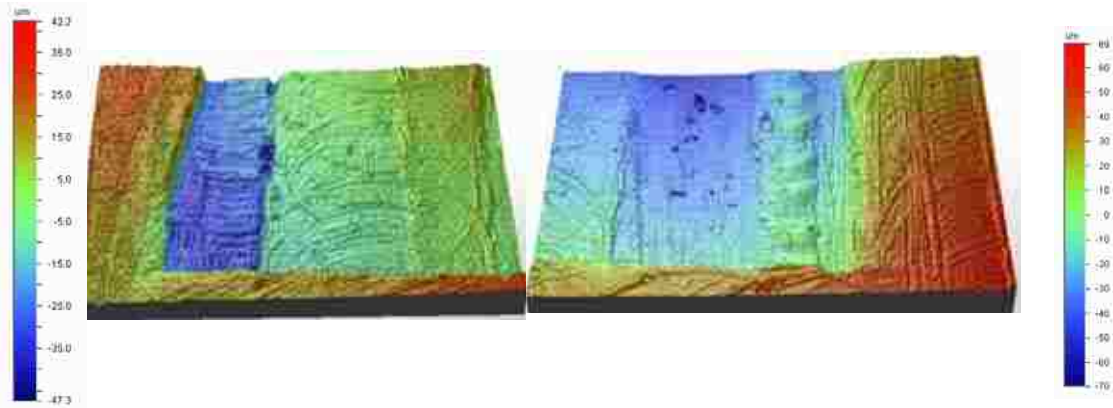
Insert 4- Void 1



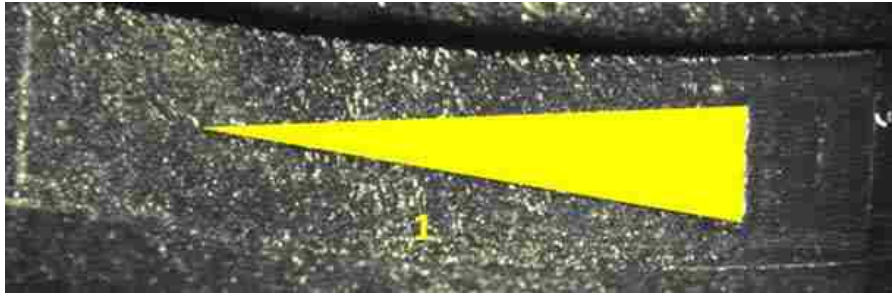
Insert 4- Void 1 cont'd



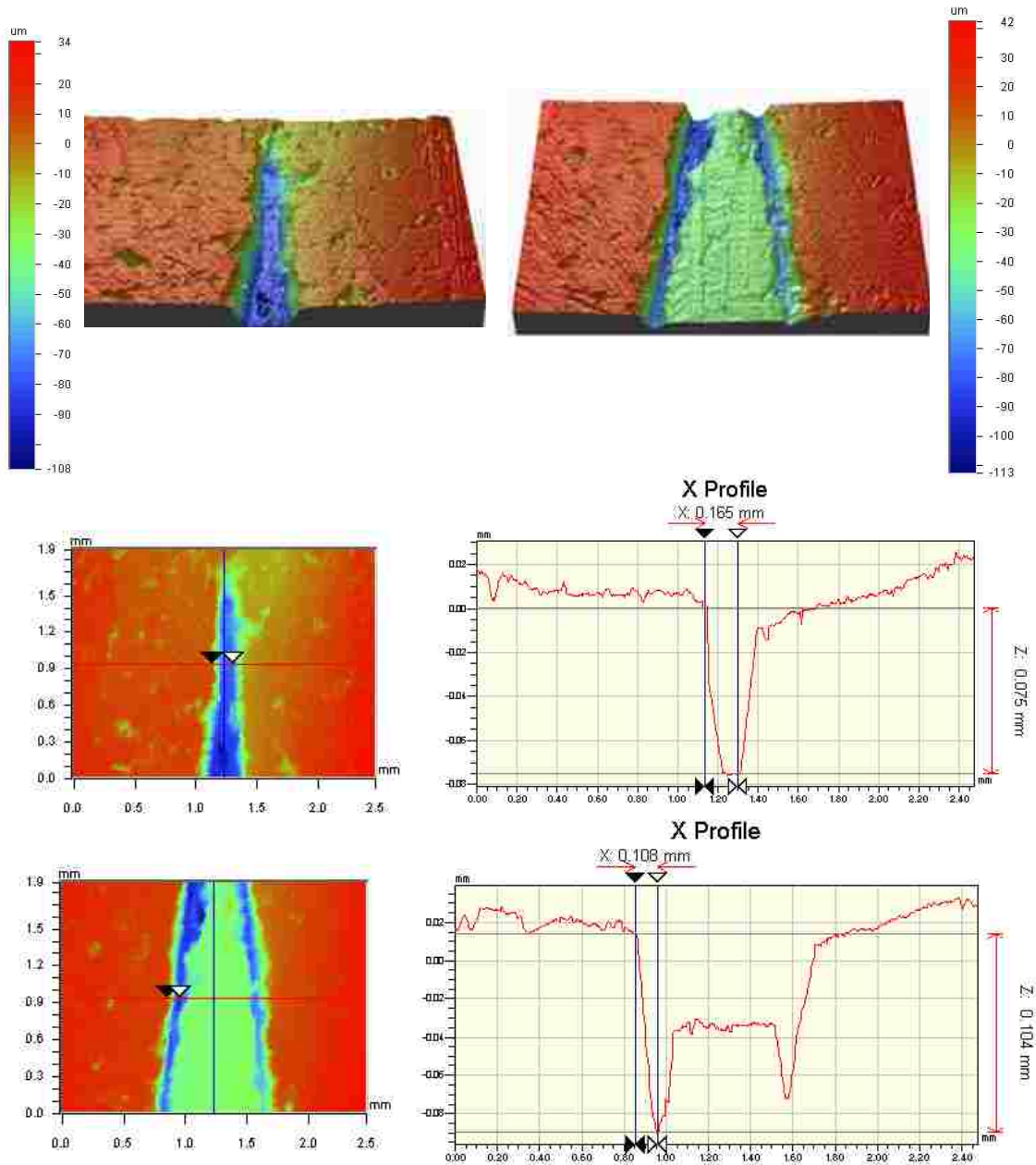
Insert 4- Void 1 cont'd



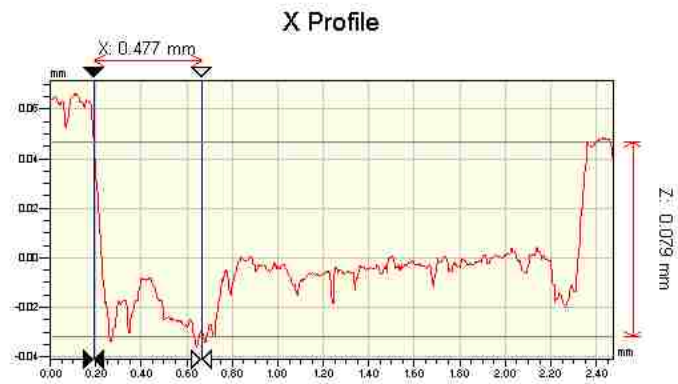
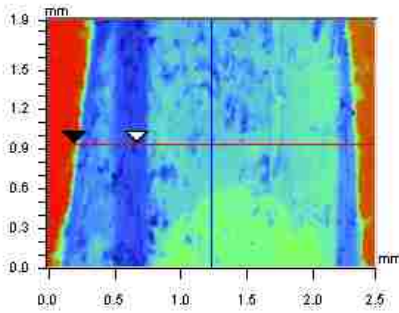
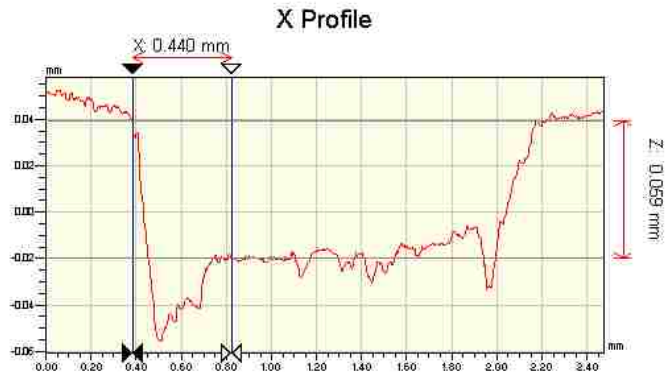
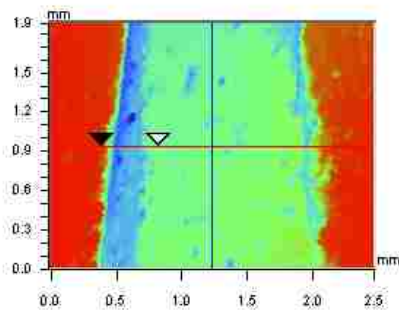
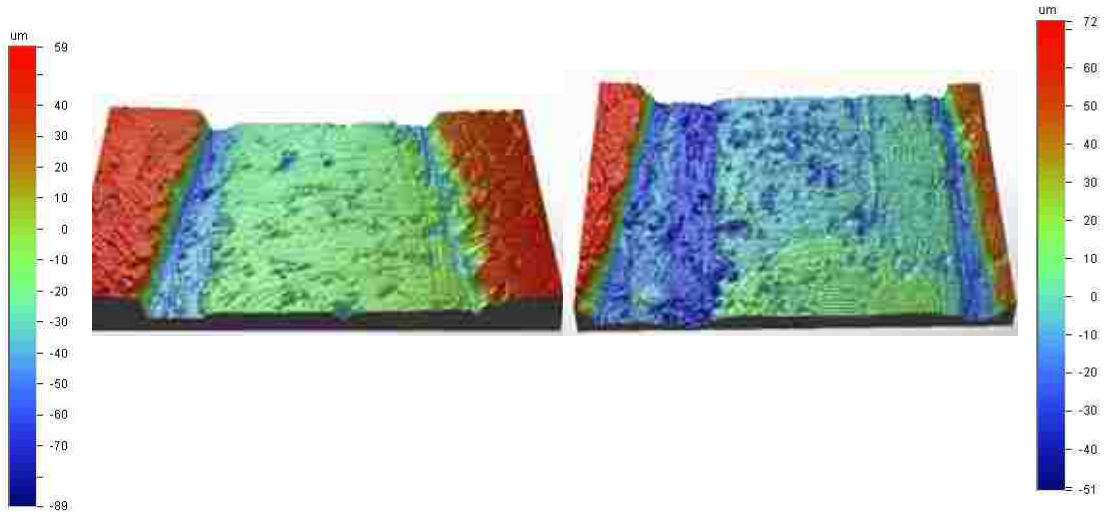
Insert 5



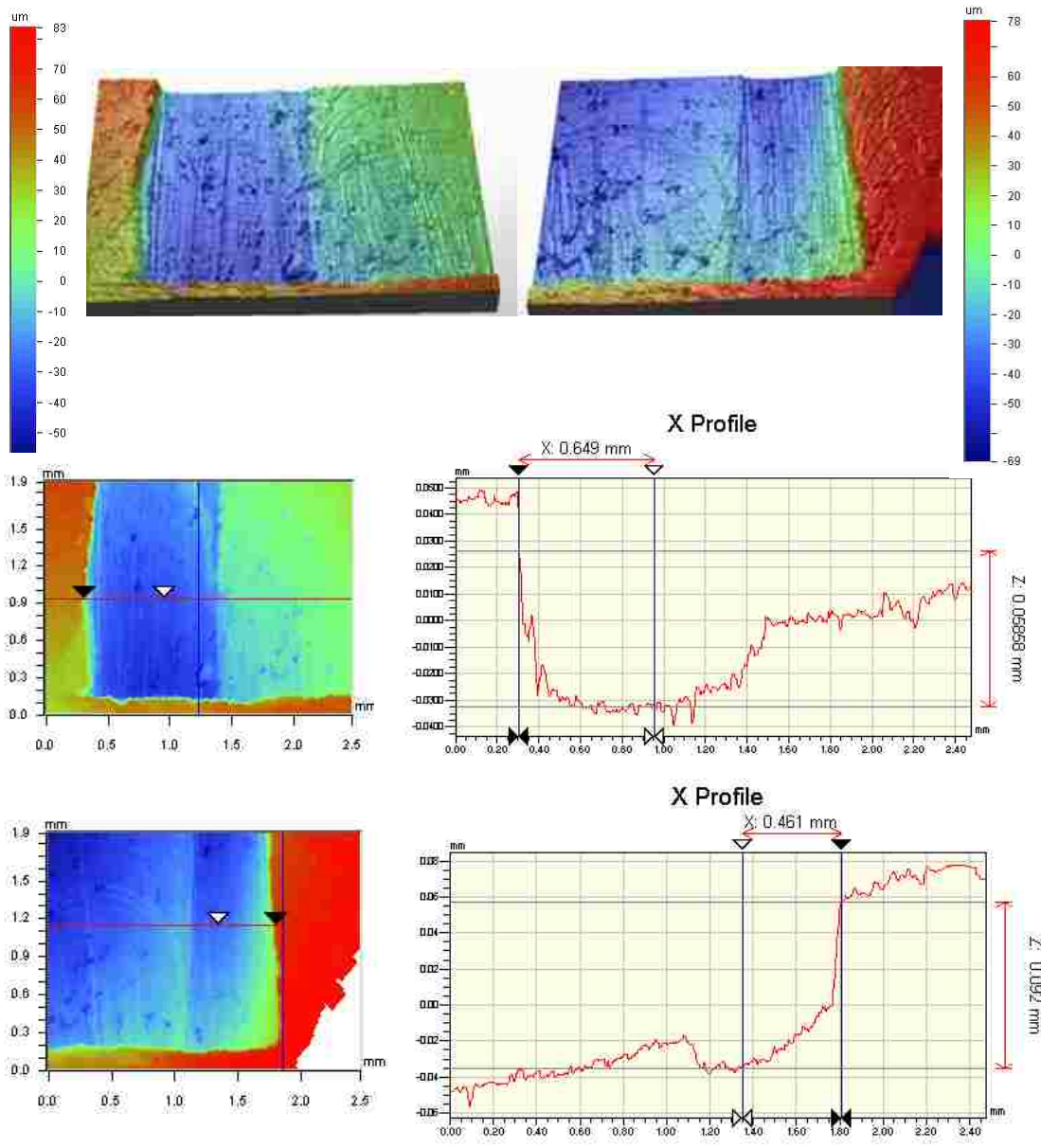
Insert 5- Void 1



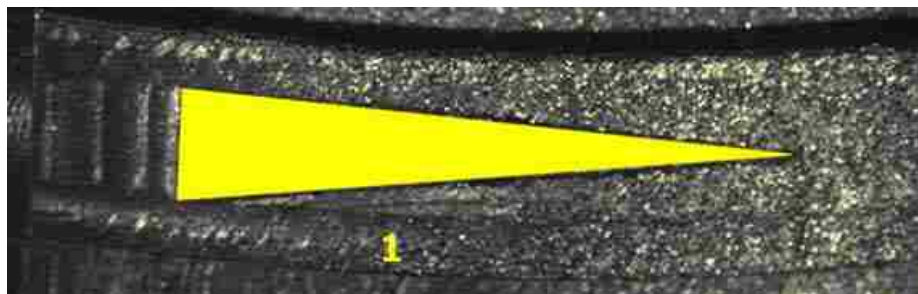
Insert 5- Void 1 cont'd



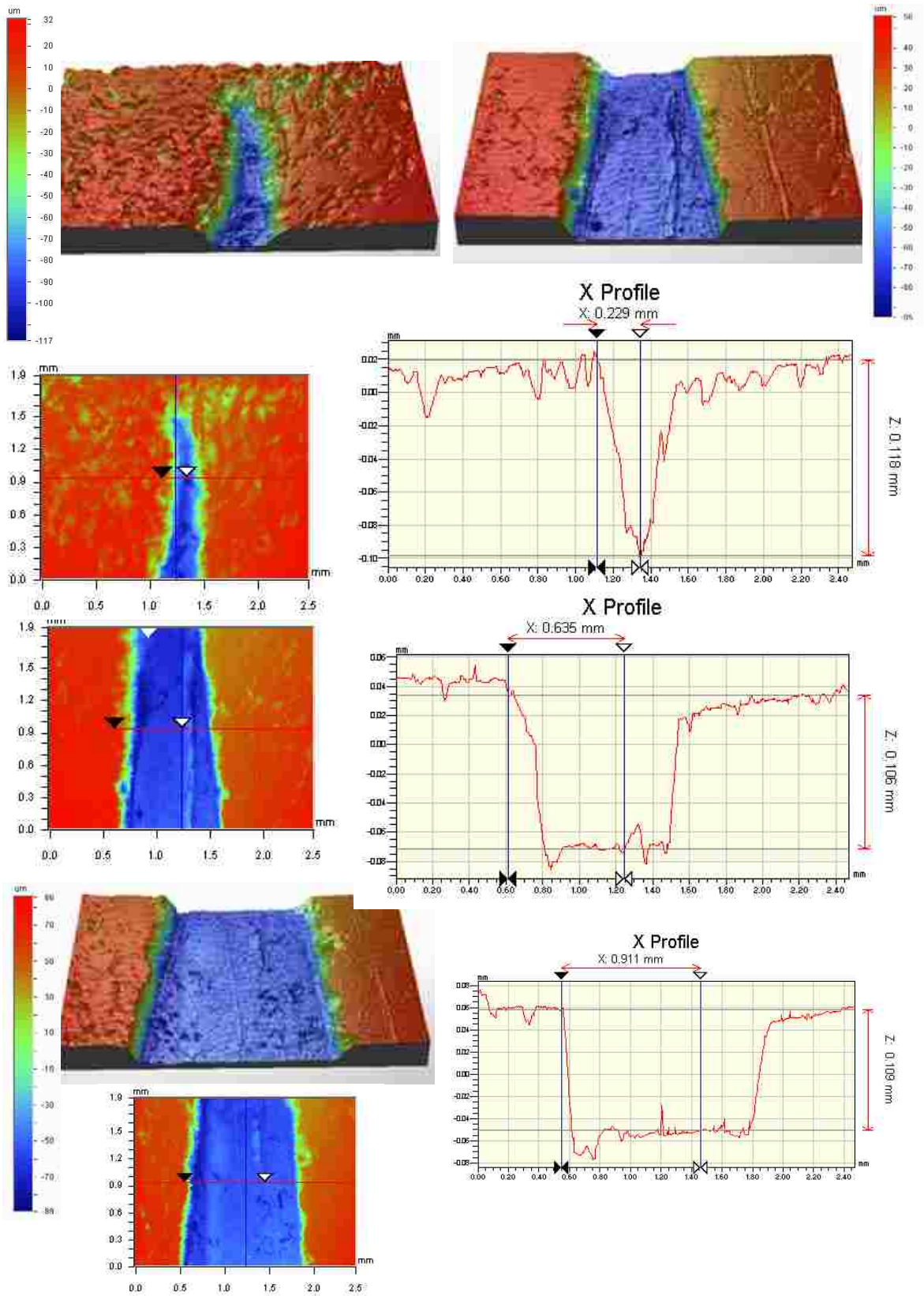
Insert 5- Void 1 cont'd



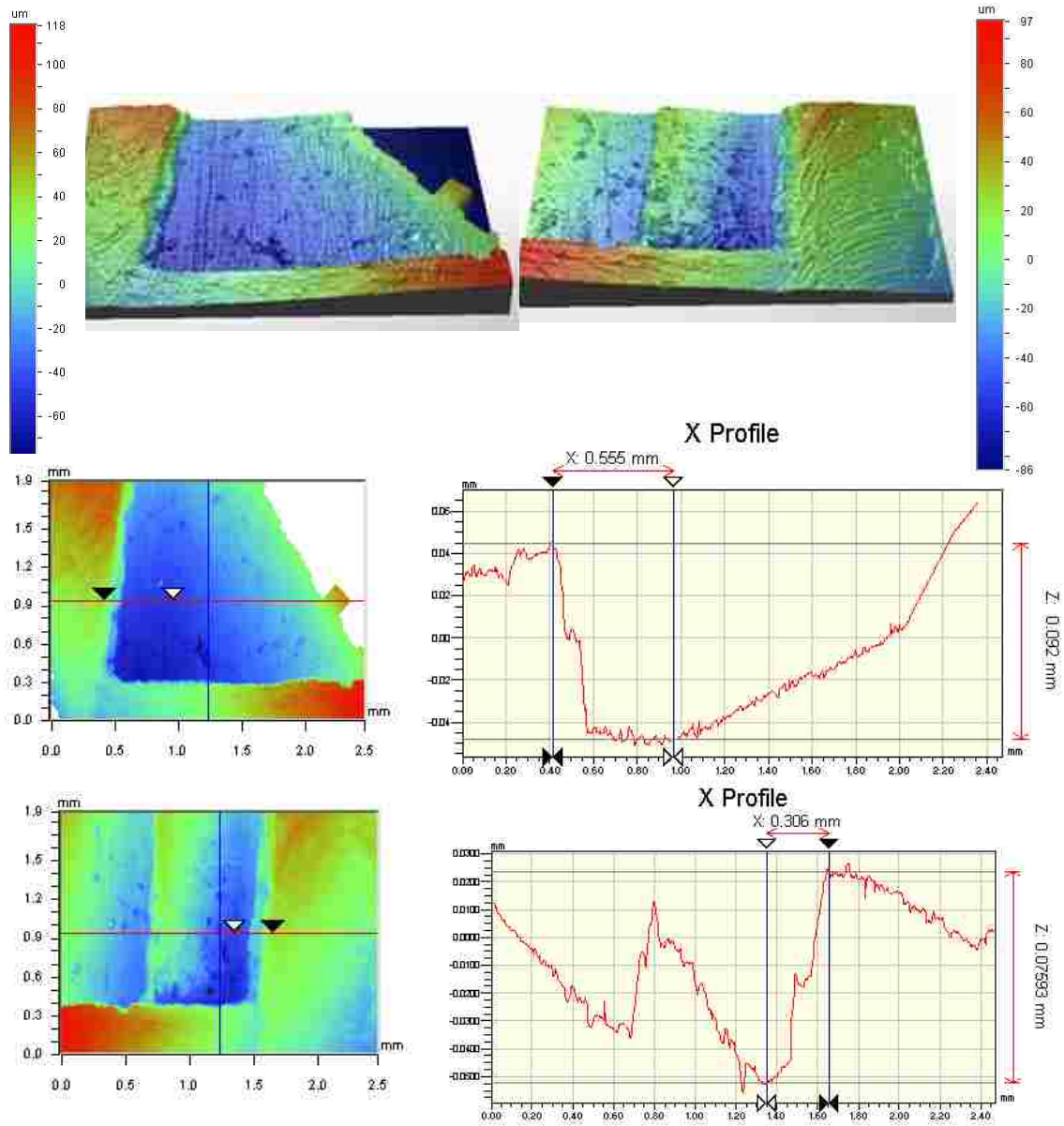
Insert 6



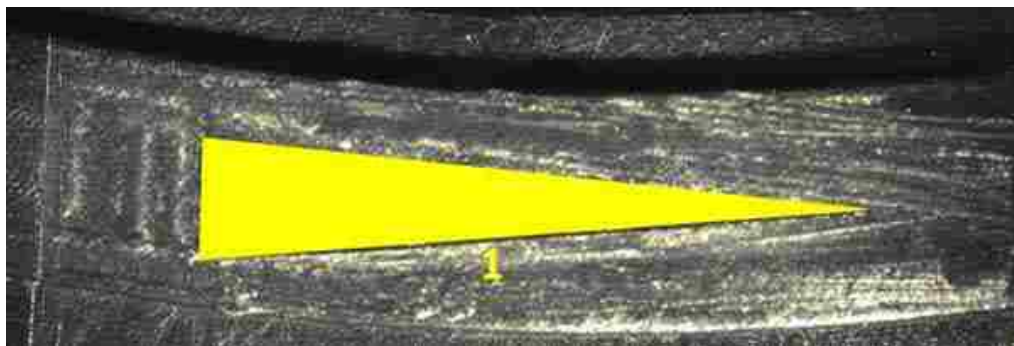
Insert 6- Void 1



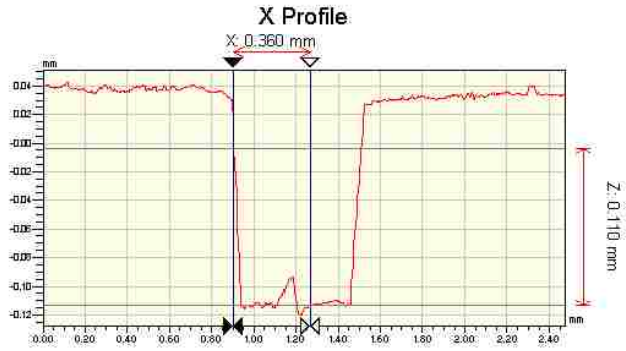
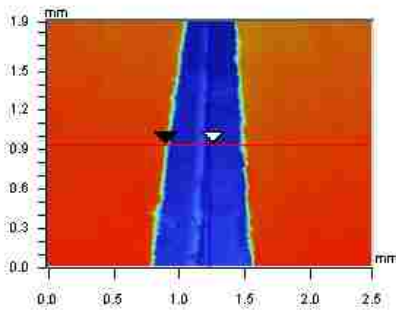
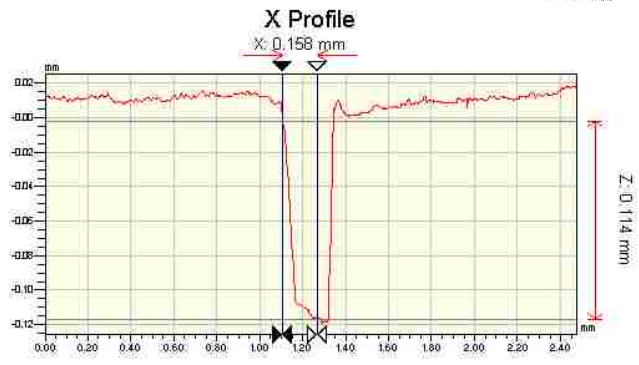
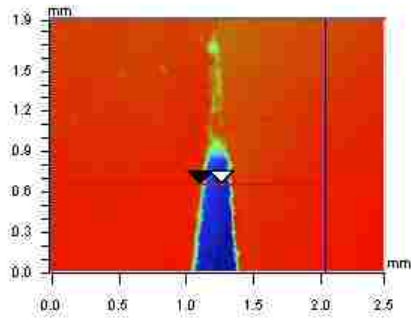
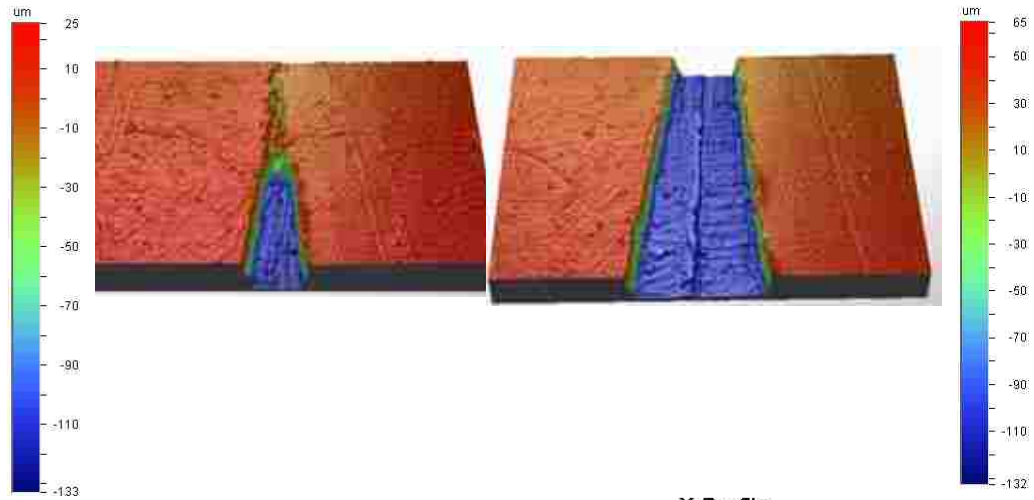
Insert 6- Void 1 cont'd



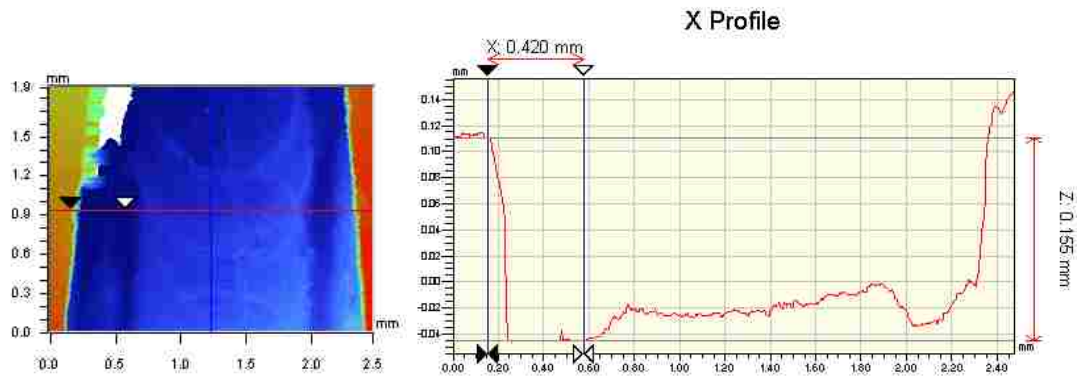
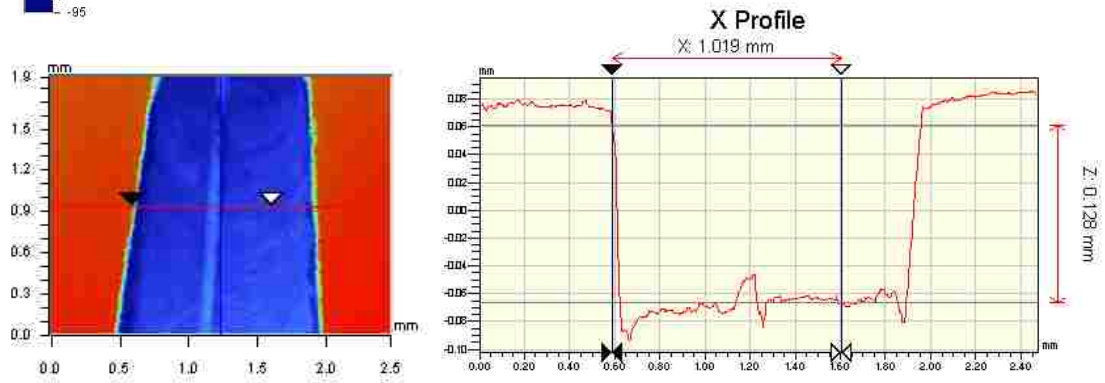
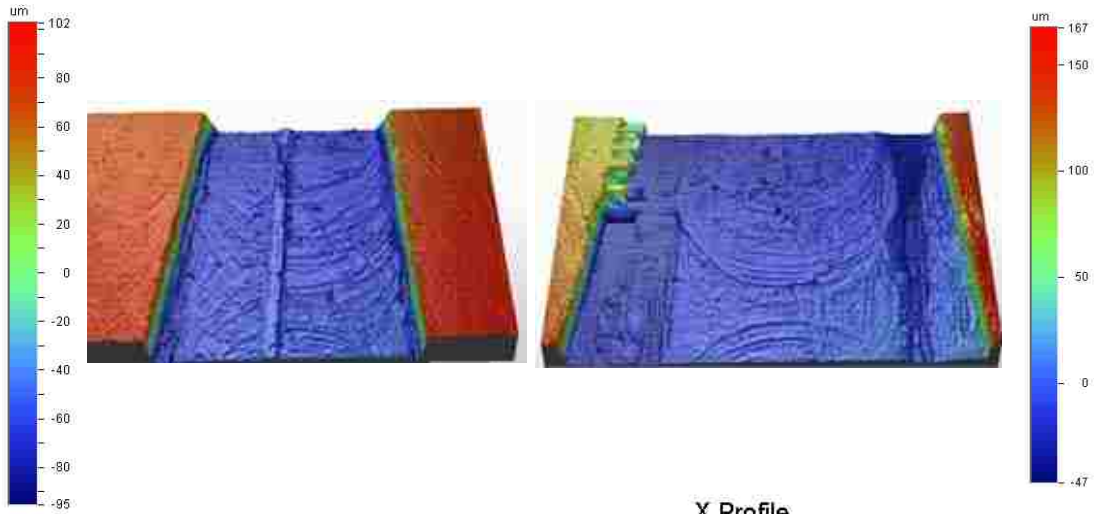
Insert 7



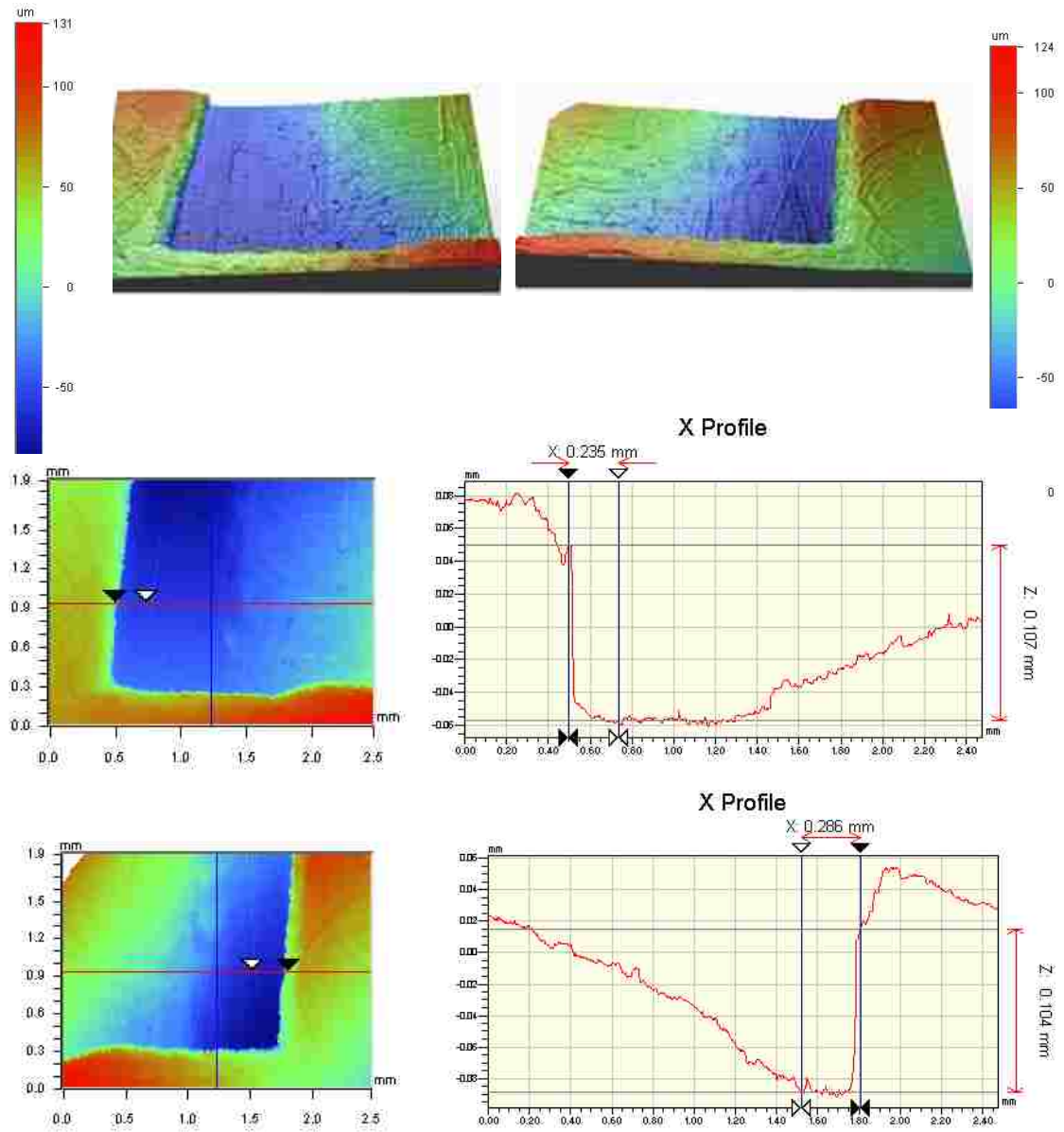
Insert 7- Void 1



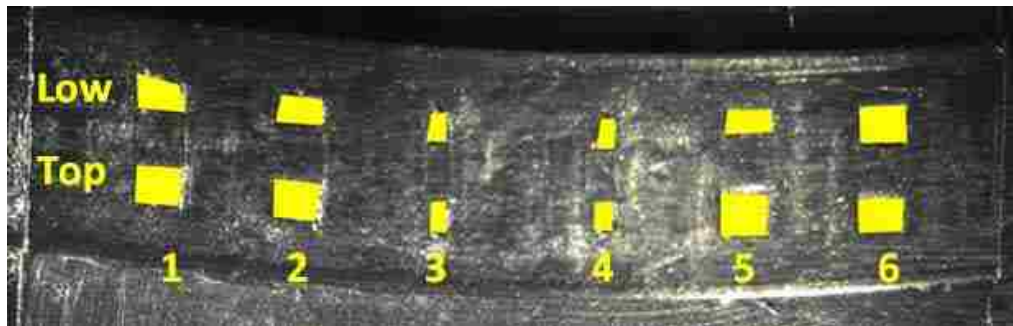
Insert 7- Void 1 cont'd



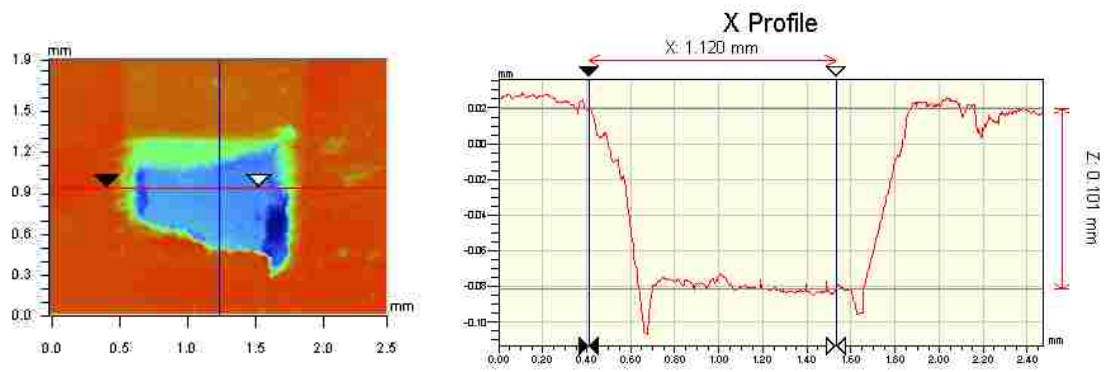
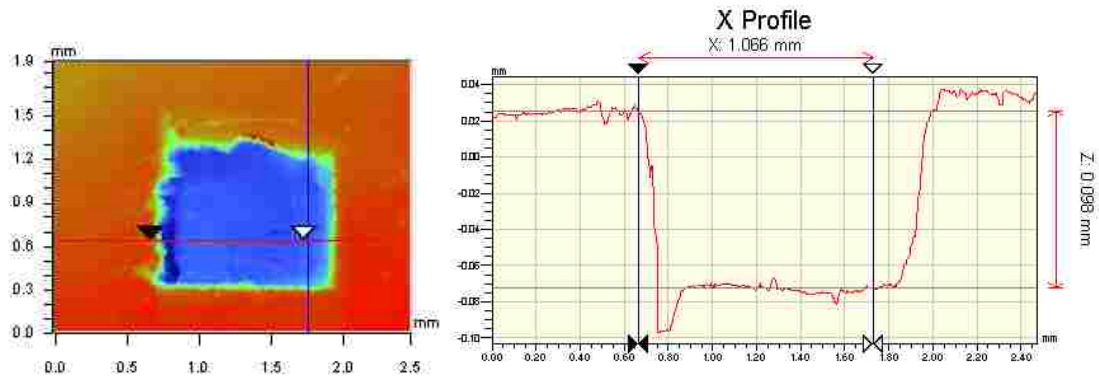
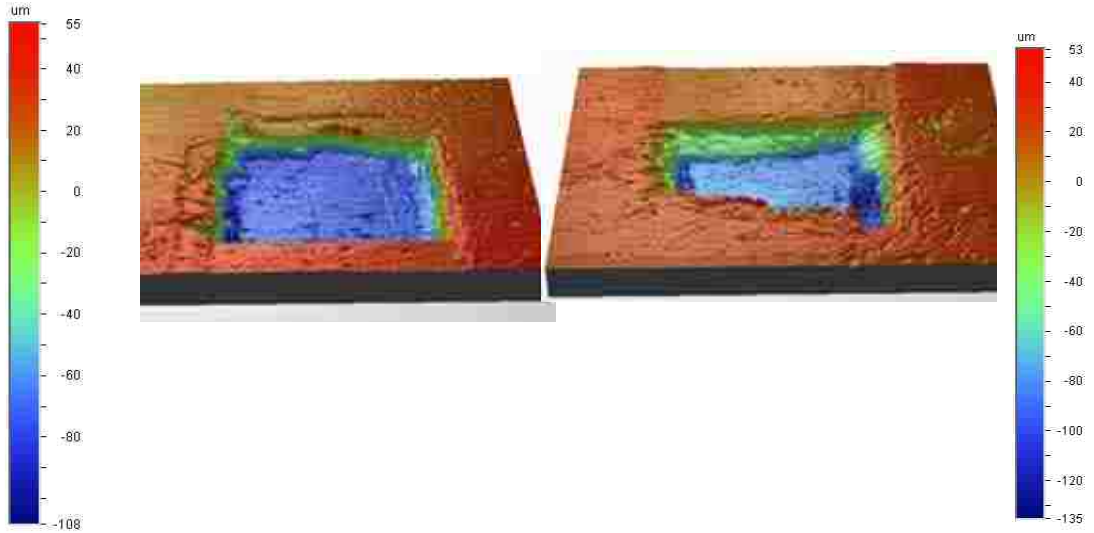
Insert 7- Void 1 cont'd



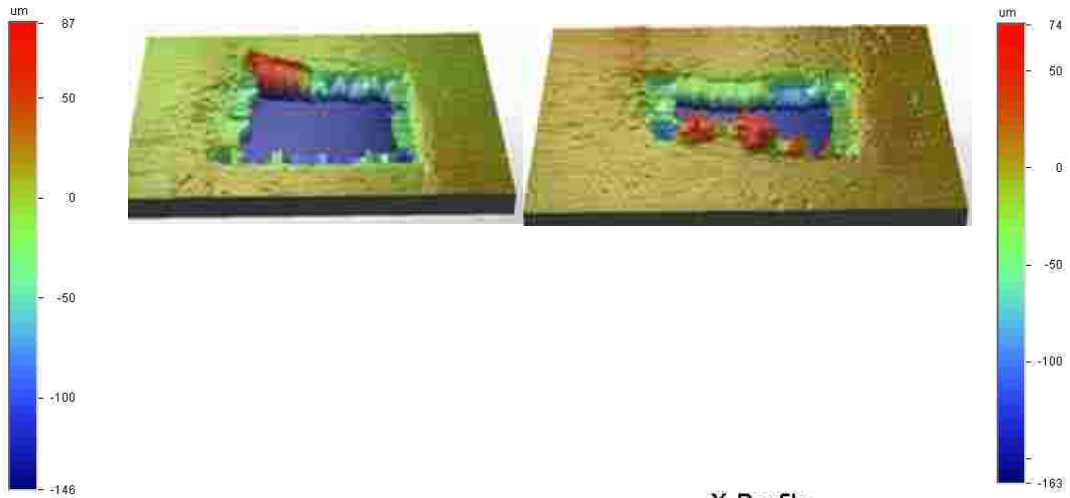
Insert 8



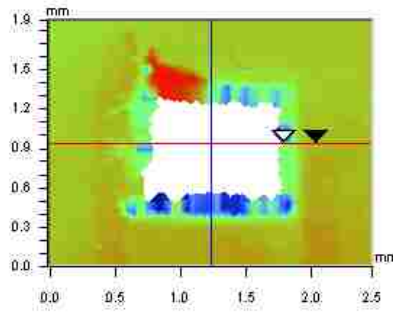
Insert 8- Void 1 “Top and Low”



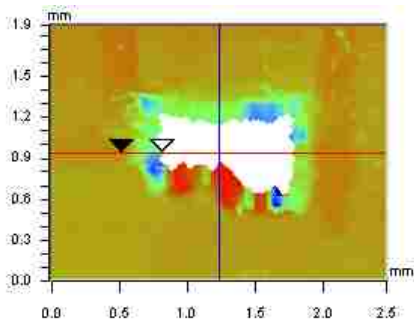
Insert 8- Void 2 “Top and Low”



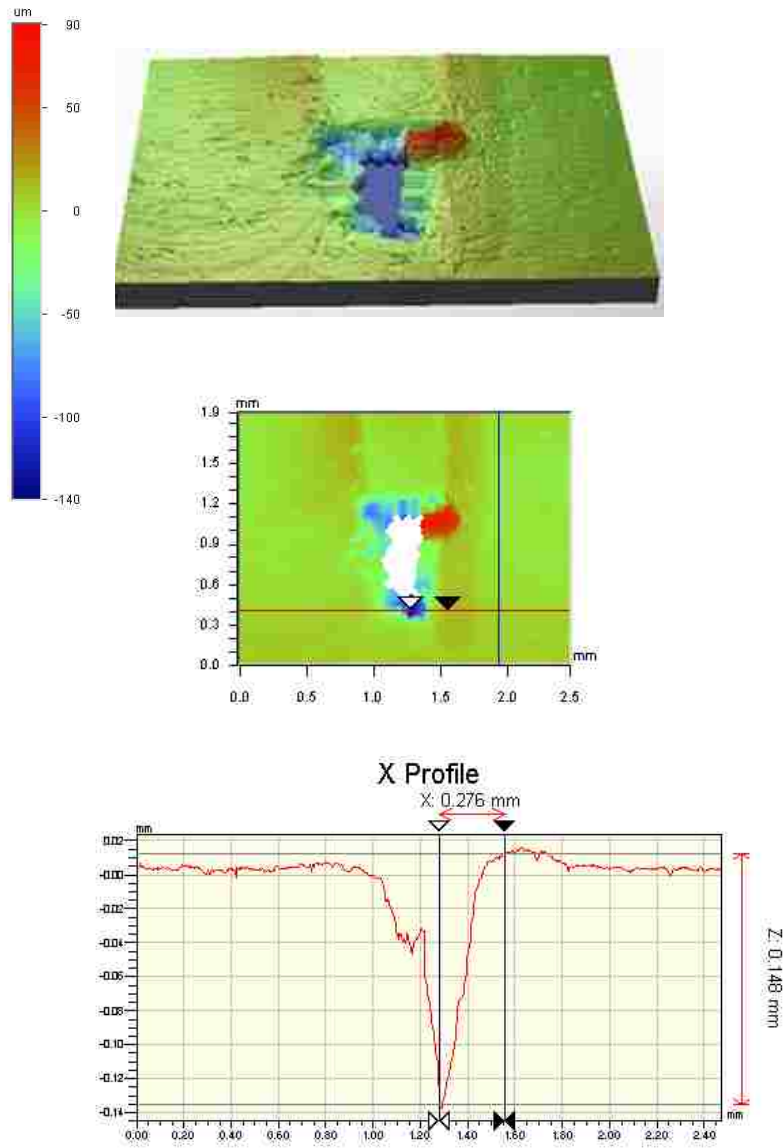
X Profile



X Profile

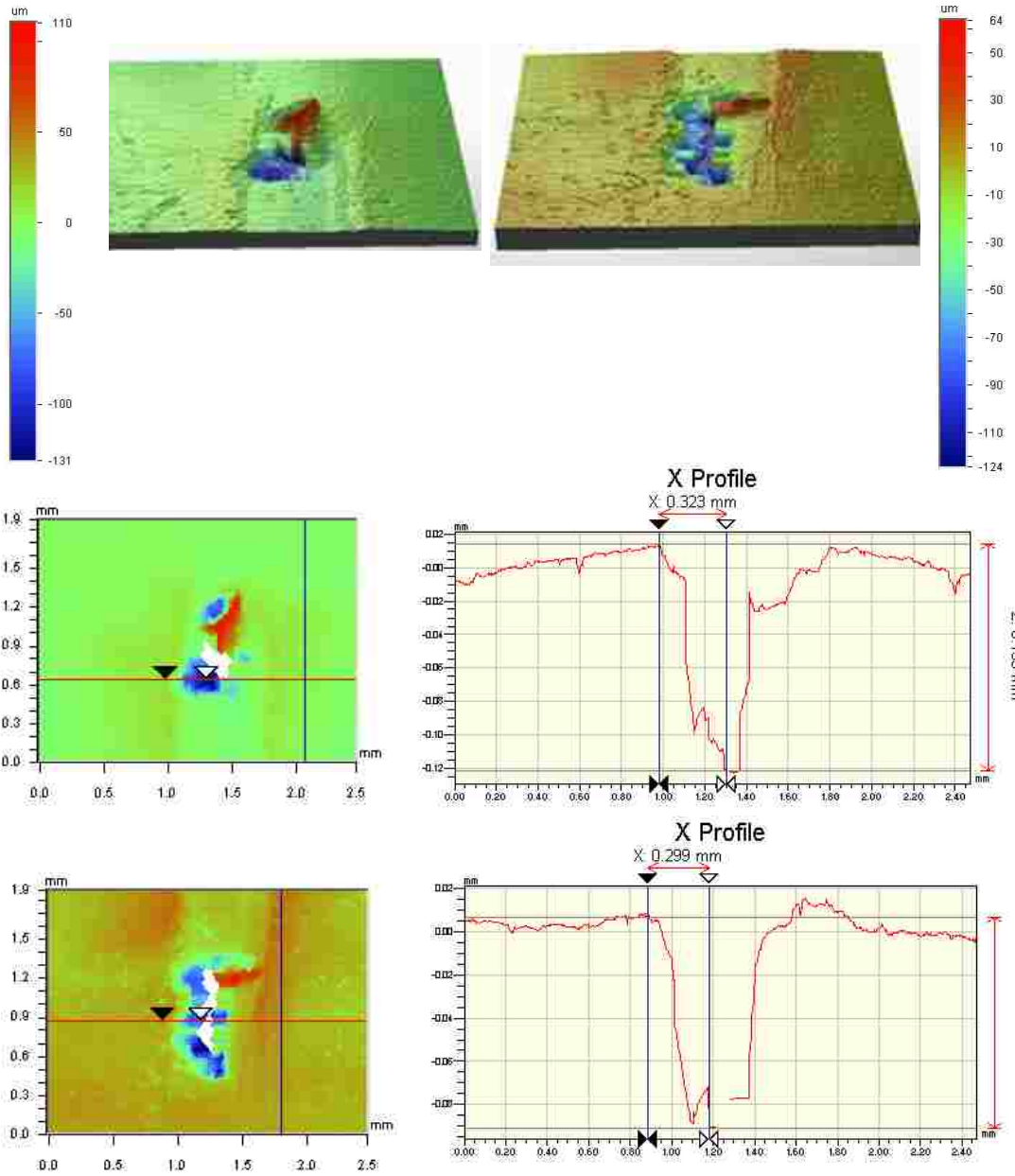


Insert 8- Void 3 “Low”

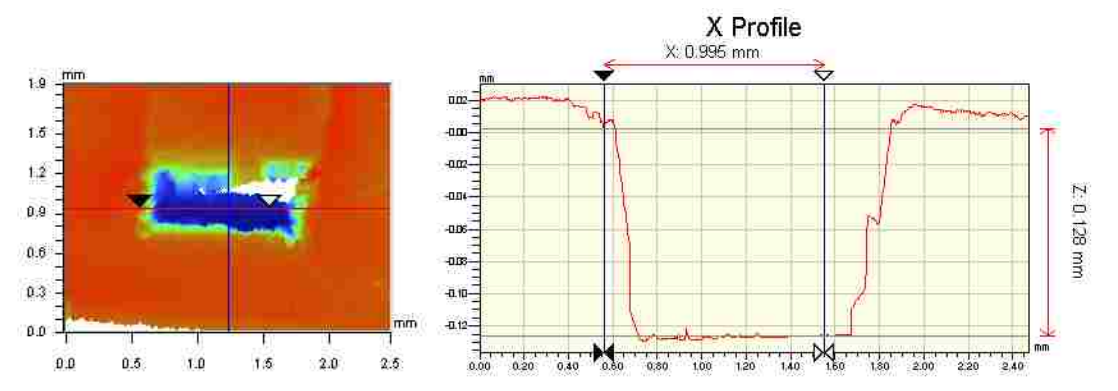
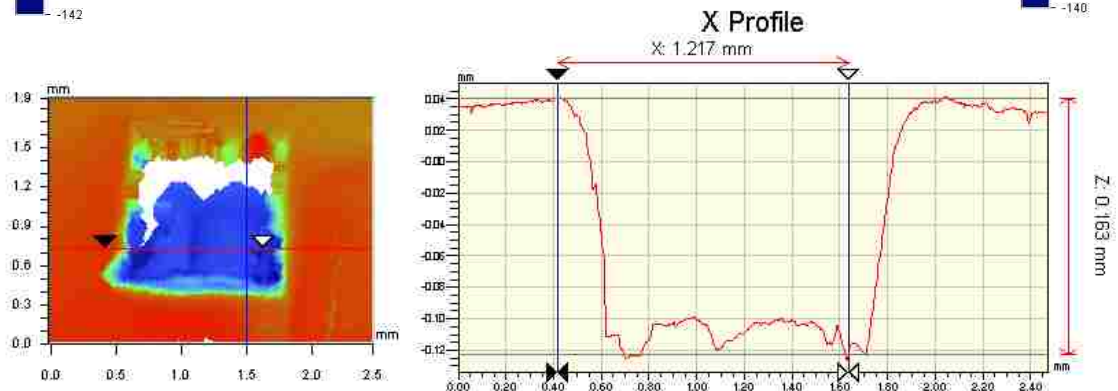
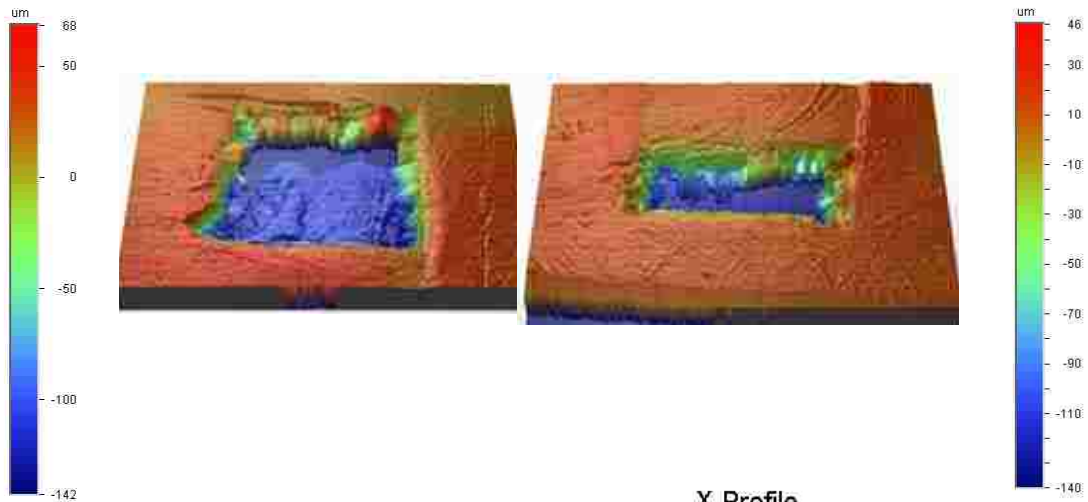


Insert 8- Void 3 Top N/A

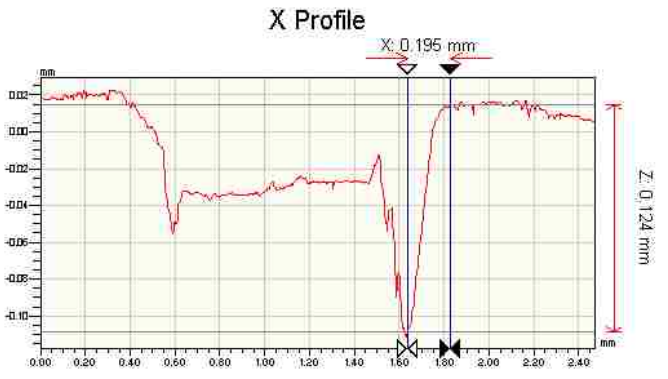
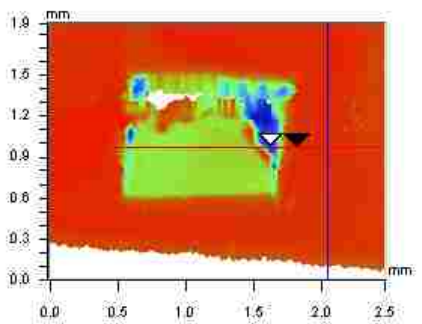
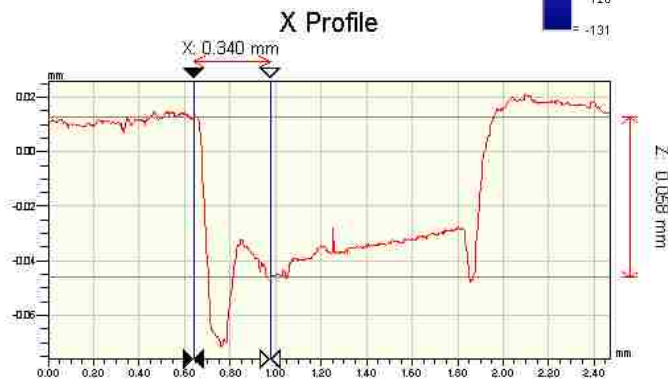
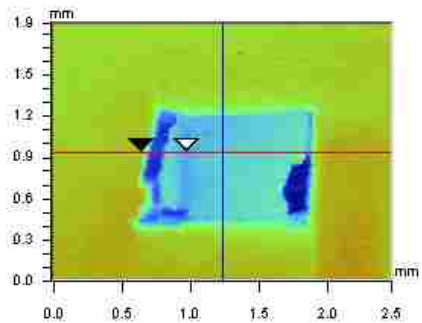
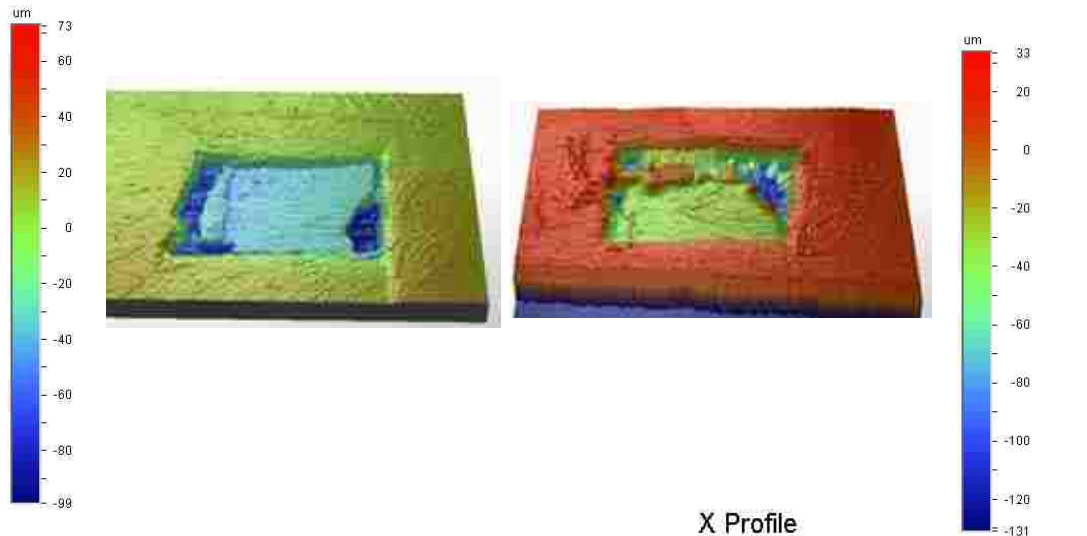
Insert 8- Void 4 “Top and Low”



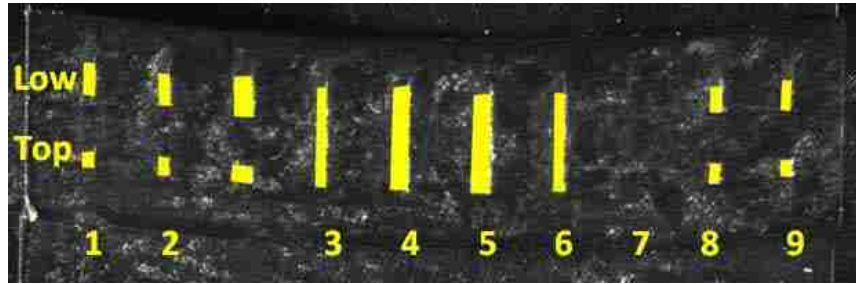
Insert 8- Void 5 "Top and Low"



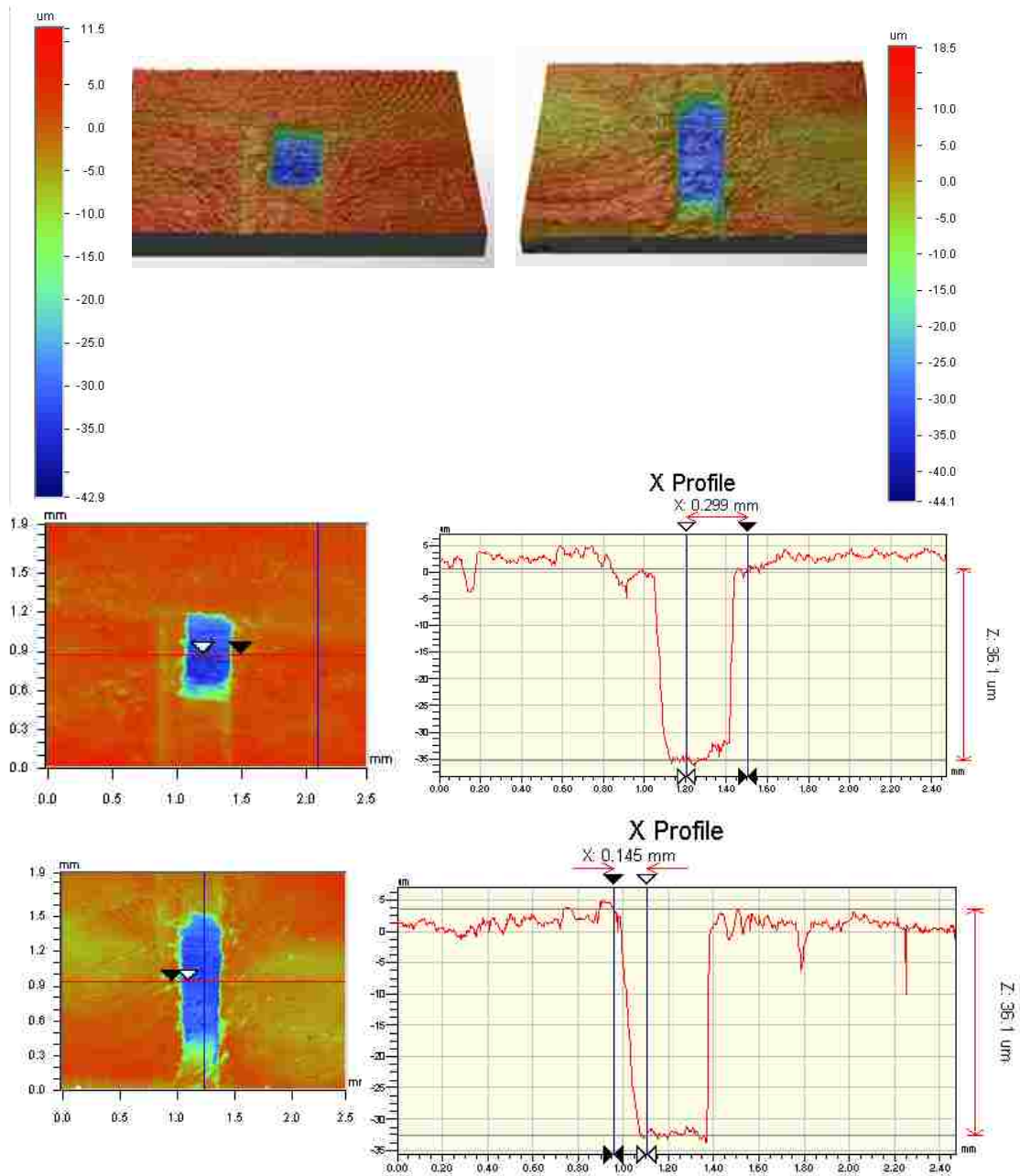
Insert 8- Void 6 "Top and Low"



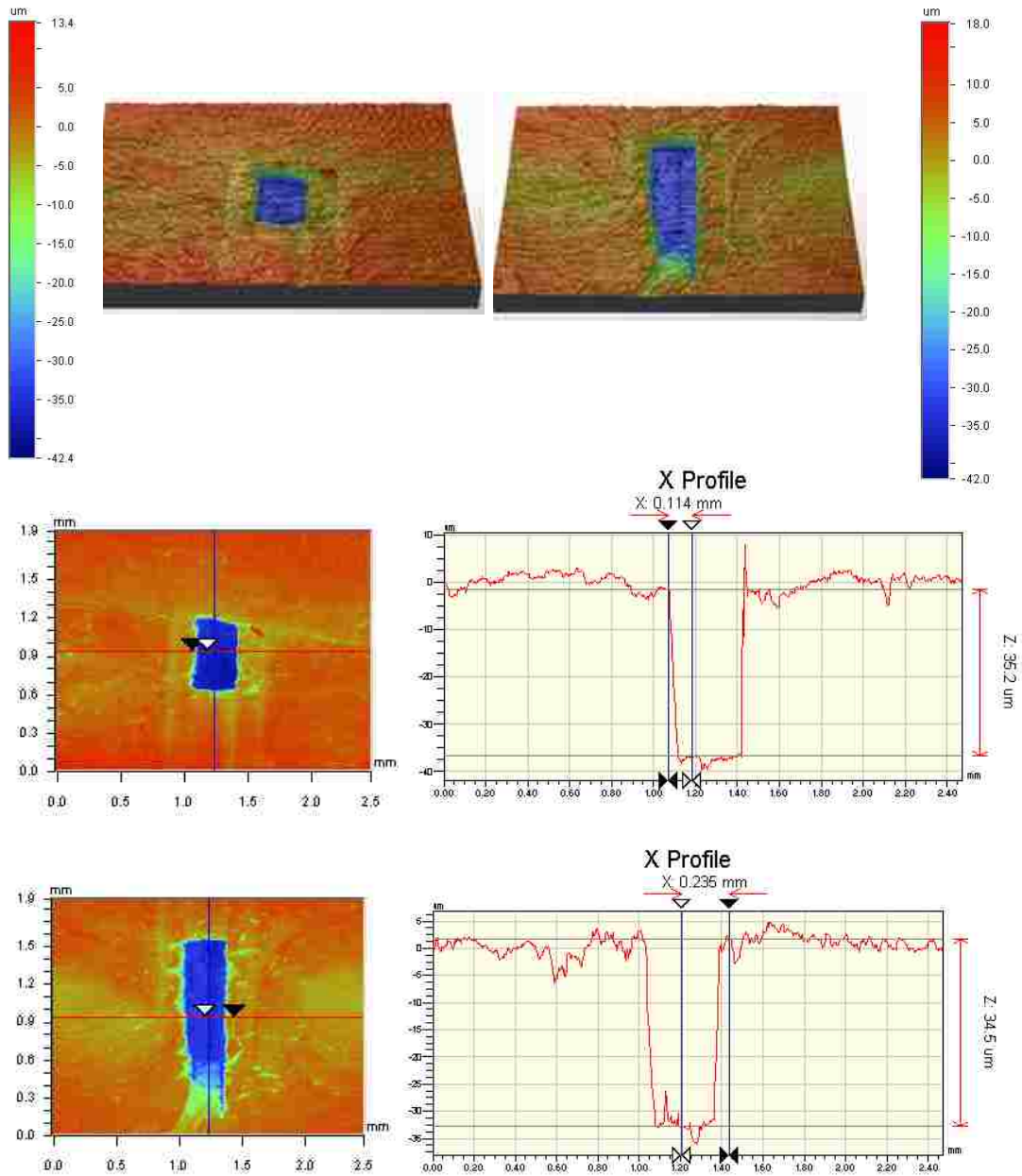
Insert 9



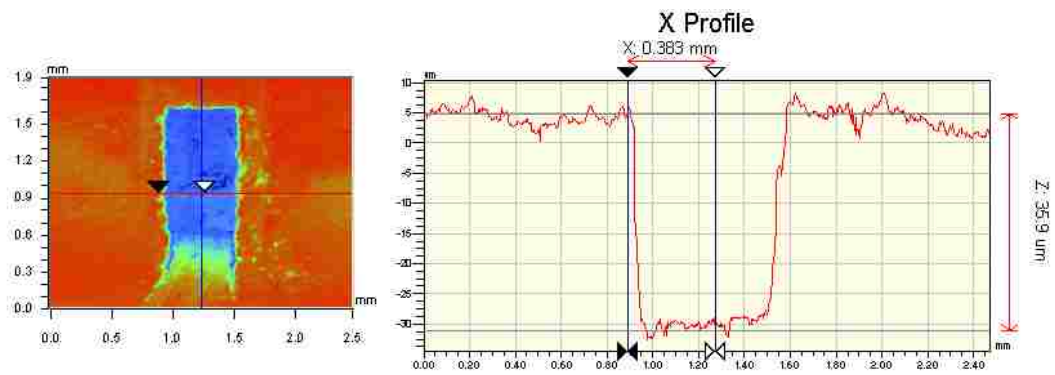
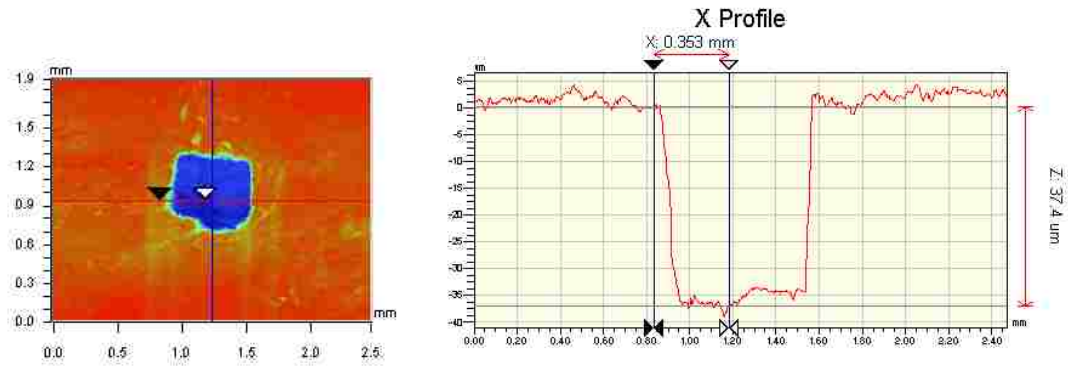
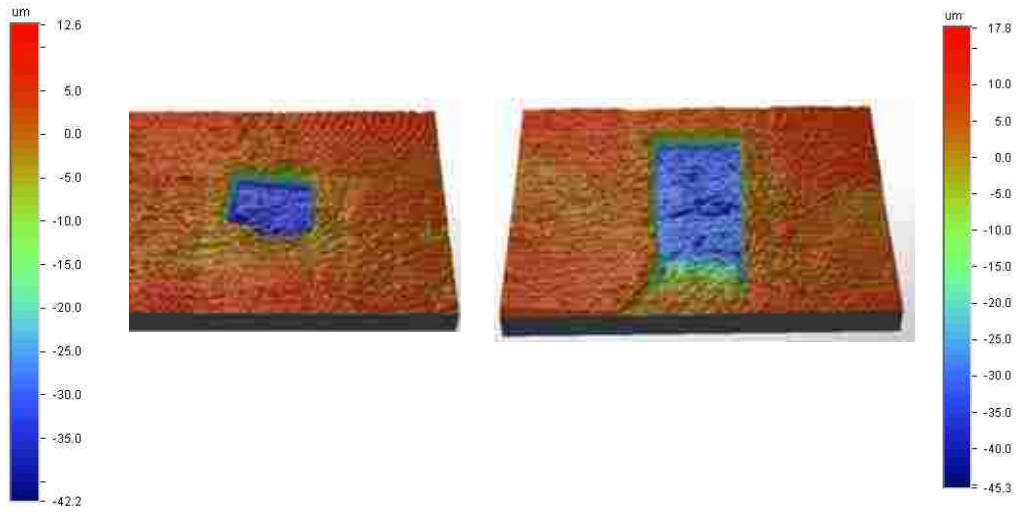
Insert 9- Void 1 “Top and Low”



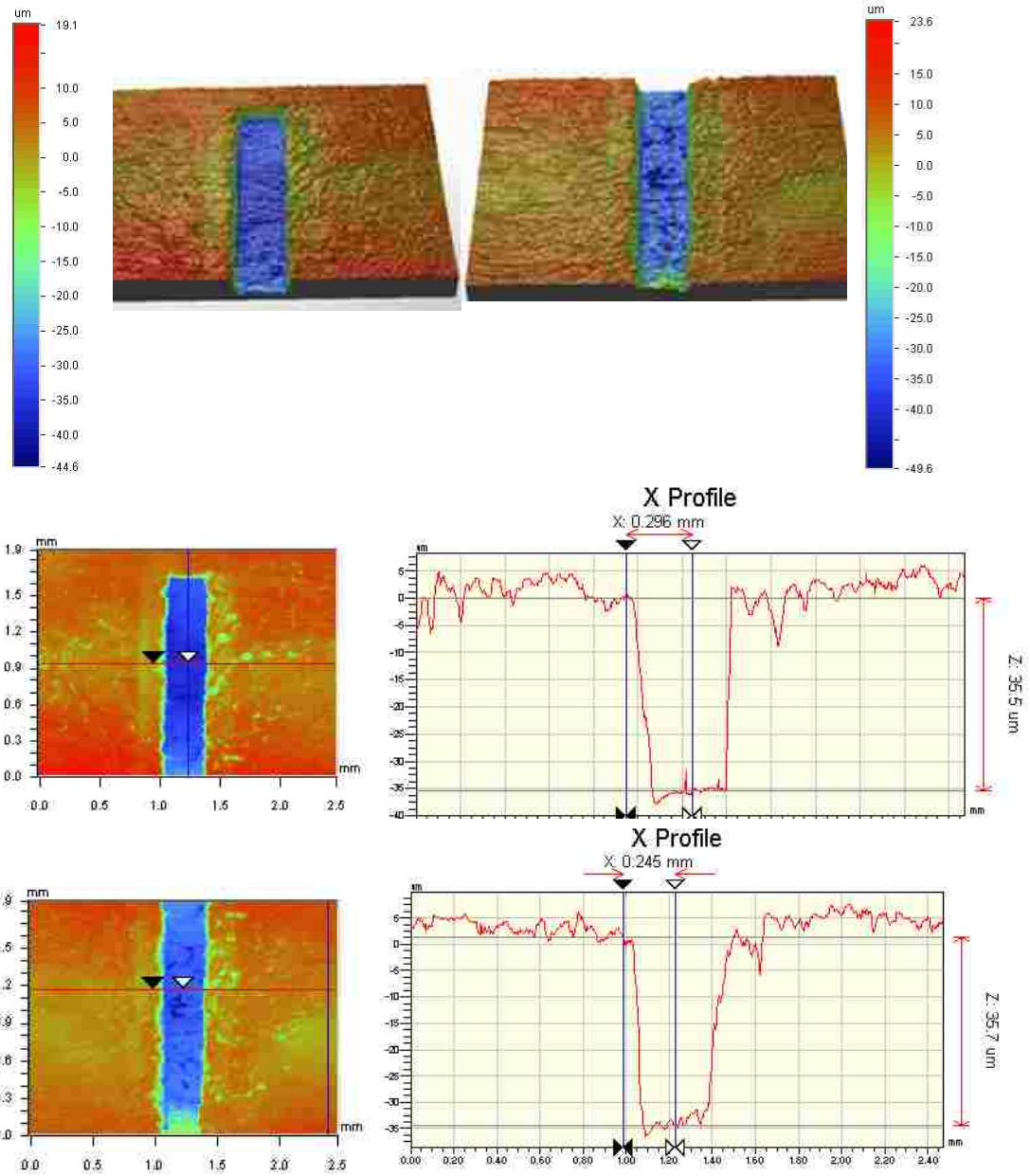
Insert 9- Void 2 “Top and Low”



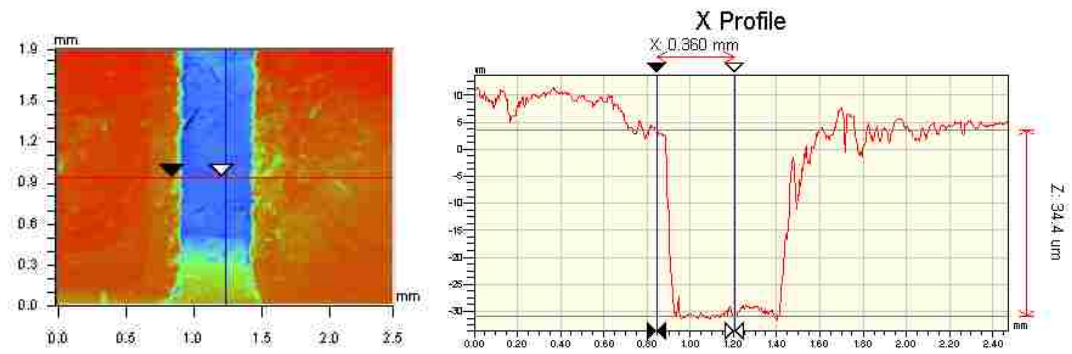
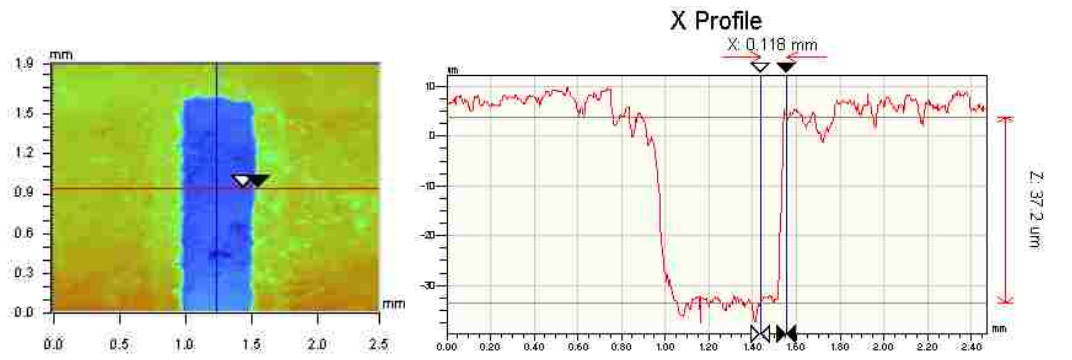
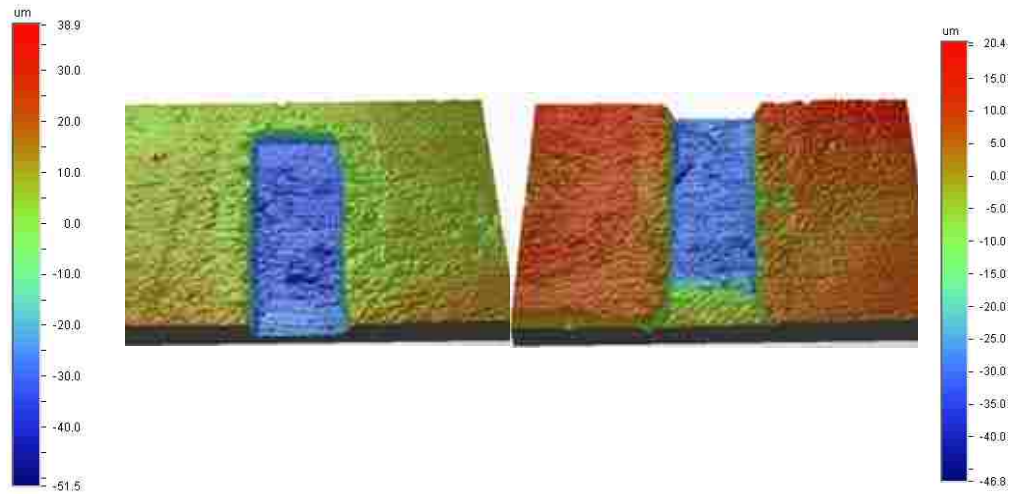
Insert 9- Void 3 “Top and Low”



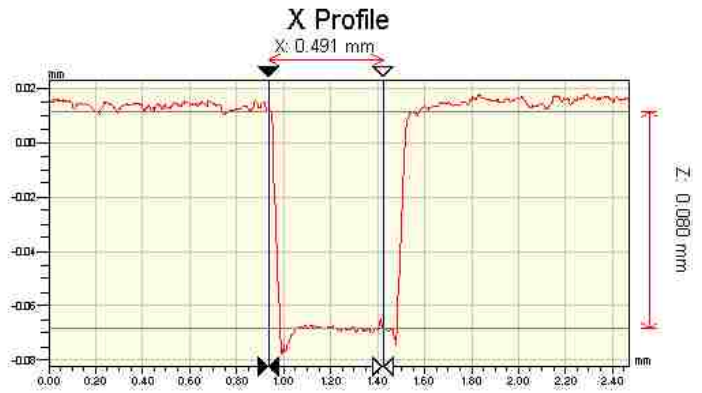
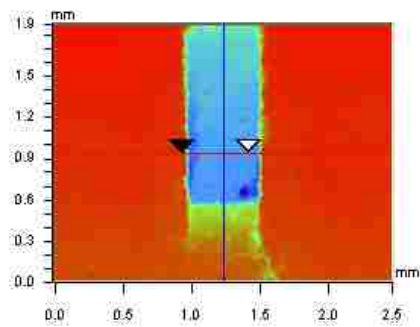
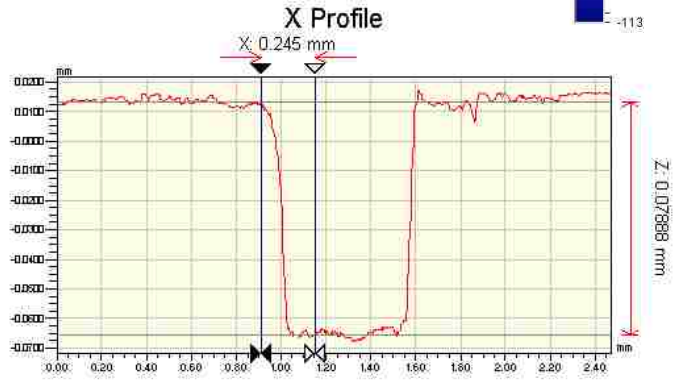
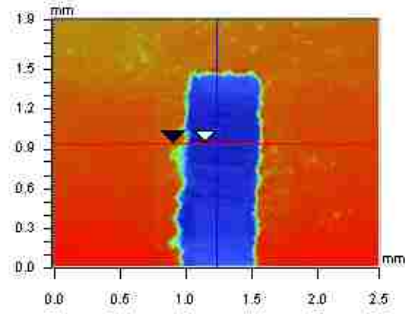
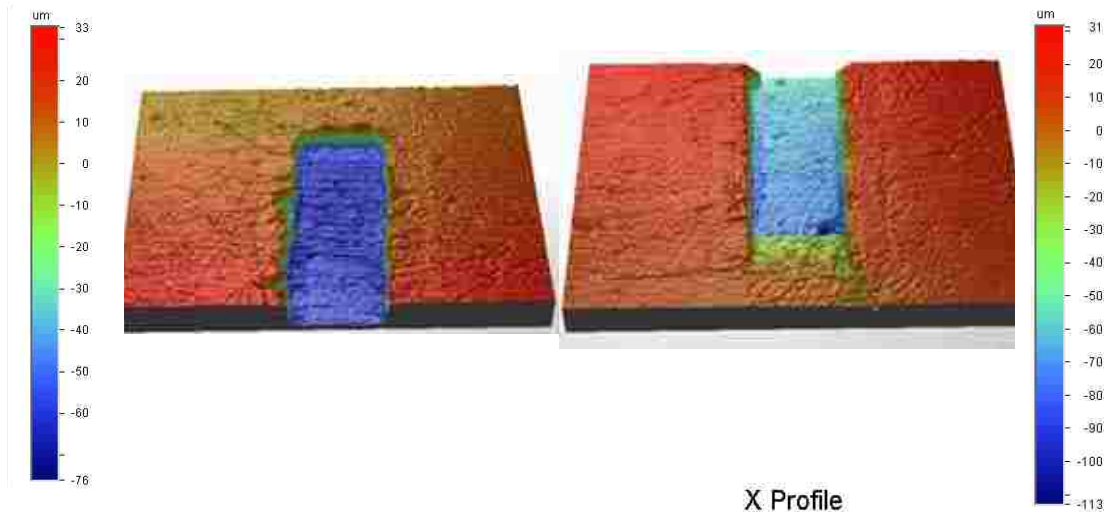
Insert 9- Void 4



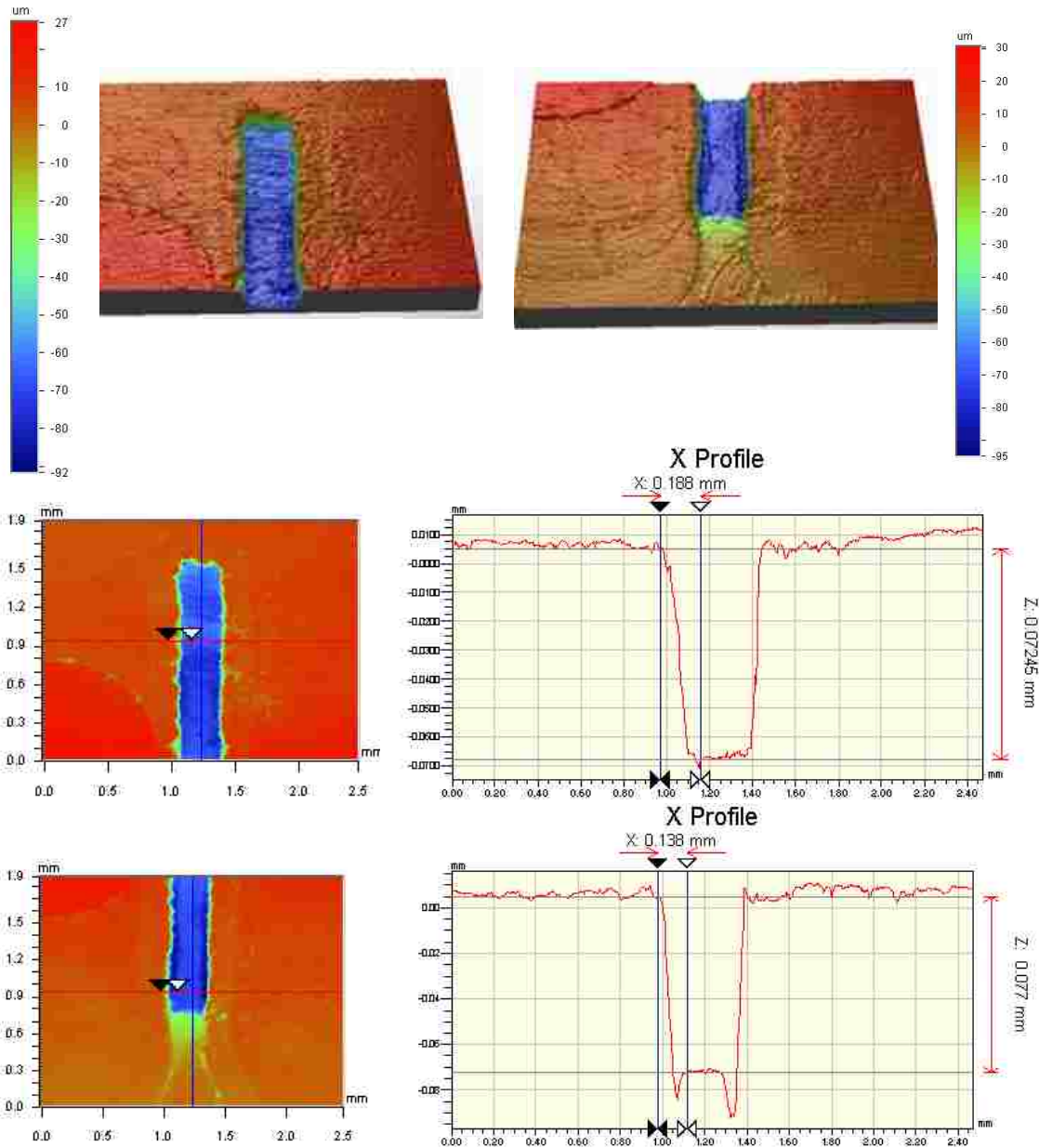
Insert 9- Void 5



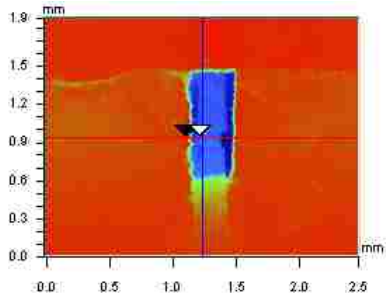
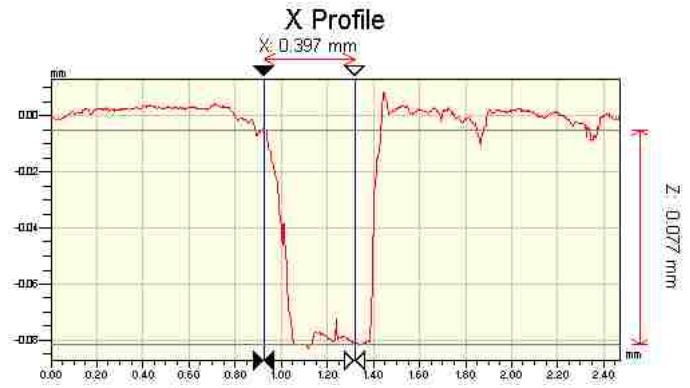
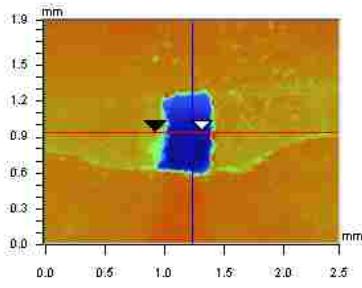
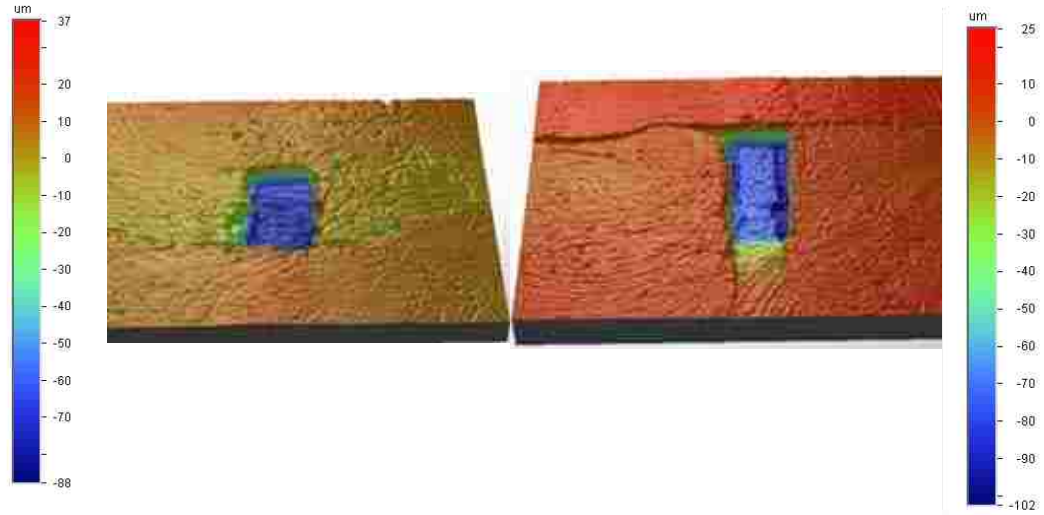
Insert 9- Void 6



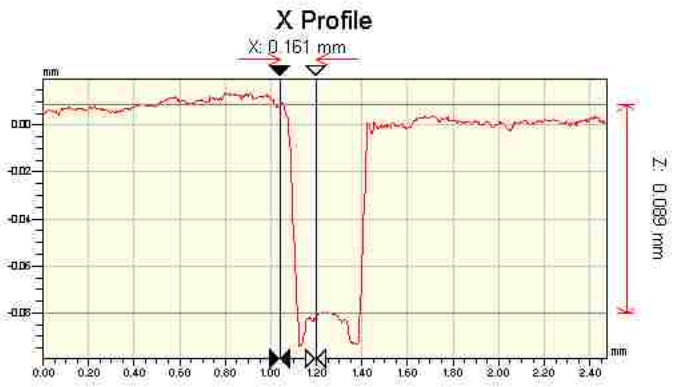
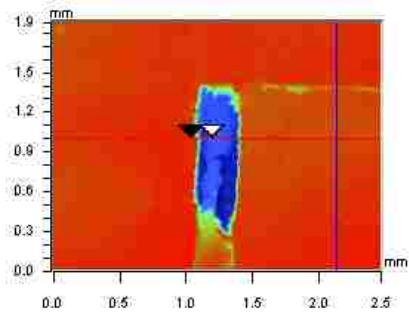
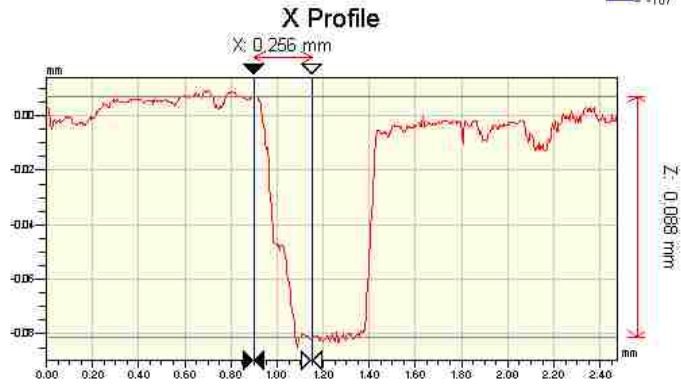
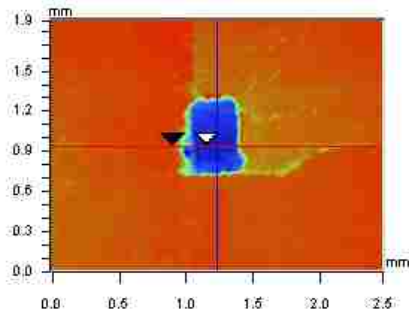
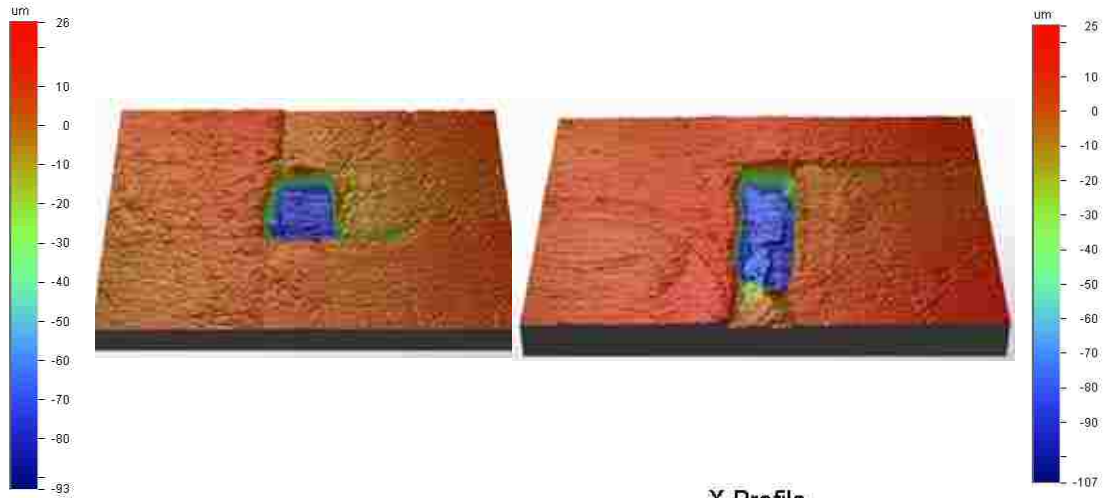
Insert 9- Void 7



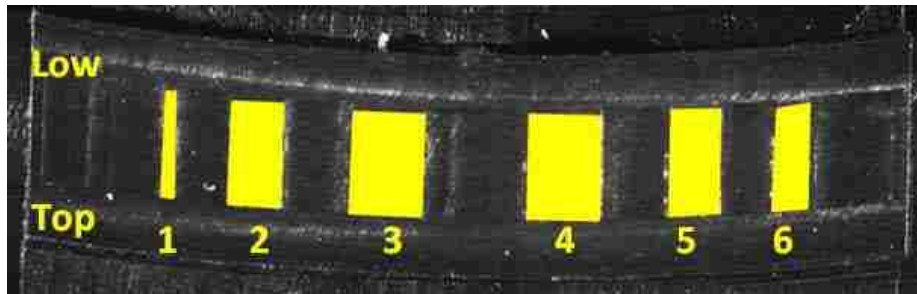
Insert 9- Void 8 “Top and Low”



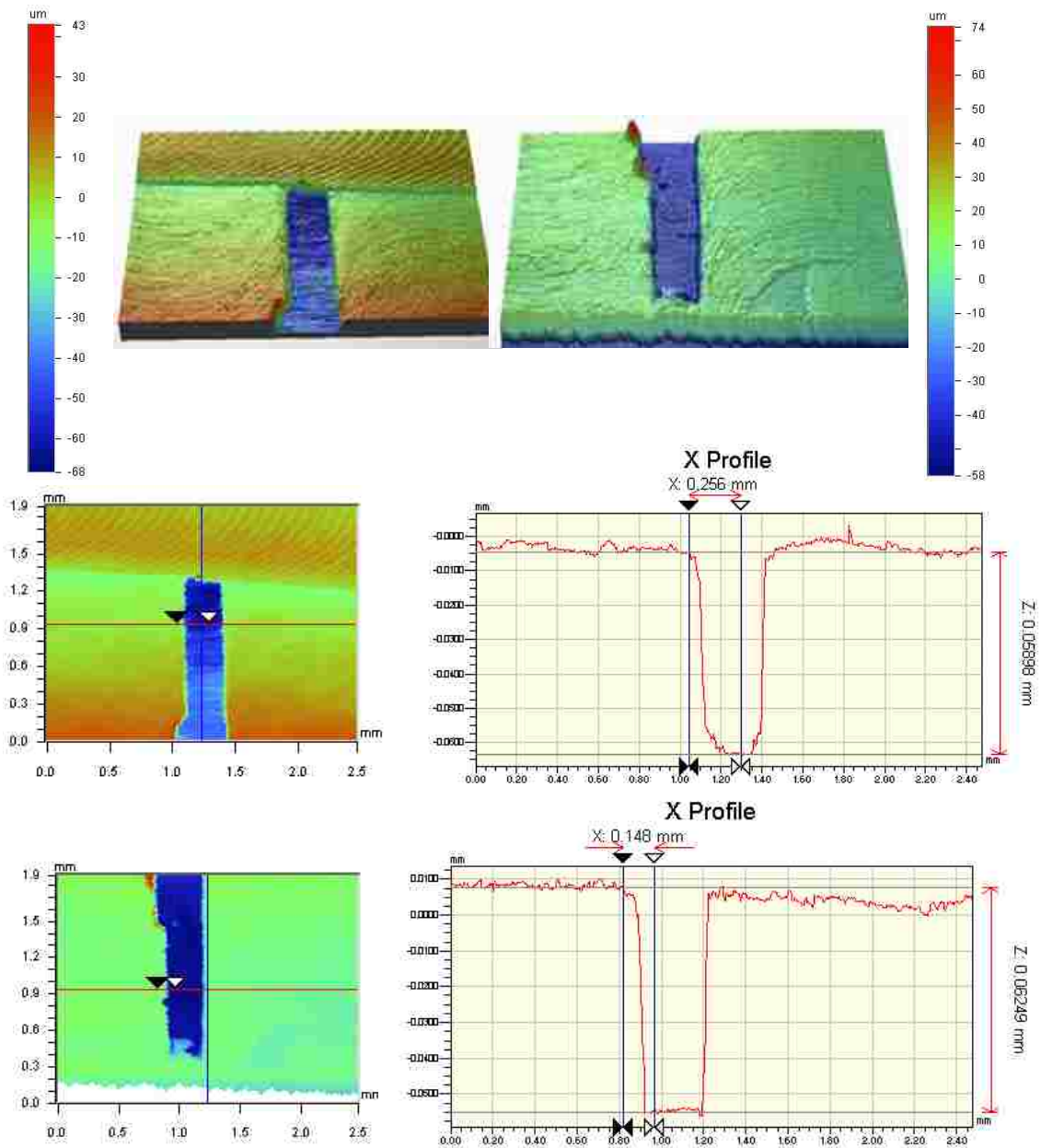
Insert 9- Void 9 “Top and Low”



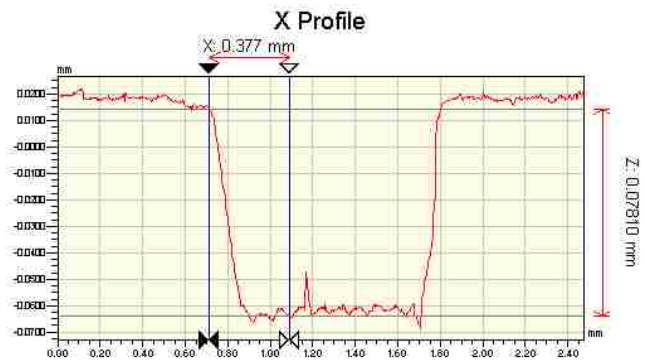
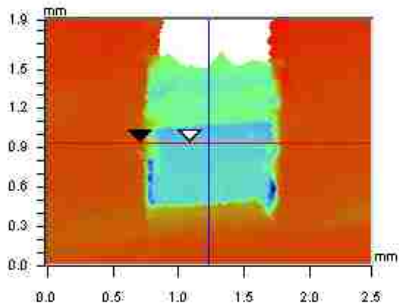
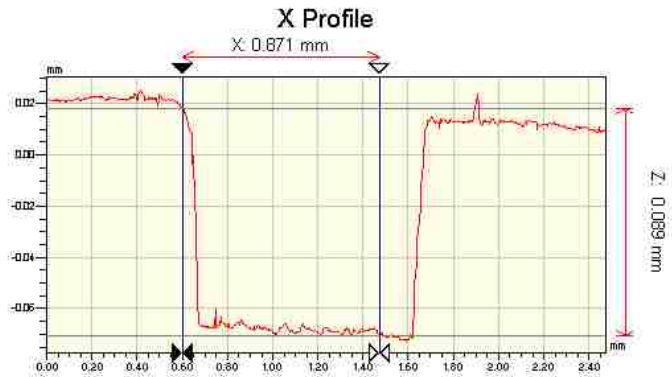
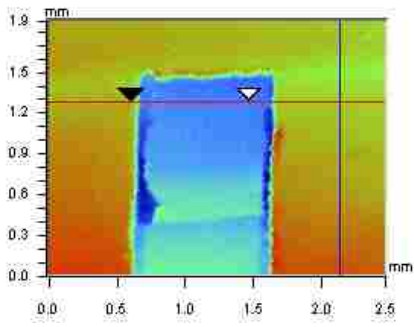
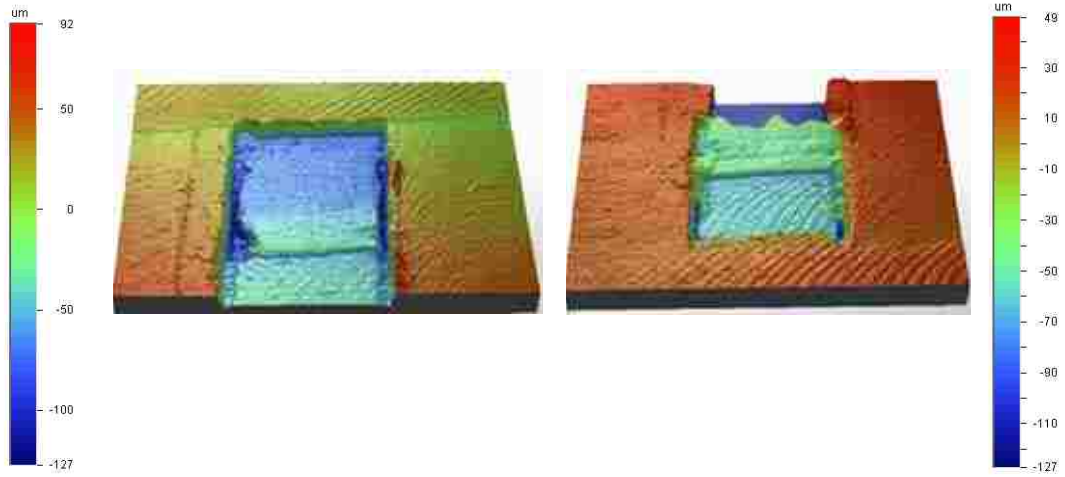
Insert 10



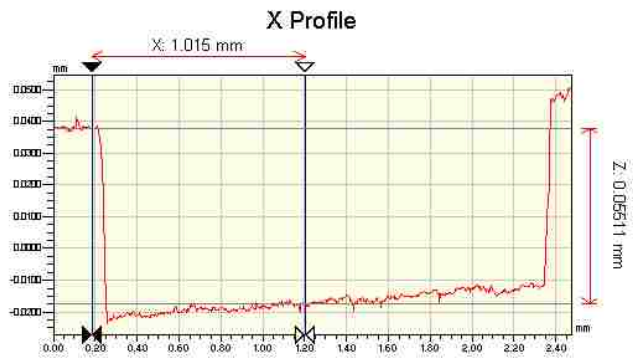
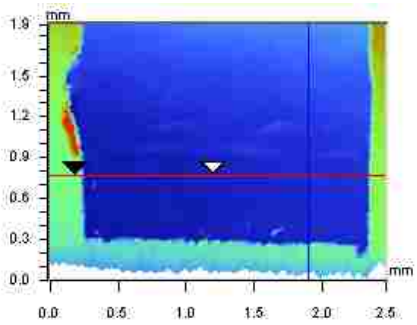
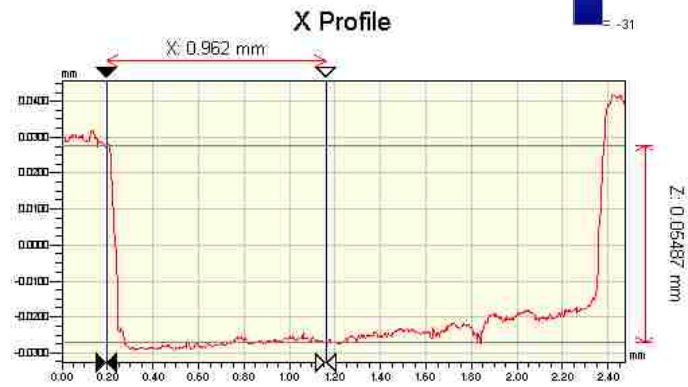
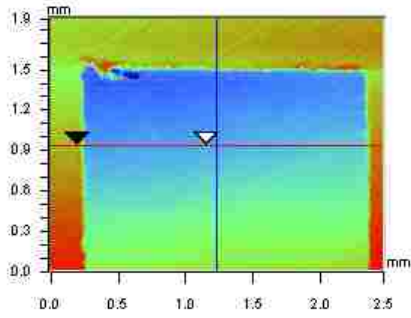
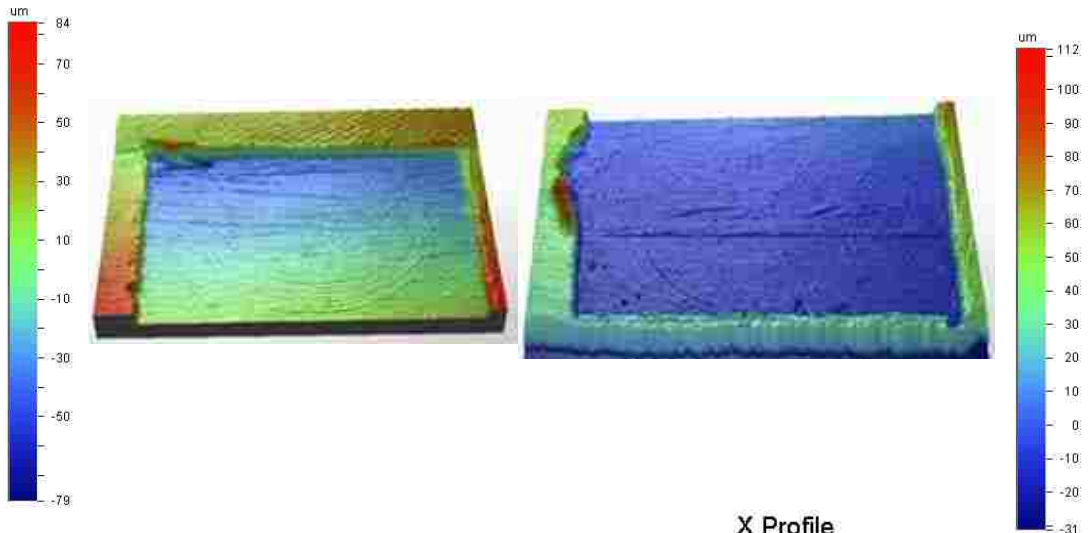
Insert 10- Void 1



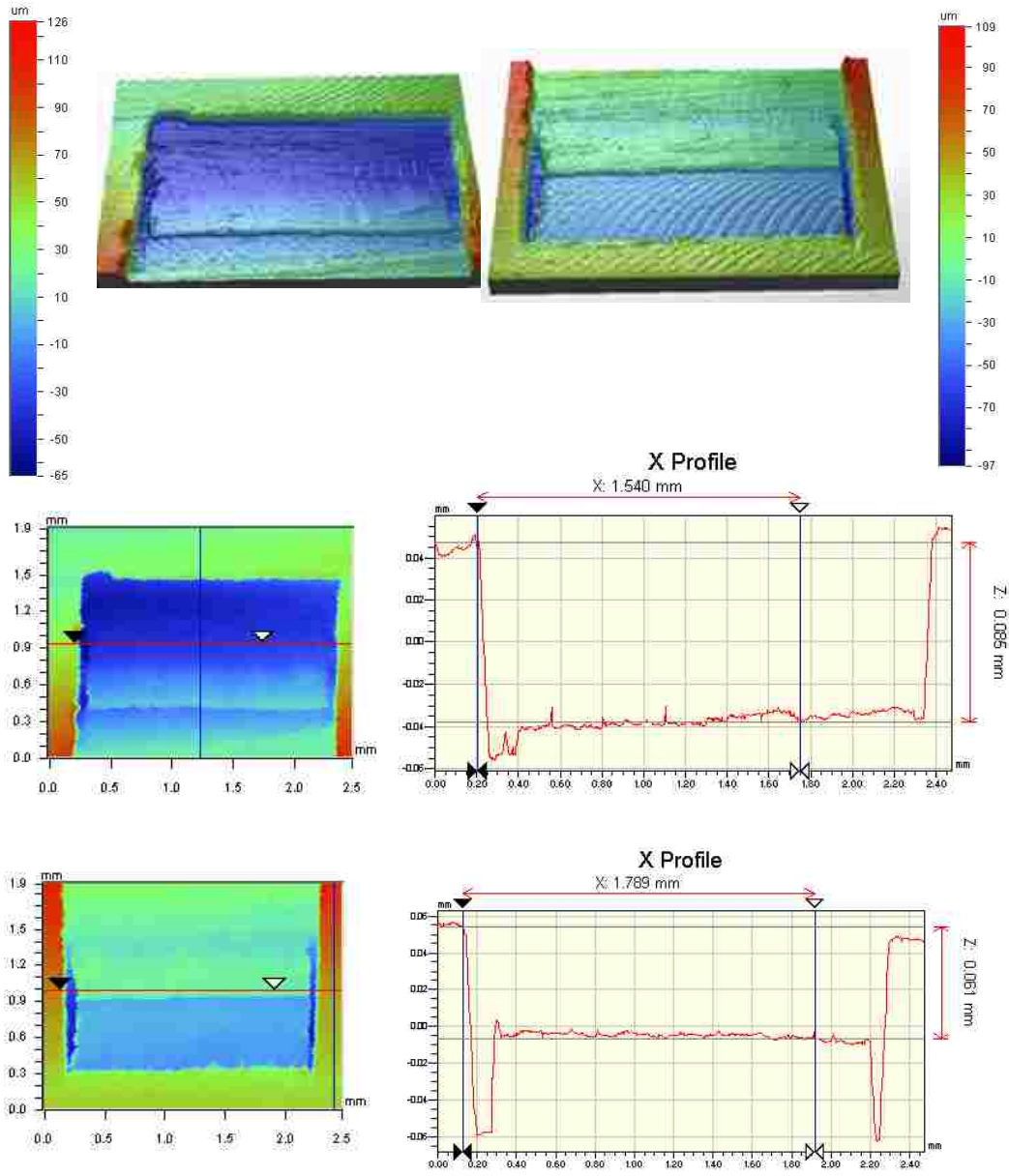
Insert 10- Void 2



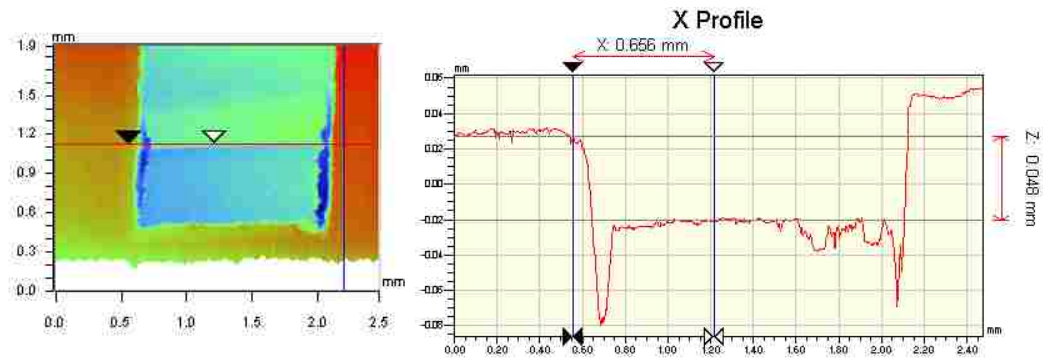
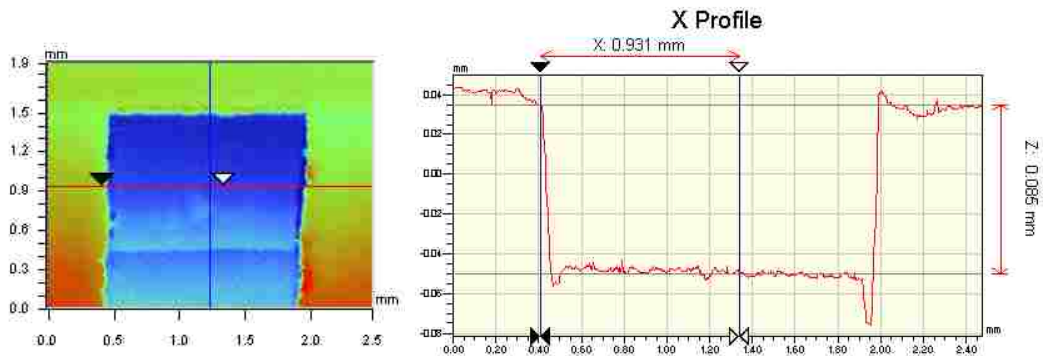
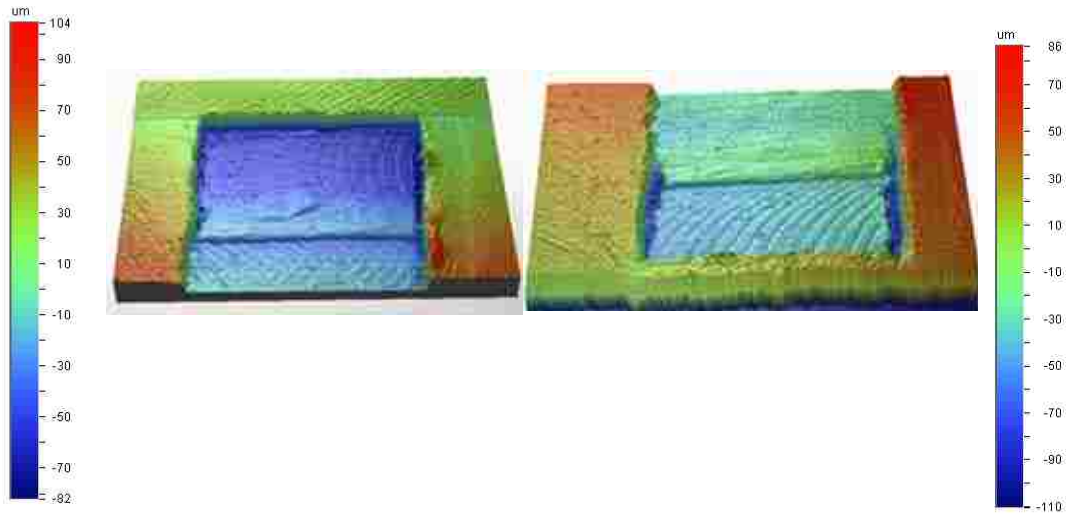
Insert 10- Void 3



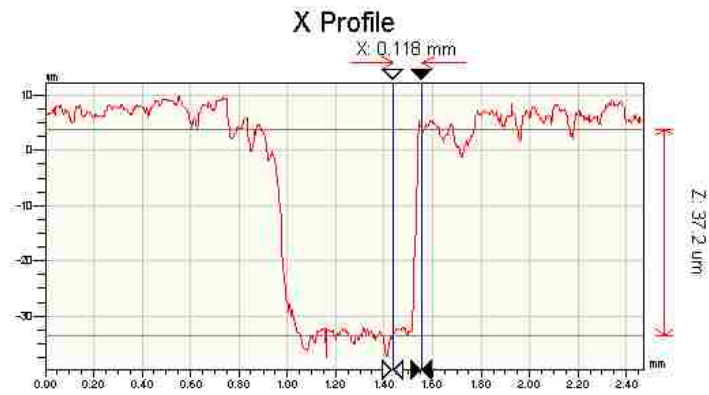
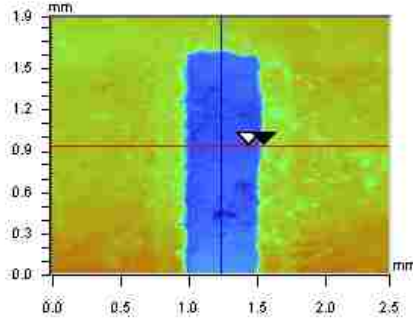
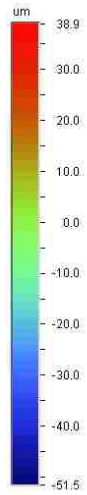
Insert 10- Void 4



Insert 10- Void 5 top



Insert 10- Void 6 (partial)



Appendix II : Microstructural Section Data and Micrographs

A- HG 26 (129N-106B, 180W, 1500mm/min, 0.12J/mm, carbon black-S/2) Insert 3N-8B							
Section	Total Area Porosity (mm ²)	Length (mm)	Area/Length (mm ² /mm)	# of pores	Average area of pore (mm ²)	Depth (mm)	
0	0.00000	28	0	0	0.000000	0	
1	0.00000	28	0	0	0.000000	0.45	
2	0.00000	28	0	0	0.000000	0.72	
3	0.00000	28	0	0	0.000000	0.85	
4	0.00000	28	0	0	0.000000	1.21	
5	0.00000	28	0	0	0.000000	1.56	
6	0.00000	28	0	0	0.000000	1.85	
7	0.54656	28	0.01951991	7	0.078080	2.04	
8	1.05458	28	0.03766347	9	0.111715	2.18	
9	1.75756	28	0.06277007	17	0.103386	2.50	
10	1.55519	28	0.05554257	37	0.042032	2.84	
11	1.14851	28	0.04101827	28	0.041018	3.06	
12	0.82530	28	0.02947499	30	0.027510	3.29	
13	0.30514	28	0.01089785	33	0.009247	3.48	
14	0.05575	28	0.00199106	12	0.004646	3.68	
15	0.05913	28	0.00211165	12	0.004927	3.68	
16	0.09999	28	0.00357121	18	0.005555	3.87	
17	0.05616	28	0.0020057	10	0.005616	4.15	
18	0.08590	28	0.00306778	14	0.006136	4.37	
19	0.23821	28	0.00850757	45	0.005294	4.61	
20	0.45525	28	0.01625881	60	0.007587	4.90	
21	0.20402	28	0.00728658	31	0.006581	5.07	
22	0.20229	28	0.00722459	42	0.004816	5.27	
23	0.10006	28	0.00357351	34	0.002943	5.56	
24	0.07908	28	0.00282446	28	0.002824	5.79	
25	0.14505	28	0.0051802	47	0.003086	6.08	
26	0.09618	28	0.0034351	27	0.003562	6.26	
27	0.13590	28	0.00485362	37	0.003673	6.54	



Figure 1: Section 1, Depth 0.45 mm



Figure 2: Section 2, Depth 0.72 mm



Figure 3: Section 3, Depth 0.85 mm



Figure 4: Section 4, Depth 1.21 mm



Figure 5: Section 5, Depth 1.56 mm



Figure 6: Section 6, Depth 1.85 mm



Figure 7: Section 7, Depth 2.04 mm



Figure 8: Section 8, Depth 2.18 mm



Figure 9: Section 9, Depth 2.50 mm



Figure 10: Section 10, Depth 2.84 mm



Figure 11: Section 11, Depth 3.06 mm



Figure 12: Section 12, Depth 3.29 mm



Figure 13: Section 13, Depth 3.48 mm



Figure 14: Section 14, Depth 3.68 mm



Figure 15: Section 15, Depth 3.68 mm



Figure 16: Section 16, Depth 3.87 mm



Figure 17: Section 17, Depth 4.15 mm



Figure 18: Section 18, Depth 4.37 mm



Figure 19: Section 19, Depth 4.61 mm



Figure 20: Section 20, Depth 4.90 mm



Figure 21: Section 21, Depth 5.07 mm



Figure 22: Section 22, Depth 5.27 mm



Figure 23: Section 23, Depth 5.56 mm



Figure 24: Section 24, Depth 5.79 mm



Figure 25: Section 25, Depth 6.08 mm



Figure 26: Section 26, Depth 6.26 mm



Figure 27: Section 27, Depth 6.54 mm

A- HG 26 (129N-106B, 180W, 1500mm/min, 0.12J/mm, carbon black-S/2) Insert 4N-7B						
Section	Total Area Porosity (mm ²)	Length (mm)	Area/Length (mm ² /mm)	# of pores	Average area of pore (mm ²)	Depth (mm)
0	0.00000	28.3	0	0	0.000000	0
1	0.00000	28.3	0	0	0.000000	0.55
2	0.00000	28.3	0	0	0.000000	0.97
3	0.00000	28.3	0	0	0.000000	1.24
4	0.15860	28.3	0.00560416	38	0.004174	1.58
5	0.86938	28.3	0.03072014	162	0.005367	2.03
6	0.87965	28.3	0.03108291	209	0.004209	2.28
7	1.34408	28.3	0.04749388	246	0.005464	2.54
8	2.87183	28.3	0.1014781	221	0.012995	2.80
9	3.55421	28.3	0.12559042	133	0.026723	3.22
10	3.39505	28.3	0.1199666	191	0.017775	3.59
11	3.30599	28.3	0.11681932	249	0.013277	3.89
12	2.56357	28.3	0.0905854	269	0.009530	4.08
13	2.69653	28.3	0.09528386	300	0.008988	4.35
14	2.25756	28.3	0.07977231	412	0.005480	4.63
15	2.61470	28.3	0.09239223	431	0.006067	4.63
16	2.19182	28.3	0.07744963	409	0.005359	5.04
17	1.21319	28.3	0.04286895	257	0.004721	5.40
18	1.84853	28.3	0.0653192	390	0.004740	5.69
19	1.72184	28.3	0.06084257	324	0.005314	6.05
20	1.44196	28.3	0.05095261	276	0.005224	6.36
21	1.83928	28.3	0.06499211	283	0.006499	6.56
22	0.92370	28.3	0.03263958	195	0.004737	6.62



Figure 28: Section 1, Depth 0.55 mm



Figure 29: Section 2, Depth 0.97 mm



Figure 30: Section 3, Depth 1.24 mm



Figure 31: Section 4, Depth 1.58 mm



Figure 32: Section 5, Depth 2.03 mm



Figure 33: Section 6, Depth 2.28 mm



Figure 34: Section 7, Depth 2.54 mm



Figure 35: Section 8, Depth 2.80 mm



Figure 36: Section 9, Depth 3.22 mm



Figure 37: Section 10, Depth 3.59 mm



Figure 38: Section 11, Depth 3.89 mm



Figure 39: Section 12, Depth 4.08 mm



Figure 40: Section 13, Depth 4.35 mm



Figure 41: Section 14, Depth 4.63 mm



Figure 42: Section 15, Depth 4.63mm



Figure 43: Section 16, Depth 5.04 mm



Figure 44: Section 17, Depth 5.40 mm



Figure 45: Section 18, Depth 5.69 mm



Figure 46: Section 19, Depth 6.05 mm



Figure 47: Section 20, Depth 6.36 mm



Figure 48: Section 21, Depth 6.56 mm



Figure 49: Section 22, Depth 6.62 mm

A- HG 26 (129N-106B, 180W, 1500mm/min, 0.12J/mm, carbon black-S/2) No Insert							
Section	Total Area Porosity (mm ²)	Length (mm)	Area/Length (mm ² /mm)	# of pores	Average area of pore (mm ²)	Depth (mm)	
1	0.000000	23	0	0	0.000000	0.00	
2	0.000000	23	0	0	0.000000	0.42	
3	0.000000	23	0	0	0.000000	1.04	
4	0.000000	23	0	0	0.000000	1.55	
5	0.273635	23	0.01189719	24	0.011401	2.07	
6	0.389887	23	0.0169516	48	0.008123	2.54	
7	0.808614	23	0.03515715	122	0.006628	3.10	
8	0.060658	23	0.00263729	20	0.003033	3.70	
9	0.000000	23	0	0	0.000000	4.19	
10	0.000000	23	0	0	0.000000	4.59	
11	0.000000	23	0	0	0.000000	5.10	
12	0.000000	23	0	0	0.000000	5.76	
13	0.000000	23	0	0	0.000000	6.01	



Figure 50: Section 1, Depth 0 mm



Figure 51: Section 2, Depth 0.42 mm



Figure 52: Section 3, Depth 1.04 mm



Figure 53: Section 4, Depth 1.55 mm



Figure 54: Section 5, Depth 2.07 mm



Figure 55: Section 6, Depth 2.54 mm



Figure 56: Section 7, Depth 3.10 mm



Figure 57: Section 8, Depth 3.70 mm



Figure 58: Section 9, Depth 4.19 mm



Figure 59: Section 10, Depth 4.59 mm



Figure 60: Section 11, Depth 5.10 mm



Figure 61: Section 12, Depth 5.76 mm



Figure 62: Section 13, Depth 6.01 mm

B- HG 29 (175N-82B, 270W, 1500mm/min, 0.18J/mm, carbon black-S/2) Insert 3N-8B							
Section	Total Area Porosity (mm ²)	Length (mm)	Area/Length (mm ² /mm)	# of pores	Average area of pore (mm ²)	Depth (mm)	
0	0	0	0	0	0	0	
1	0.611310	28	0.021832	119	0.005137	0.86	
2	1.525356	28	0.054477	175	0.008716	1.32	
3	1.284653	28	0.045880	172	0.007469	1.56	
4	1.777297	28	0.063475	323	0.005502	1.75	
5	2.053292	28	0.073332	236	0.008700	2.04	
6	1.679747	28	0.059991	161	0.010433	2.30	
7	1.318257	28	0.047081	120	0.010985	2.51	
8	2.592885	28	0.092603	272	0.009533	2.75	
9	2.467094	28	0.088110	249	0.009908	2.98	
10	2.169436	28	0.077480	215	0.010090	3.20	
11	2.377206	28	0.084900	246	0.009663	3.37	
12	2.616539	28	0.093448	228	0.011476	3.61	
13	2.899763	28	0.103563	314	0.009235	3.94	
14	2.396803	28	0.085600	266	0.009011	4.16	
15	2.651643	28	0.094702	335	0.007915	4.32	
16	3.213422	28	0.114765	304	0.010570	4.58	
17	3.360038	28	0.120001	240	0.014000	4.77	
18	3.103526	28	0.110840	278	0.011164	4.98	
19	3.154835	28	0.112673	325	0.009707	5.18	
20	2.830252	28	0.101080	324	0.008708	5.38	
21	2.774459	28	0.099088	315	0.008808	5.60	
22	2.712775	28	0.096885	376	0.007215	5.90	
23	1.806426	28	0.064515	274	0.006593	6.14	
24	1.957247	28	0.069902	206	0.009501	6.36	
25	2.158972	28	0.077106	335	0.006445	6.50	



Figure 63: Section 1, Depth 0.86 mm



Figure 64: Section 2, Depth 1.32 mm



Figure 65: Section 3, Depth 1.56 mm



Figure 66: Section 4, Depth 1.75 mm



Figure 67: Section 5, Depth 2.04 mm



Figure 68: Section 6, Depth 2.30 mm



Figure 69: Section 7, Depth 2.51 mm



Figure 70: Section 8, Depth 2.75 mm



Figure 71: Section 9, Depth 2.98 mm



Figure 72: Section 10, Depth 3.20 mm



Figure 73: Section 11, Depth 3.37 mm



Figure 74: Section 12, Depth 3.61 mm



Figure 75: Section 13, Depth 3.94 mm



Figure 76: Section 14, Depth 4.16 mm



Figure 77: Section 15, Depth 4.32 mm



Figure 78: Section 16, Depth 4.58 mm



Figure 79: Section 17, Depth 4.77 mm



Figure 80: Section 18, Depth 4.98 mm



Figure 81: Section 19, Depth 5.18 mm



Figure 82: Section 20, Depth 5.38 mm



Figure 83: Section 21, Depth 5.60 mm



Figure 84: Section 22, Depth 5.90 mm



Figure 85: Section 23, Depth 6.14 mm

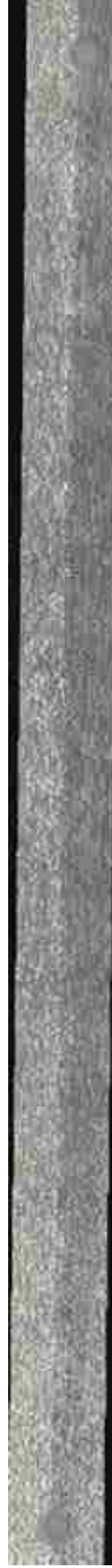


Figure 86: Section 24, Depth 6.36 mm



Figure 87: Section 25, Depth 6.50 mm

B- HG 29 (175N-82B, 270W, 1500mm/min, 0.18J/mm, carbon black-S/2) Insert 4N-7B						
Section	Total Area Porosity (mm ²)	Length (mm)	Area/Length (mm ² /mm)	# of pores	Average area of pore (mm ²)	Depth (mm)
0	0	0	0	0	0	0.00
1	1.328841036	29.6	0.044893	175	0.007593	0.95
2	1.956645056	29.6	0.066103	301	0.006500	1.31
3	1.849546802	29.6	0.062485	222	0.008331	1.74
4	2.617168282	29.6	0.088418	295	0.008872	2.00
5	3.234742024	29.6	0.109282	283	0.011430	2.37
6	3.307313049	29.6	0.111734	207	0.015977	2.72
7	4.386338707	29.6	0.148187	328	0.013373	3.11
8	3.899422946	29.6	0.131737	288	0.013540	3.32
9	4.814829821	29.6	0.162663	317	0.015189	3.69
10	4.277645166	29.6	0.144515	321	0.013326	4.03
11	4.304703342	29.6	0.145429	324	0.013286	4.25
12	4.150985556	29.6	0.140236	367	0.011311	4.62
13	3.313719346	29.6	0.111950	401	0.008264	4.98
14	2.849253977	29.6	0.096259	380	0.007498	5.29
15	3.125850905	29.6	0.105603	350	0.008931	5.61
16	2.513706749	29.6	0.084923	231	0.010882	5.91
17	2.103672023	29.6	0.071070	425	0.004950	6.32
18	1.902339816	29.6	0.064268	271	0.007020	6.49
19	1.700557401	29.6	0.057451	292	0.005824	6.69



Figure 88: Section 1, Depth 0.95 mm



Figure 89: Section 2, Depth 1.31 mm



Figure 90: Section 3, Depth 1.74 mm



Figure 91: Section 4, Depth 2.00 mm



Figure 92: Section 5, Depth 2.37 mm



Figure 93: Section 6, Depth 2.72 mm



Figure 94: Section 7, Depth 3.11 mm



Figure 95: Section 8, Depth 3.32 mm



Figure 96: Section 9, Depth 3.69 mm



Figure 97: Section 10, Depth 4.03 mm



Figure 98: Section 11, Depth 4.25 mm



Figure 99: Section 12, Depth 4.62 mm



Figure 100: Section 13, Depth 4.98 mm



Figure 101: Section 14, Depth 5.29 mm



Figure 102: Section 15, Depth 5.61 mm



Figure 103: Section 16, Depth 5.91 mm



Figure 104: Section 17, Depth 6.32 mm



Figure 105: Section 18, Depth 6.49 mm



Figure 106: Section 19, Depth 6.69 mm

B- HG 29 (175N-82B, 270W, 1500mm/min, 0.18J/mm, carbon black-S/2) No Insert							
Section	Total Area Porosity (mm ²)	Length (mm)	Area/Length (mm ² /mm)	# of pores	Average area of pore (mm ²)	Depth (mm)	
1	0.320566	21.2	0.015121	117	0.002740	0.00	
2	0.981590	21.2	0.046301	284	0.003456	0.50	
3	1.666319	21.2	0.078600	317	0.005257	1.29	
4	1.832921	21.2	0.086459	307	0.005970	1.80	
5	1.954644	21.2	0.092200	320	0.006108	2.41	
6	1.642434	21.2	0.077473	281	0.005845	2.89	
7	1.698271	21.2	0.080107	262	0.006482	3.44	
8	2.007656	21.2	0.094701	301	0.006670	3.90	
9	1.914701	21.2	0.090316	349	0.005486	4.39	
10	2.644415	21.2	0.124737	355	0.007449	4.93	
11	2.372932	21.2	0.111931	356	0.006666	5.55	
12	1.154571	21.2	0.054461	234	0.004934	6.01	
13	0.929188	21.2	0.043830	159	0.005844	6.23	



Figure 107: Section 1, Depth 0 mm



Figure 108: Section 2, Depth 0.50 mm



Figure 109: Section 3, Depth 1.29 mm



Figure 110: Section 4, Depth 1.80 mm



Figure 111: Section 5, Depth 2.41 mm



Figure 112: Section 6, Depth 2.89 mm



Figure 113: Section 7, Depth 3.44 mm



Figure 114: Section 8, Depth 3.90 mm



Figure 115: Section 9, Depth 4.39 mm



Figure 116: Section 10, Depth 4.93 mm



Figure 117: Section 11, Depth 5.55 mm



Figure 118: Section 12, Depth 6.01 mm



Figure 119: Section 13, Depth 6.23mm

C- HG 9 (151N-45B, 180W, 1500mm/min, 0.12l/mm, carbon black-S) Insert 3N-8B						
Section	Total Area Porosity (mm ²)	Length (mm)	Area/Length (mm ² /mm)	# of pores	Average area of pore (mm ²)	Depth (mm)
0	0.000000	26.6	0.000000	0	0.000000	0.00
1	0.756509	26.6	0.028440	197	0.003840	0.45
2	1.551967	26.6	0.058345	565	0.002747	0.72
3	0.777263	26.6	0.029220	194	0.004007	0.85
4	1.627678	26.6	0.061191	271	0.006006	1.21
5	1.960888	26.6	0.073718	381	0.005147	1.56
6	2.347973	26.6	0.088270	284	0.008268	1.85
7	1.793683	26.6	0.067432	212	0.008461	2.04
8	1.575148	26.6	0.059216	267	0.005899	2.18
9	2.266746	26.6	0.085216	402	0.005639	2.50
10	1.195828	26.6	0.044956	273	0.004380	2.84
11	1.161893	26.6	0.043680	497	0.002338	3.06
12	1.365962	26.6	0.051352	383	0.003566	3.29
13	1.243136	26.6	0.046734	450	0.002763	3.48
14	0.804941	26.6	0.030261	329	0.002447	3.68
15	1.086672	26.6	0.040852	385	0.002823	3.68
16	1.478669	26.6	0.055589	327	0.004522	3.87
17	1.057352	26.6	0.039750	289	0.003659	4.15
18	1.287234	26.6	0.048392	288	0.004470	4.37
19	1.084660	26.6	0.040777	243	0.004464	4.61
20	1.289142	26.6	0.048464	320	0.004029	4.90
21	0.874601	26.6	0.032880	315	0.002777	5.07
22	0.854216	26.6	0.032113	319	0.002678	5.27
23	0.732411	26.6	0.027534	323	0.002268	5.56
24	0.573979	26.6	0.021578	353	0.001626	5.79
25	0.566893	26.6	0.021312	227	0.002497	6.08



Figure 120: Section 1, Depth 0.45 mm



Figure 121: Section 2, Depth 0.72 mm



Figure 122: Section 3, Depth 0.85 mm



Figure 123: Section 4, Depth 1.21 mm



Figure 124: Section 5, Depth 1.56 mm

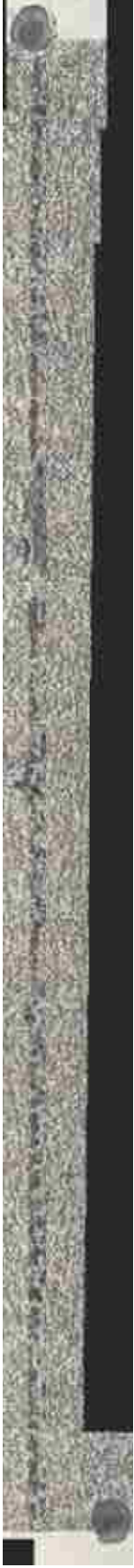


Figure 125: Section 6, Depth 1.85 mm



Figure 126: Section 7, Depth 2.04 mm

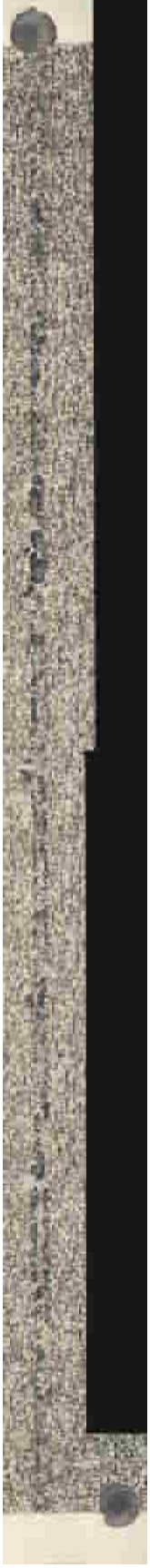


Figure 127: Section 8, Depth 2.18 mm



Figure 128: Section 9, Depth 2.50 mm



Figure 129: Section 10, Depth 2.84 mm



Figure 130: Section 11, Depth 3.06 mm



Figure 131: Section 12, Depth 3.29 mm



Figure 132: Section 13, Depth 3.48 mm



Figure 133: Section 14, Depth 3.68 mm



Figure 134: Section 15, Depth 3.68 mm



Figure 135: Section 16, Depth 3.87 mm



Figure 136: Section 17, Depth 4.15 mm



Figure 137: Section 18, Depth 4.37 mm



Figure 138: Section 19, Depth 4.61 mm



Figure 139: Section 20, Depth 4.90 mm



Figure 140: Section 21, Depth 5.07 mm



Figure 141: Section 22, Depth 5.27 mm



Figure 142: Section 23, Depth 5.56 mm



Figure 143: Section 24, Depth 5.79 mm

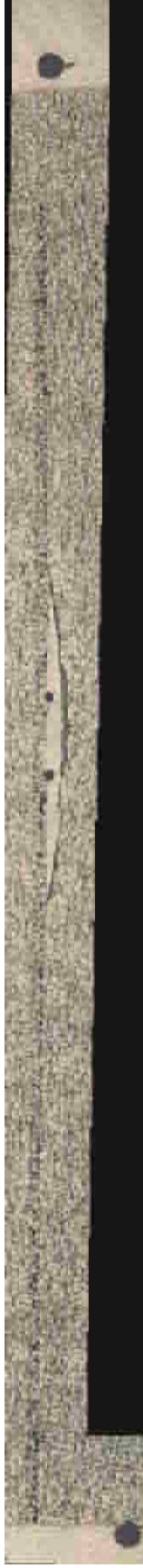


Figure 144: Section 25, Depth 6.08 mm

C- HG 9 (151N-45B, 180W, 1500mm/min, 0.12l/mm, carbon black-S) Insert 4N-7B						
Section	Total Area Porosity (mm ²)	Length (mm)	Area/Length (mm ² /mm)	# of pores	Average area of pore (mm ²)	Depth (mm)
1	0.000000	30	0.000000	0	0.000000	0.00
2	0.772574	30	0.025752	149	0.005185	0.55
3	2.192456	30	0.073082	311	0.007050	0.97
4	1.478343	30	0.049278	317	0.004664	1.24
5	3.450858	30	0.115029	425	0.008120	1.58
6	4.344438	30	0.144815	398	0.010916	2.03
7	3.825325	30	0.127511	300	0.012751	2.28
8	3.931820	30	0.131061	335	0.011737	2.54
9	3.055355	30	0.101845	314	0.009730	2.80
10	3.998151	30	0.133272	306	0.013066	3.22
11	4.100148	30	0.136672	420	0.009762	3.59
12	3.396612	30	0.113220	545	0.006232	3.89
13	2.305325	30	0.076844	375	0.006148	4.08
14	2.807914	30	0.093597	478	0.005874	4.35
15	2.085414	30	0.069514	567	0.003678	4.63
16	2.422737	30	0.080758	463	0.005233	4.63
17	1.529009	30	0.050967	365	0.004189	5.04
18	1.603861	30	0.053462	403	0.003980	5.40
19	1.264822	30	0.042161	340	0.003720	5.69
20	1.245399	30	0.041513	372	0.003348	6.05
21	0.700562	30	0.023352	267	0.002624	6.36
22	1.332234	30	0.044408	661	0.002015	6.56
23	0.821479	30	0.027383	203	0.004047	6.62



Figure 145: Section 1, Depth 0 mm



Figure 146: Section 2, Depth 0.55 mm



Figure 147: Section 3, Depth 0.97 mm



Figure 148: Section 4, Depth 1.24 mm



Figure 149: Section 5, Depth 1.58 mm



Figure 150: Section 6, Depth 2.03 mm



Figure 151: Section 7, Depth 2.28 mm



Figure 152: Section 8, Depth 2.54 mm



Figure 153: Section 9, Depth 2.80 mm



Figure 154: Section 10, Depth 3.22 mm



Figure 155: Section 11, Depth 3.59 mm



Figure 156: Section 12, Depth 3.89 mm



Figure 157: Section 13, Depth 4.08 mm



Figure 158: Section 14, Depth 4.35 mm



Figure 159: Section 15, Depth 4.63 mm



Figure 160: Section 16, Depth 4.63 mm



Figure 161: Section 17, Depth 5.04 mm



Figure 162: Section 18, Depth 5.40 mm



Figure 163: Section 19, Depth 5.69 mm



Figure 164: Section 20, Depth 6.05 mm



Figure 165: Section 21, Depth 6.36 mm



Figure 166: Section 22, Depth 6.56 mm

C- HG 9 (151N-45B, 180W, 1500mm/min, 0.12J/mm, carbon black-S)

No Insert

Section	Total Area Porosity (mm ²)	Length (mm)	Area/Length (mm ² /mm)	# of pores	Average area of pore (mm ²)	Depth (mm)
1	0.199305	21.4	0.009313	26	0.007666	0.00
2	0.442382	21.4	0.020672	212	0.002087	0.33
3	1.167944	21.4	0.054577	318	0.003673	0.75
4	1.406095	21.4	0.065705	298	0.004718	1.37
5	1.728550	21.4	0.080773	402	0.004300	1.88
6	1.541124	21.4	0.072015	452	0.003410	2.40
7	1.272692	21.4	0.059472	415	0.003067	2.87
8	1.121524	21.4	0.052408	555	0.002021	3.43
9	0.925192	21.4	0.043233	566	0.001635	4.03
10	0.897396	21.4	0.041934	450	0.001994	4.52
11	1.035355	21.4	0.048381	397	0.002608	4.92
12	1.119305	21.4	0.052304	445	0.002515	5.43
13	0.854645	21.4	0.039937	308	0.002775	6.09
14	1.100237	21.4	0.051413	261	0.004215	6.34



Figure 167: Section 1, Depth 0 mm



Figure 168: Section 2, Depth 0.33 mm



Figure 169: Section 3, Depth 0.75 mm



Figure 170: Section 4, Depth 1.37 mm



Figure 171: Section 5, Depth 1.88 mm



Figure 172: Section 6, Depth 2.40 mm



Figure 173: Section 7, Depth 2.87 mm



Figure 174: Section 8, Depth 3.43 mm



Figure 175: Section 9, Depth 4.03 mm



Figure 176: Section 10, Depth 4.52 mm



Figure 177: Section 11, Depth 4.92 mm



Figure 178 : Section 12, Depth 5.43 mm



Figure 179: Section 13, Depth 6.09 mm



Figure 180: Section 14, Depth 6.34 mm

D- HG 35 (127N-79B, 270W, 1800mm/min, 0.15J/mm, carbon black-S/2) Insert 3N-8B							
Section	Total Area Porosity (mm ²)	Length (mm)	Area/Length (mm ² /mm)	# of pores	Average area of pore (mm ²)	Depth (mm)	
0	0.00000	29	0.00000	0	0.00000	0.00	
1	0.133314	29	0.004597	54	0.002469	0.83	
2	0.213033	29	0.007346	135	0.001578	1.16	
3	0.420858	29	0.014512	67	0.006281	1.25	
4	0.340370	29	0.011737	121	0.002813	1.61	
5	0.405932	29	0.013998	176	0.002306	1.96	
6	0.470710	29	0.016231	216	0.002179	2.21	
7	0.890607	29	0.030711	303	0.002939	2.45	
8	1.042944	29	0.035964	201	0.005189	2.67	
9	1.046435	29	0.036084	232	0.004510	3.26	
10	0.863388	29	0.029772	230	0.003754	3.56	
11	0.646331	29	0.022287	296	0.002184	3.79	
12	1.026642	29	0.035401	452	0.002271	3.99	
13	0.779201	29	0.026869	427	0.001825	4.19	
14	0.885888	29	0.030548	291	0.003044	4.39	
15	1.279882	29	0.044134	324	0.003950	4.39	
16	1.851346	29	0.063840	360	0.005143	4.58	
17	0.821997	29	0.028345	275	0.002989	4.79	
18	1.471923	29	0.050756	330	0.004460	4.98	
19	1.441997	29	0.049724	356	0.004051	5.22	
20	1.906672	29	0.065747	353	0.005401	5.44	
21	1.349704	29	0.046542	465	0.002903	5.63	
22	1.044172	29	0.036006	402	0.002597	5.83	
23	1.058476	29	0.036499	394	0.002686	6.13	
24	0.690843	29	0.023822	330	0.002093	6.48	
25	1.028166	29	0.035454	301	0.003416	6.76	



Figure 181: Section 1, Depth 0.83 mm



Figure 182: Section 2, Depth 1.16 mm



Figure 183: Section 3, Depth 1.25 mm



Figure 184: Section 4, Depth 1.61 mm



Figure 185: Section 5, Depth 1.96 mm



Figure 186: Section 6, Depth 2.21 mm



Figure 187: Section 7, Depth 2.45 mm



Figure 188: Section 8, Depth 2.67 mm



Figure 189: Section 9, Depth 3.26 mm



Figure 190: Section 10, Depth 3.56 mm



Figure 191: Section 11, Depth 3.79 mm



Figure 192: Section 12, Depth 3.99 mm



Figure 193: Section 13, Depth 4.19 mm



Figure 194: Section 14, Depth 4.39 mm



Figure 195: Section 15, Depth 4.39 mm

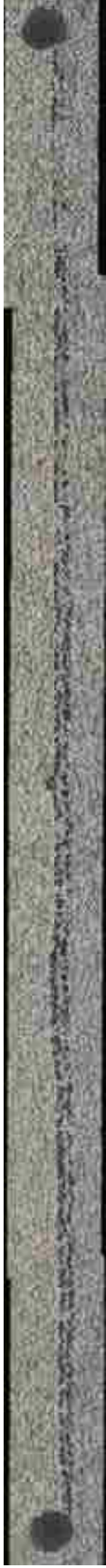


Figure 196: Section 16, Depth 4.58 mm



Figure 197: Section 17, Depth 4.79 mm



Figure 198: Section 18, Depth 4.98 mm

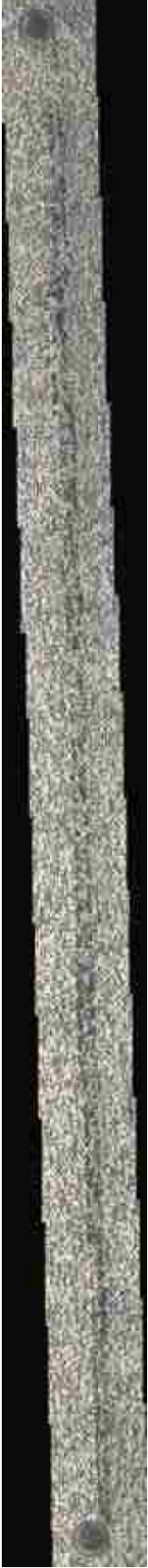


Figure 199: Section 19, Depth 5.22 mm



Figure 200: Section 20, Depth 5.44 mm



Figure 201: Section 21, Depth 5.63 mm



Figure 202: Section 22, Depth 5.83 mm



Figure 203: Section 23, Depth 6.13 mm



Figure 204: Section 24, Depth 6.48 mm



Figure 205: Section 25, Depth 6.76 mm

D- HG 35 (127N-79B, 270W, 1800mm/min, 0.15J/mm, carbon black-S/2) Insert 4N-7B							
Section	Total Area Porosity (mm ²)	Length (mm)	Area/Length (mm ² /mm)	# of pores	Average area of pore (mm ²)	Depth (mm)	
0	0.000000	27.2	0.000000	0	0.000000	0.00	
1	0.357988	27.2	0.013161	91	0.003934	0.83	
2	0.718195	27.2	0.026404	350	0.002052	1.16	
3	0.327692	27.2	0.012048	123	0.002664	1.25	
4	0.799719	27.2	0.029401	184	0.004346	1.61	
5	0.805547	27.2	0.029616	207	0.003892	1.96	
6	0.821923	27.2	0.030218	270	0.003044	2.21	
7	1.167988	27.2	0.042941	252	0.004635	2.45	
8	0.642012	27.2	0.023603	207	0.003102	2.67	
9	2.214719	27.2	0.081423	313	0.007076	3.26	
10	2.308402	27.2	0.084868	289	0.007988	3.56	
11	3.103595	27.2	0.114103	716	0.004335	3.79	
12	2.418743	27.2	0.088924	367	0.006591	3.99	
13	2.016361	27.2	0.074131	271	0.007440	4.19	
14	1.648136	27.2	0.060593	302	0.005457	4.39	
15	2.404512	27.2	0.088401	320	0.007514	4.39	
16	2.780044	27.2	0.102208	332	0.008374	4.58	
17	2.037426	27.2	0.074905	298	0.006837	4.79	
18	1.717426	27.2	0.063141	306	0.005613	4.98	
19	2.248787	27.2	0.082676	304	0.007397	5.22	
20	1.922751	27.2	0.070689	342	0.005622	5.44	
21	1.224867	27.2	0.045032	336	0.003645	5.63	
22	1.234349	27.2	0.045380	357	0.003458	5.83	
23	1.293299	27.2	0.047548	447	0.002893	6.13	
24	1.323757	27.2	0.048668	391	0.003386	6.48	
25	0.894837	27.2	0.032898	320	0.002796	6.76	
26	1.445118	27.2	0.053129	538	0.002686	6.90	
27	0.708580	27.2	0.026051	269	0.002634	6.96	



Figure 206: Section 1, Depth 0.83 mm



Figure 207: Section 2, Depth 1.16 mm



Figure 208: Section 3, Depth 1.25 mm



Figure 209: Section 4, Depth 1.61 mm



Figure 210: Section 5, Depth 1.96 mm



Figure 211: Section 6, Depth 2.21 mm



Figure 212: Section 7, Depth 2.45 mm



Figure 213: Section 8, Depth 2.67 mm



Figure 214: Section 9, Depth 3.26 mm



Figure 215: Section 10, Depth 3.56 mm



Figure 216: Section 11, Depth 3.79 mm



Figure 217: Section 12, Depth 3.99 mm



Figure 218: Section 13, Depth 4.19 mm



Figure 219: Section 14, Depth 4.39 mm



Figure 220: Section 15, Depth 4.39 mm



Figure 221: Section 16, Depth 4.58 mm



Figure 222: Section 17, Depth 4.79 mm



Figure 223: Section 18, Depth 4.98 mm



Figure 224: Section 19, Depth 5.22 mm



Figure 225: Section 20, Depth 5.44 mm



Figure 226: Section 21, Depth 5.63 mm



Figure 227: Section 22, Depth 5.83 mm



Figure 228: Section 23, Depth 6.13 mm



Figure 229: Section 24, Depth 6.48 mm



Figure 230: Section 25, Depth 6.76 mm



Figure 231: Section 26, Depth 6.90 mm



Figure 232: Section 27, Depth 6.96 mm

D- HG 35 (127N-79B, 270W, 1800mm/min, 0.15J/mm, carbon black-S/2)							
No Insert							
Section	Total Area Porosity (mm ²)	Length (mm)	Area/Length (mm ² /mm)	# of pores	Average area of pore (mm ²)	Depth (mm)	
1	0.000000	23	0.000000	0	0.000000	0.00	
2	0.754689	23	0.032813	185	0.004079	0.40	
3	1.427234	23	0.062054	250	0.005709	0.90	
4	2.079734	23	0.090423	183	0.011365	1.69	
5	1.403151	23	0.061007	537	0.002613	2.20	
6	1.107766	23	0.048164	418	0.002650	2.81	
7	1.066243	23	0.046358	421	0.002533	3.29	
8	1.043817	23	0.045383	425	0.002456	3.84	
9	0.731405	23	0.031800	329	0.002223	4.30	
10	1.05296	23	0.045882	362	0.002915	4.80	
11	1.141953	23	0.049650	503	0.002270	5.34	
12	1.144615	23	0.049766	493	0.002322	5.96	
13	1.053861	23	0.045820	164	0.006426	6.41	



Figure 233: Section 1, Depth 0 mm



Figure 234: Section 2, Depth 0.40 mm

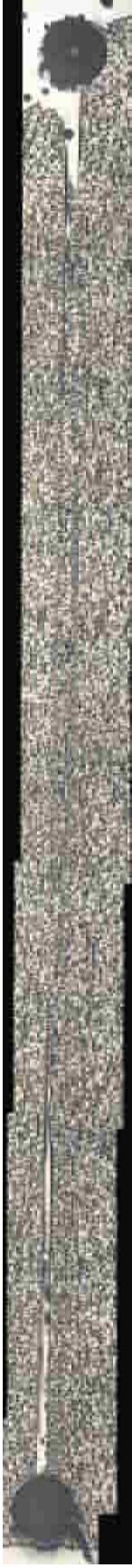


Figure 235: Section 3, Depth 0.90 mm



Figure 236: Section 4, Depth 1.69 mm



Figure 237: Section 5, Depth 2.20 mm



Figure 238: Section 6, Depth 2.81 mm



Figure 239: Section 7, Depth 3.29 mm



Figure 240: Section 8, Depth 3.84 mm



Figure 241: Section 9, Depth 4.30 mm



Figure 242: Section 10, Depth 4.80 mm



Figure 243: Section 11, Depth 5.34 mm



Figure 244: Section 12, Depth 5.96 mm



Figure 245: Section 13, Depth 6.41 mm

E- HG 3 (171N-60B, 240W, 2000mm/min, 0.12J/mm, carbon black-S) Insert 3N-8B							
Section	Total Area Porosity (mm ²)	Length (mm)	Area/Length (mm ² /mm)	# of pores	Average area of pore (mm ²)	Depth (mm)	
1	0.00000	28.8	0.00000	0	0.00000	0.00	
2	0.00000	28.8	0.00000	0	0.00000	0.25	
3	0.047309	28.8	0.001643	11	0.004301	0.47	
4	0.107301	28.8	0.003726	39	0.002751	0.73	
5	0.244930	28.8	0.008505	32	0.007654	0.95	
6	0.609554	28.8	0.021165	51	0.011952	1.29	
7	0.924702	28.8	0.032108	101	0.009155	1.51	
8	1.373670	28.8	0.047697	122	0.011260	1.75	
9	1.381686	28.8	0.047975	113	0.012227	1.95	
10	1.014468	28.8	0.035225	112	0.009058	2.15	
11	0.878789	28.8	0.030514	168	0.005231	2.36	
12	0.948918	28.8	0.032949	157	0.006044	2.57	
13	1.165049	28.8	0.040453	196	0.005944	2.82	
14	1.288262	28.8	0.044731	267	0.004825	3.03	
15	1.733827	28.8	0.060202	289	0.005999	3.25	
16	2.283043	28.8	0.079272	355	0.006431	3.44	
17	2.604425	28.8	0.090431	335	0.007774	3.68	
18	2.386540	28.8	0.082866	297	0.008035	3.88	
19	2.774694	28.8	0.096344	356	0.007794	4.11	
20	2.553664	28.8	0.088669	384	0.006650	4.37	
21	2.549405	28.8	0.088521	396	0.006438	4.57	
22	2.184208	28.8	0.075841	448	0.004875	4.81	
23	2.236114	28.8	0.077643	488	0.004582	5.03	
24	1.621846	28.8	0.056314	408	0.003975	5.21	
25	1.935368	28.8	0.067200	425	0.004554	5.42	
26	1.585727	28.8	0.055060	412	0.003849	5.59	



Figure 246: Section 1, Depth 0 mm



Figure 247: Section 2, Depth 0.25 mm



Figure 248: Section 3, Depth 0.47 mm



Figure 249: Section 4, Depth 0.73 mm



Figure 250: Section 5, Depth 0.95 mm



Figure 251: Section 6, Depth 1.29 mm



Figure 252: Section 7, Depth 1.51 mm



Figure 253: Section 8, Depth 1.75 mm



Figure 254: Section 9, Depth 1.95 mm



Figure 255: Section 10, Depth 2.15 mm



Figure 256: Section 11, Depth 2.36 mm



Figure 257: Section 12, Depth 2.57 mm



Figure 258: Section 13, Depth 2.82 mm



Figure 259: Section 14, Depth 3.03 mm



Figure 260: Section 15, Depth 3.25 mm



Figure 261: Section 16, Depth 3.44 mm



Figure 262: Section 17, Depth 3.68 mm



Figure 263: Section 18, Depth 3.88 mm



Figure 264: Section 19, Depth 4.11 mm



Figure 265: Section 20, Depth 4.37 mm



Figure 266: Section 21, Depth 4.57 mm



Figure 267: Section 22, Depth 4.81 mm



Figure 268: Section 23, Depth 5.03 mm



Figure 269: Section 24, Depth 5.21 mm



Figure 270: Section 25, Depth 5.42 mm



Figure 271: Section 26, Depth 5.59 mm

E- HG 3 (171N-60B, 240W, 2000mm/min, 0.12I/mm, carbon black-S) Insert 4N-7B						
Section	Total Area Porosity (mm ²)	Length (mm)	Area/Length (mm ² /mm)	# of pores	Average area of pore (mm ²)	Depth (mm)
1	0.000000	28.3	0.000000	7	0.003257	0.00
2	0.236760	28.3	0.008366	72	0.003288	0.25
3	0.285725	28.3	0.010096	96	0.002976	0.47
4	0.634689	28.3	0.022427	196	0.003238	0.73
5	0.423209	28.3	0.014954	127	0.003332	0.95
6	1.147751	28.3	0.040557	249	0.004609	1.29
7	1.511420	28.3	0.053407	231	0.006543	1.51
8	1.874157	28.3	0.066225	262	0.007153	1.75
9	2.092692	28.3	0.073947	287	0.007292	1.95
10	2.345296	28.3	0.082873	272	0.008622	2.15
11	2.562959	28.3	0.090564	276	0.009286	2.36
12	2.201287	28.3	0.077784	334	0.006591	2.57
13	2.525947	28.3	0.089256	300	0.008420	2.82
14	3.108476	28.3	0.109840	362	0.008587	3.03
15	2.592766	28.3	0.091617	401	0.006466	3.25
16	2.879068	28.3	0.101734	376	0.007657	3.44
17	2.671391	28.3	0.094395	400	0.006678	3.68
18	2.155207	28.3	0.076156	384	0.005613	3.88
19	2.044275	28.3	0.072236	503	0.004064	4.11
20	1.454896	28.3	0.051410	383	0.003799	4.37
21	1.105976	28.3	0.039080	307	0.003603	4.57
22	1.403195	28.3	0.049583	372	0.003772	4.81
23	1.458772	28.3	0.051547	512	0.002849	5.03
24	1.313802	28.3	0.046424	416	0.003158	5.21
25	1.406598	28.3	0.049703	494	0.002847	5.42
26	1.029660	28.3	0.036384	370	0.002783	5.59
27	1.728994	28.3	0.061095	275	0.006287	5.81



Figure 272: Section 1, Depth 0 mm



Figure 273: Section 2, Depth 0.25mm



Figure 274: Section 3, Depth 0.47 mm



Figure 275: Section 4, Depth 0.73 mm



Figure 276: Section 5, Depth 0.95 mm



Figure 277: Section 6, Depth 1.29 mm



Figure 278: Section 7, Depth 1.51 mm



Figure 279: Section 8, Depth 1.75 mm



Figure 280: Section 9, Depth 1.95 mm



Figure 281: Section 10, Depth 2.15 mm



Figure 282: Section 11, Depth 2.36 mm



Figure 283: Section 12, Depth 2.57 mm



Figure 284: Section 13, Depth 2.82 mm



Figure 285: Section 14, Depth 3.03 mm



Figure 286: Section 15, Depth 3.25 mm



Figure 287: Section 16, Depth 3.44 mm



Figure 288: Section 17, Depth 3.68 mm



Figure 289: Section 18, Depth 3.88 mm



Figure 290: Section 19, Depth 4.11 mm



Figure 291: Section 20, Depth 4.37 mm



Figure 292: Section 21, Depth 4.57 mm



Figure 293: Section 22, Depth 4.81 mm



Figure 294: Section 23, Depth 5.03 mm



Figure 295: Section 24, Depth 5.21 mm



Figure 296: Section 25, Depth 5.42 mm



Figure 297: Section 26, Depth 5.59 mm



Figure 298: Section 27, Depth 5.81 mm

E- HG 3 (171N-60B, 240W, 2000mm/min, 0.12I/mm, carbon black-S) No Insert							
Section	Total Area Porosity (mm ²)	Length (mm)	Area/Length (mm ² /mm)	# of pores	Average area of pore (mm ²)	Depth (mm)	
1	0	0	0	0	0	0.00	
2	0.261405	23	0.011365	52	0.005027	0.42	
3	0.770666	23	0.033507	169	0.004560	1.04	
4	0.741672	23	0.032247	136	0.005453	1.55	
5	1.105473	23	0.048064	158	0.006997	2.07	
6	1.265311	23	0.055014	243	0.005207	2.54	
7	0.959320	23	0.041710	211	0.004547	3.10	
8	0.955370	23	0.041538	152	0.006285	3.70	
9	1.046731	23	0.045510	114	0.009182	4.19	
10	1.374467	23	0.059759	255	0.005390	4.59	
11	1.244438	23	0.054106	286	0.004351	5.10	
12	0.996657	23	0.043333	193	0.005164	5.76	
13	1.064896	23	0.046300	263	0.004049	6.01	
14	1.314941	23	0.057171	201	0.006542	6.13	



Figure 299: Section 1, Depth 0 mm



Figure 300: Section 2, Depth 0.42 mm



Figure 301: Section 3, Depth 1.04 mm



Figure 302: Section 4, Depth 1.55 mm



Figure 303: Section 5, Depth 2.07 mm



Figure 304: Section 6, Depth 2.54 mm



Figure 305: Section 7, Depth 3.10 mm



Figure 306: Section 8, Depth 3.70 mm



Figure 307: Section 9, Depth 4.19 mm



Figure 308: Section 10, Depth 4.59 mm



Figure 309: Section 11, Depth 5.10 mm



Figure 310: Section 12, Depth 5.79 mm



Figure 311: Section 13, Depth 6.01 mm



Figure 312: Section 14, Depth 6.13 mm

Un-welded Insert Sections

Insert 3N un-welded



Figure 313: Section 1, Depth 0.86 mm



Figure 314: Section 2, Depth 1.32 mm



Figure 315: Section 3, Depth 1.56 mm



Figure 316: Section 4, Depth 1.75 mm



Figure 317: Section 5, Depth 2.04 mm



Figure 318: Section 6, Depth 2.30 mm

Insert 3N un-welded



Figure 319: Section 7, Depth 2.51 mm



Figure 320: Section 8, Depth 2.75 mm



Figure 321: Section 9, Depth 2.98 mm



Figure 322: Section 10, Depth 3.20 mm



Figure 323: Section 11, Depth 3.37 mm



Figure 324: Section 12, Depth 3.61 mm



Figure 325: Section 13, Depth 3.94 mm



Figure 326: Section 14, Depth 4.16 mm



Figure 327: Section 15, Depth 4.32 mm



Figure 328: Section 16, Depth 4.58 mm



Figure 329: Section 17, Depth 4.77 mm



Figure 330: Section 18, Depth 4.98 mm



Figure 331: Section 19, Depth 5.18 mm



Figure 332: Section 20, Depth 5.30 mm



Figure 333: Section 21, Depth 5.60 mm



Figure 334: Section 22, Depth 5.90 mm



Figure 335: Section 23, Depth 6.14 mm



Figure 336: Section 24, Depth 6.36 mm

Insert 3N un-welded

Insert 8B un-welded



Figure 337: Section 1, Depth 0.86 mm



Figure 338: Section 2, Depth 1.32 mm



Figure 339: Section 3, Depth 1.56 mm



Figure 340: Section 4, Depth 1.75 mm



Figure 341: Section 5, Depth 2.04 mm



Figure 342: Section 6, Depth 2.30 mm

Insert 8B un-welded



Figure 343: Section 7, Depth 2.51 mm



Figure 344: Section 8, Depth 2.75 mm



Figure 345: Section 9, Depth 2.98 mm



Figure 346: Section 10, Depth 3.20 mm



Figure 347: Section 11, Depth 3.37 mm



Figure 348: Section 12, Depth 3.61 mm

Insert 8B un-welded



Figure 349: Section 13, Depth 3.94 mm



Figure 350: Section 14, Depth 4.16 mm



Figure 351: Section 15, Depth 4.32 mm



Figure 352: Section 16, Depth 4.58 mm



Figure 353: Section 17, Depth 4.77 mm



Figure 354: Section 18, Depth 4.98 mm

Insert 8B un-welded



Figure 355: Section 19, Depth 5.18 mm



Figure 356: Section 20, Depth 5.30 mm



Figure 357: Section 21, Depth 5.60 mm



Figure 358: Section 22, Depth 5.90 mm



Figure 359: Section 23, Depth 6.14 mm



Figure 360: Section 24, Depth 6.36 mm

Insert 4N un-welded



Figure 361: Section 1, Depth 0.95 mm



Figure 362: Section 2, Depth 1.31 mm



Figure 363: Section 3, Depth 1.74 mm



Figure 364: Section 4, Depth 2.00 mm



Figure 365: Section 5, Depth 2.37 mm



Figure 366: Section 6, Depth 2.72 mm

Insert 4N un-welded



Figure 367: Section 7, Depth 3.11 mm



Figure 368: Section 8, Depth 3.32 mm



Figure 369: Section 9, Depth 3.69 mm



Figure 370: Section 10, Depth 4.03 mm



Figure 371: Section 11, Depth 4.25 mm



Figure 372: Section 12, Depth 4.62 mm

Insert 4N un-welded



Figure 373: Section 13, Depth 4.98 mm



Figure 374: Section 14, Depth 5.29 mm



Figure 375: Section 15, Depth 5.61 mm



Figure 376: Section 16, Depth 5.91 mm



Figure 377: Section 17, Depth 6.32 mm



Figure 378: Section 18, Depth 6.49 mm

Insert 4N un-welded

Insert 7B un-welded



Figure 379: Section 1, Depth 0.95 mm



Figure 380: Section 2, Depth 1.31 mm



Figure 381: Section 3, Depth 1.74 mm



Figure 382: Section 4, Depth 2.00 mm



Figure 383: Section 5, Depth 2.37 mm



Figure 384: Section 6, Depth 2.72 mm

Insert 7B un-welded



Figure 385: Section 7, Depth 3.11 mm



Figure 386: Section 8, Depth 3.32 mm



Figure 387: Section 9, Depth 3.69 mm



Figure 388: Section 10, Depth 4.03 mm



Figure 389: Section 11, Depth 4.25 mm



Figure 390: Section 12, Depth 4.62 mm



Figure 391: Section 13, Depth 4.98 mm



Figure 392: Section 14, Depth 5.29 mm



Figure 393: Section 15, Depth 5.61 mm



Figure 394: Section 16, Depth 5.91 mm



Figure 395: Section 17, Depth 6.32 mm



Figure 396: Section 18, Depth 6.49 mm

Insert 7B un-welded

Conference Publication and Presentation

Watt, D. F., Masse, S., & Baylis, B., An Experimental Method to Study the Sensitivity of Transmission Laser Welding of Plastic Parts to Interfacial Gaps, in SAE World Congress 2009, SAE International: Technical Paper 2009-01-1298.

Vita Auctoris

NAME: Stephanie Lynn Masse
PLACE OF BIRTH: Windsor, Ontario
DATE OF BIRTH: 1985
EDUCATION: Ontario Secondary School Diploma
General Amherst Secondary School
Amherstburg, ON
1999-2003

Bachelor of Applied Science
Mechanical Engineering – Materials Option
University of Windsor
Windsor, ON
2003-2007

Master of Applied Science
Engineering Materials
University of Windsor
Windsor, ON
2008 – 2010